Ambient Ground Vibration Measurements at the Hanford, Washington LIGO Site

Alan Rohay, Pacific Northwest Laboratory

1.0 Introduction

An analysis of ground vibration measurements taken at the Laser Interferometer Gravitational Wave Observatory (LIGO) site at Hanford, Washington, was conducted to characterize the ambient seismic noise conditions, anthropogenic noise, and wind and acoustic noise sources at the LIGO site. The purpose of this study is to establish site-specific ground vibration statistics for the design of vibration-sensitive systems.

The instrumentation used, and its calibration and noise characteristics are described below in Sections 2 and 3. The method of recording at the LIGO site and the observations that were taken is then described (Section 4). The methods used to prepare spectrograms (a time-frequency analysis), frequency spectra, and noise amplitude histograms are described in Sections 5, 6, and 7. The plots of the data and analysis results are included as separate appendices that generally correspond to each of the major sections of this report. Special studies of highway traffic, heavy equipment, wind, and acoustic noise sources are contained in Section 8. A study of wind noise at a large nearby building is presented in Section 9. Section 10 briefly reviews the results and some lessons learned.

In summary, it was found that the original LIGO design spectrum is a close approximation to the ambient ground vibrations measured at the site. The design spectrum below 1 Hz is usually slightly lower than the observed "microseism peak" during the period of the measurements. From 1 to 10 Hz, several transient phenomena including rush hour traffic, heavy equipment operations within 4 km, and wind speeds in excess of 10 m/s are observed to increase ground vibration to levels above the design spectrum. Above 10 Hz, the design spectrum nearly always envelops the observed ground vibration.

2.0 Instrumentation System Description

The instrumentation used to make the vibration measurements consisted of modern seismological instruments conventionally used to record small earthquake signals. This system consists of three orthogonally-mounted seismometers to sense the ground motion and a recording system that digitally records the data in the field. A low-frequency (infrasonic) microphone was recorded in parallel with the seismic data. Wind speed and direction were also recorded at each site using a separate, low-speed data logger. This section describes the components and systems used to make these measurements, and the parameters used to record the data.

Seismometers. The measurements at the LIGO site were made with a CMG-40T three-component broad band seismometer, manufactured by Guralp Systems, Ltd. and distributed in the U.S. by Digital Technology Associates, Concord, CA. This instrument detects the relative displacement of the seismometer mass due to an input acceleration with a capacitive transducer. This signal is amplified and a feedback force is applied to a coil/magnet assembly to restore the mass position. The instrument has acceleration-, velocity-, and displacement-proportional outputs derived from the feedback signal. The data were collected from the low-gain (nominally 800 V/m/s) velocity output. The velocity output is attenuated by 3 dB (70%) at 0.05 and 50 Hz. The frequency response and noise floor of the CMG-40T seismometer were measured and are described in greater detail in the next section on system calibration and noise.

In addition to the CMG-40T seismometer, a second CMG-40T seismometer and a CMG-3T seismometer were used for some of the measurements. The CMG3-T has a similar design, but has a different frequency response outside of the 0.05 - 50 Hz range, and has a noise floor that is reported to be a factor of 10 or more lower than that of the CMG-40T. A comparison of these three seismometers is also included in the next section.

Digital Recorder. The data acquisition system was a Model 72A-02 from Refraction Technology, Inc. (Reftek), Dallas, TX. It amplifies and then digitizes up to six input signals with 16-bit precision at 1000 samples/s and digitally applies an anti-alias filter to the output stream at selected sub-rates. This data acquisition system can record each input channel at a different amplification and digitizing rate, and can record continuous data, data from pre-programmed time periods, or can record based on a variety of signal threshold triggers. All data collected at the LIGO site were collected continuously using a sample rate of 250 samples/s. The system used stores up to 2.5 Mb of data internally and periodically copies the data to one of two 1 Gb disk drives. Precise time is obtained from a Global Positioning Satellite (GPS) receiver and maintained by an internal crystal oscillator. Control of the data acquisition system was provided by a hand-held PC and software provided by Reftek.

Playback and analysis software. The Reftek disk drives were connected to a SUN/UNIX workstation and playback software, obtained from the Incorporated Research Institutions for Seismology (IRIS, Arlington, VA), was used to copy the data from the field disk to the computer system's disk. IRIS software was then used to view the data on the computer screen, and reformat, merge, and otherwise manipulate the data. All data were copied to 8mm tape in UNIX tar format. The IRIS software was used to convert selected portions of the data to SAC format (Seismic Analysis Code, from Lawrence Livermore National Laboratory), and the spectral analyses were conducted using the SAC programs. In addition to the IRIS and SAC software, the Splus statistical package (from StatSci, Seattle, WA) was used to generate histograms and some additional graphics.

Infrasound Microphone. The infrasound instrument used was a Model 2 Microphone from Chaparral Physics Consultants, Albuquerque, NM. It has a 0.4 V/Pa response at the sensitivity selected and its response to pressure is essentially constant between 0.3 and 100 Hz. Its response is attenuated by 3 dB (70%) at 0.1 and 300 Hz. This instrument was not calibrated and has only been used for qualitative comparisons to the seismic noise sig-

nals to date. The infrasound signals were recorded as the fourth channel on the Reftek digital recorder at the same rate (250 samples/s) as the seismic data.

Wind measurement system. Wind speed and direction were measured using an F-460 cross-arm assembly from Climatronix, Bohemia, NY, and recorded on a Campbell 21X data logger (Campbell Scientific, Inc., Logan, UT). Wind speed was measured with a cup anemometer and wind direction was measured with a vane. Wind speed and direction were measured every second, and the average wind speed and direction over a one-minute period were calculated and recorded by the data logger. In addition to the one-minute mean, the peak wind speed during the last minute and the time it occurred was also recorded. The data were downloaded to a portable PC and converted to ASCII files using Campbell PC-208 software.

3.0 System Calibration and System Noise

3.1 Seismometer Calibration

Calibration method. Electrical signals were input to the calibration coil of the seismometers to check the calibration constants of the seismometers. The current in the coil (determined by a 10 K ohm resistor) induces an acceleration of all three transducers. Two types of input signals were used, step offsets and sinusoidal inputs. Sinusoidal inputs were input for a duration of 10 or more cycles, at frequencies ranging from 0.025 to 150 Hz. Different amplitudes of input signals were used in different frequency ranges to obtain as near to full scale digitization when recorded on the Reftek recorder. The step test was repeated over fifteen times at 20-s intervals with alternating polarity. The seismometer velocity outputs were digitized at 250 samples/s at a gain of 1, and the calibration input signal was recorded as a fourth channel at a digitization rate of 1000 samples/s and the same gain. The input and output signals recorded on the Reftek disk were then copied to the workstations for spectral analysis. Figure 3-1 shows examples of the seismometer output for the vertical channel of the two seismometers. The response fall-off at high frequency was measured from 4 to 140 Hz (the first and sixth panels of Figure 3-1, with the first being repeated in descending order). Low-frequency response was measured on one seismometer, in descending order from 2 to 0.25 Hz in panels 2 and 3, and then in ascending order in panels 4 and 5. The signal output was clipped by the digitizer at 0.05 Hz (the second-lowest frequency) and these calibrations were repeated (shown in the last two panels of Figure 3-1). The two seismometers' response to step-function inputs is shown in the panels 7 to 10; measurements were made after the interval between the alternate-polarity steps was adjusted to approximately 40 s.

Analysis of Step Calibration. Spectral analysis was performed on both the calibration signal and the output signals of the six components tested. The Fourier spectra of the inputs and outputs was calculated over 16 different step intervals and the average taken to reduce the variance. The ratio of the output to input voltage spectra (obtained by converting the input acceleration spectra to velocity spectra) was calculated, and normalized to the calibration circuit resistance and the feedback coil constant appropriate to each component. The result is shown in Figure 3-2 for the two three-component seismometers, nor-

malized to the velocity transduction constants provided by the manufacturer. The original values agree with those measured to within 5%. This calibration begins to fail at frequencies higher than approximately 5 Hz because background noise at this location is high and the power in the step inputs is relatively low when referred to a velocity spectrum.

Analysis of Sinusoidal Calibration. Amplitudes were measured from the sinusoidal input and output signals. The best results were obtained when the root-mean-square (r.m.s.) amplitude of the signals was measured, although comparable results (not presented here) were obtained for peak amplitude measurements. The ratio of the output to input signal amplitude was again normalized to the calibration circuit resistance and the feedback coil constant appropriate to each component. Figure 3-3 shows the results, normalized to the velocity transduction constants provided by the manufacturer. The results are again within 5% of the provided constants in the flat portion of the velocity spectrum, and the high-frequency filters of the seismometer are well-resolved. The effect of the anti-alias filtering done by the Reftek recorder appears at 100 Hz.

Spectral Amplitude Corrections 0.1 to 100 Hz. Equations to correct the velocity output of the seismometers to be flat from 0.1 to 100 Hz were derived and their effect on the spectrum is shown in Figures 3-4 and 3-5. However, these have not been used to correct the spectra in this report because the response of the seismometers above approximately 40 Hz is strongly affected by resonances or coupling problems in the field installations. No correction would have been needed at frequencies as low as 0.1 Hz, the lowest frequency considered here. The velocity output is flat within 10% for frequencies between 0.1 and 30 Hz. The velocity output rolls off by 30% at 50 Hz.

3.2 Seismometer Noise

A different, quieter site than was used for the seismometer calibration was located at an abandoned subterranean Nike missile bunker located 7.8 km southwest of the LIGO Southwest End. The two CMG-40T were set on the concrete floor and covered with an inverted 55-gallon drum lined with 3"-thick foam to maintain temperature stability, eliminate air currents, and to reduce acoustic noises. The seismometers were mutually oriented and recorded at the same gain and digitizing rate on the six channels of the Reftek recorder. A one hour segment was selected that was among the quietest periods, and spectra were calculated using identical methods to the spectral calculations made on the LIGO site measurements. This involves taking 39 180-s overlapping samples and calculating the mean of the logarithm of the squared spectral amplitudes (see below for greater detail).

Figure 3-6 shows the two spectra from the two vertical channels of the two seismometers, which practically overlie one another, and the spectrum of the signal obtained by subtracting one of the time series from the other. The latter represents the portion of the signal that is not common to both sensors and which is interpreted as sensor noise. However, there are additional signal differences that are due to the method of emplacement, including misalignment of the horizontal components and possible differences in coupling on the concrete floor. Assuming each of the two sensors contribute equally to this noise signal, the noise caused by each sensor would be estimated to be reduced by a factor of sqrt(2) relative to the values plotted in the figure. At frequencies above 20 Hz, the signal and

noise spectra overly one another and it is clear that only sensor noise is recorded and not actual ground motion from 20-100 Hz. The sensor noise is more than a factor of 10 below the LIGO design spectrum throughout this entire range.

At frequencies near 1 Hz, the signal difference spectrum is nearly equal to the individual sensor spectra, and it is in this range that the two sensor spectra can be seen to diverge. This indicates that these sensors have only marginally detected actual ground noise in the 1 Hz frequency range. The noise signal spectrum lies approximately a factor of 3 below the LIGO design spectrum at 1 Hz (not including the sqrt(2) factor). The noise spectrum falls as approximately f^5/2 from 0.1 to 10 Hz and then flattens at higher frequencies. This flattening is believed to be due to the sequential sampling of the six input channels of the digitizer, which results in an increasing phase difference at frequencies approaching the Nyquist frequency.

Figures 3-7 and 3-8 show the same spectra taken for the "north" and "east" horizontal channels. Practically all of the comments made about the vertical channel also apply to the two horizontals, but the horizontal noise is essentially a factor of two lower than the vertical at frequencies below 10 Hz (along the portion with the f^5/2 fall off).

In addition to comparing the two identical seismometers, the CMG-40T #4160, used for all measurements at the LIGO sites, was also operated in parallel with the CMG-3T that was used to make the measurements at the Moses Lake aircraft hangar. The CMG-3T is reported to be approximately a factor of 10 quieter than the CMG-40T at frequencies below 30 Hz.

Figures 3-9, 3-10, and 3-11 compare the spectra for an hour period on the vertical, north, and east channels (note the amplitude scale is shifted from the previous figures). At frequencies above 20 Hz, it is not apparent that the high frequency noise is any lower for the CMG-3T sensor than for the CMG-40T. But around 1 Hz, the CMG-40 vertical noise spectrum is observably higher than the CMG-3T vertical noise spectrum, confirming the result obtained by the inter-comparison of two CMG-40 signals and differences. This effect is significantly reduced on the two horizontal noise comparisons, being somewhat more apparent on the "east" channel.

3.3 Amplifier and Digitizer Noise

Figure 3-12 provides a comparison of the CMG-40T signal difference spectra for all three channels and an estimate of the noise generated by the Reftek amplifier and digitizer (lowest curve). The two horizontal signal difference spectra are offset by factors of 10 for clarity. The vertical noise spectrum is approximately a factor of two higher than those of the horizontals to nearly 10 Hz, as observed previously. The lowest curve is a spectrum estimated from a simulated white noise signal with a r.m.s. amplitude corresponding to 1 count on the digitizer. (The evenly-spaced spikes in this spectrum are an artifact of the random number generator, as using different seeds changed their position). At the gain actually used in making the LIGO site measurements, this corresponds to 0.89 microvolts r.m.s. Actual tests by Reftek indicate that at this gain, the noise is approximately 1.2 uV, so that the noise plotted here should be increased nominally 30%. Actual quantization noise

due to rounding (a signal with a uniform distribution between -0.5 and +0.5 counts) was also checked and is found to be a factor of 1/sqrt(12) below the plotted estimate, in agreement with theory. This figure shows that the seismometer noise signal is well resolved by the Reftek system at the gain used, but the margin was quite small at frequencies near 10 Hz.

3.4 Coupling

Returning to the high frequency noise difference spectra in Figure 3-12, there a large increase in the noise signals for the two horizontal sensors at frequencies between 70 and 80 Hz. A second peak at approximately 90 Hz is also observed. These are attributed to an amplification of the actual noise by a rocking oscillation of the seismometers, termed a "coupling" problem. The effect is much smaller for the vertical channel (not offset in this plot). The coupling problem will also appear in the actual LIGO data, although this is ultimately found to be worse in the sandy soil compared to the hard concrete surface at the Nike missile bunker.

4.0 Description of Noise Measurements

4.1 LIGO Site Installation Description

Measurement Period and Timing of Seismic Data. Seismic data were recorded at the LIGO site from November 23 through December 14, 1994. Data were taken at the Northwest End from November 23 to December 1, which included the Thanksgiving Holiday weekend (November 24, Thursday to November 27, Sunday). Data were taken from Thursday, December 1 to Wednesday, December 7 at the Southwest End and from December 7 to Wednesday, December 14 at the Corner. This resulted in obtaining at least two week-end and three work-week days of recording at each site.

Sunday	Monday	Tuesday	Wednesday	Thursday	Friday	Saturday
			327 (11/23) NW End	328 (11/24) NW End	329 (11/25) NW End	330 (11/26) NW End
331 (11/27) NW End	332 (11/28) NW End	333 (11/29) NW End	334 (11/30) NW End	335 (12/01) NW End	336 (12/02) SW End	337 (12//03) SW End
338 (12//04) SW End	339 (12//05) SW End	340 (12//06) SW End	341 (12//07) SW End	342 (12//08) Corner	343 (12//09) Corner	344 (12//10) Corner
345 (12//11) Corner	346 (12//12) Corner	347 (12//13) Corner	348 (12//14) Corner			

The measurements were conducted during the period of active grading, graveling, and packing of the site, and although this presented the opportunity to evaluate the effects of nearby construction activity, it prevented obtaining representative data during the daytime

hours of the work-week. It also prevented operation of the system at the exact location of the planned location of the Corner and End Stations.

Time was synchronized to Greenwich Meridian Time (GMT) and day of year (termed "Day" in this report) using the GPS receiver. It is important to reference these times to local time and to the day of the week. GMT is 8 hours advanced from Pacific Standard Time (PST). Therefore, 4 p.m. PST on Wednesday, November 23 (when the first measurements were made) represents the beginning of Day 328 in GMT.

Measurement Locations. A relatively flat location within approximately 200 m of the center of the LIGO arms was selected which approximated the condition of the graded arms. These sites were as close as possible to the edge of the graded area.

One of the auxiliary outputs of the GPS clock used to synchronize time to GMT was the latitude and longitude of the site. The locations determined by JUB Engineers, Inc. for the LIGO site are shown below to an approximate precision of 10 m. The distance and azimuth between the corner and the end stations were calculated to be within 20 m of the 4 km length specified, and the azimuths of the two arms were within 0.1 degrees of being perpendicular.

Location Name	Latitude	Longitude	Distance	Azimuth
LIGO Corner	46.4551	119.4077	-	-
LIGO Northwest End	46.4842	119.4383	3.993	324.00
LIGO Southwest End	46.4340	119.4496	3.983	233.89

The table below gives the locations where the seismic measurements were taken, and the distances and azimuths to the corresponding sites of the LIGO construction. These locations are mapped in Figure 4-1.

Seismometer Station Location Name	Latitude	Longitude	Distance From LIGO	Azimuth From LIGO
LIGO Corner Seismic	46.4534	119.4059	0.243	143.65
LIGO Northwest Seismic	46.4837	119.4369	0.121	116.73
LIGO Southwest Seismic	46.4358	119.4507	0.219	337.48

Equipment Installation. Figures 4-2 to 4-6 illustrate stages of the installation process. A 55-gallon drum (approximate dimensions 4' high and 2.5' in diameter) with an open bottom and a removable lid was emplaced in a hole dug in the sandy soil so that the top of the drum was just exposed to the surface. This housed batteries and the Reftek data acquisition system and disk.

A second drum was cut to 3' length and emplaced approximately 1' below grade in a second hole approximately 15' from the first (this was limited by the length of the provided cable). A cement paving stone approximately 1.5' in diameter was leveled in the sand exposed at the bottom of this drum, and the seismometer was set on the paving stone and oriented using a compass to an estimated precision of 2 degrees.

The orientation of the LIGO facility was measured from a map that indicated the orientation of the LIGO arms were 22 degrees counter-clockwise from the principal directions. The actual orientation of the arms is given in the table above, 36 degrees counter-clockwise from the principal directions. Therefore, the measurements reported here are not parallel and perpendicular to the LIGO arms, but are rotated by approximately 14 degrees clockwise from the actual orientation of the LIGO arms. It may be important in future analyses to note that no adjustment for this difference has been made to the data.

The seismometer cable was buried in the sand at the bottom of the drum and was fed to the data acquisition system through holes cut in the sides of the drums and along a shallow trench dug between the two drums. The seismometer barrel was covered to grade to dampen acoustic noise and the trench was filled to prevent damage to the cable from rodents.

Data recording setup. As described in the previous section on system calibration and noise, all measurements were made at a gain of 128 at a sample rate of 250 samples/s. This gain level represented a compromise between recording higher noise levels and the resolution of lower noise levels at high frequency. As described in the seismometer noise section, the seismometer noise is approximately 6 to 8 times lower than the LIGO design spectrum at 1 Hz. Otherwise, the noise at the LIGO site is observed to be significantly greater than system noise from 0.1 to nearly 40 Hz. Above 40 Hz, the recorded noise is often comparable to the system noise, and is subject to coupling resonances especially on the horizontal channels.

The disk was connected to the switched power connection of the data acquisition system, so that the disk drive only consumed power when data was dumped from memory to disk. The vibration caused by the disk drive operating is frequently observable in the seismic data at 90Hz, at intervals of approximately 880 seconds (the time it takes to fill approximately 70% of the 2.5 Mb of memory). Approximately 175 Mb of data were collected each day on the combined 4 channels (including the infrasound channel), which filled the 1 Gb disk drives roughly every 5 days.

Infrasound measurements. Infrasound data was recorded in parallel with the seismometer signals. Initially, the microphone was set on the ground surface, but even moderate winds blowing past the microphone aperture created too much noise. On November 28, the installation of the microphone was modified to an emplacement in a shallow pit covered by two furnace filters and a 4'x4' pegboard panel (the pegboard has 1/4" holes at 2" spacing in it). This was found to give sufficient isolation from the wind, and is not thought to affect the amplitude of the low-frequency pressure fluctuations. This installation method was used for the rest of the recording period at all three sites, although the acous-

tic system power was accidentally disconnected from December 7 to 12 while located at the Corner.

Wind measurements. Wind speed and direction data were collected from November 28 (after the Thanksgiving Holiday) to the last day of seismic data collection. The assembly has a cup anemometer and a wind vane at each end of a 1-m arm. This assembly was mounted at the top of a rigid tripod assembly approximately 2.5 m high. The orientation of the wind vane was checked by compass and the data logger's time synchronized to within approximately 5 s of the time base of the Reftek seismic recorder.

Wind speed and direction data were obtained from an existing weather station located 7 km South of the Corner for the complete time period, but observed differences between these records and the on-site measurements indicated these data could only be used as a general indication of wind conditions for the period over Thanksgiving Holiday prior to the beginning of on-site wind measurements. Plots of wind speed measurements at the three LIGO sites and at Horn Rapids are included in Appendix H.

Video documentation of anthropogenic noise sources. A videotape recorder was operated on several occasions to record the visible activities that could affect the noise at the measurement sites. In addition, narration by the video camera operator allowed for notations of activities not in the camera view, and for audible detection/description/location of other effects, such as aircraft, hums, wind speed and direction fluctuations

Video tapes of construction activity were made to document the effect of construction activities at various distances from the recording sites. Preliminary measurements were made on November 18 and 21 at temporary sites near the construction activity. Only the second provided useful data. Another time period was videotaped when construction activity was limited to the Corner and Southwest Arm and the system was operating at the Northwest End 4 km distant.

Video tapes of periods of heavy and light traffic were made at the three sites. The Northwest End is approximately 2.3 km from Route 4 South. The Southwest End is approximately 1.9 km from Highway 240, and the Corner is approximately 0.6 km from Route 10. High winds obscured any possible effect at the Northwest End. The effect of individual vehicles was detectable only at the Corner.

The video tapes were reviewed and an annotated description of the observations was written. The annotations and video tapes are included in the Video Data Package.

Data selected for analysis. The data were plotted for each day and each seismic component. These plots were used primarily to make a selection of data that was not affected by the construction activities. These plots are included as Appendix A.

In order to obtain a 24-hour long sample, the period of 4 p.m. Saturday to 4 p.m. Sunday was selected for analysis, corresponding to Day 331, 338, and 345, GMT times 00:00 - 24:00. This provides a 24 hour sample at the Northwest End, Southwest End, and Corner, respectively. Also, the time period from 6 a.m. to 7 a.m. was selected to represent the day-to-day variation in noise levels, because the LIGO construction workers did not arrive

until after 7 a.m. with the exception of Days 342 and 343. This hour-long period also includes the period of time that morning traffic is heavy past all three sites, and provides information on the day-to-day variation of microseismic noise in the 0.1 to 1 Hz frequency range.

In addition to the above time slices through the data, selections of data for analysis were made to examine the effect of anthropogenic and wind speed effects on the seismic data. These special analyses are presented as descriptions of the individual phenomena. Because many of the noise phenomena that will be observed during the 3 24-hour periods and the 6 a.m.to 7 a.m. periods selected, it may be preferable to read Section 8 prior to viewing the large number of spectrograms, spectra, and histograms in the Appendices.

5.0 Spectrograms

Acceleration and Infrasound Spectrograms. Spectrograms were produced for the vertical channel of the seismic signals for the same periods that were used to calculate the 24-hour spectra and histograms (Sections 6 and 7, below), as a means of identifying the sources of the noise signals. The spectrograms were constructed by calculating the amplitude spectrum of 720 sequential 5-second segments of a one-hour time series (900,000 points). The time series data had previously been differentiated to acceleration to flatten the spectrum between 5 to 100 Hz (this also makes the scaling parallel to the LIGO design spectrum in the range 10 to 100 Hz).The display of a spectrogram consists of arranging each spectrum (one from each 5 s of data) into a sequential table, so that the table entries correspond to the spectral amplitude at each frequency as a function of time. This table or matrix of amplitudes can then be color-coded, gray-scaled, or contoured to produce a quantitative representation of the time-frequency patterns of spectral amplitude variations. Better results were obtained by developing the following alternative method of display. The range of the spectral amplitudes was first reduced by taking the square-root of the amplitudes, so that linear contouring (e.g. contours at 1, 2, 3... amplitude units) of these transformed values would correspond to an exponential contouring (contours at 1, 4, 9... amplitude units). (Logarithmic contouring is perhaps a more logical transformation, but produced a display that was too cluttered.) By using a relatively large number of contours, the contour display begins to mimic a gray-scale plot because the density of the contours darkens the display when the spectral amplitudes change rapidly. All of the spectrograms have the same range and number of contours, and in some spectrograms, the range of contours is exceeded by the data, leaving a "hole" in the center of a densely-contoured part of these diagrams. Examples of acceleration spectrograms are shown in Figures 5-1 and 5-2. Spectrograms were also calculated in the same way for the infrasound signals for one 24-hour period (Day 338). The range of contour values for the infrasound spectrograms was selected to obtain a similar image compared to the vertical acceleration spectrograms. Examples of the acoustic spectrograms and the phenomena they exhibit are shown in Figures 5-3 and 5-4. The 24-hour spectrograms are included in Appendix B.

A set of spectrograms was also constructed from the data sampled from 6 a.m. to 7 a.m. daily. The spectrograms for the 6 a.m.to 7 a.m. period clearly show the effect of traffic at the Corner on work-week days and will be described in the section on traffic noise below.

Displacement spectrograms. In addition to the acceleration spectrograms, a set of displacement spectrograms was generated for a subset of data decimated to a sampling rate of 25 samples/s, to highlight the noise phenomena below 10 Hz. The displacement spectrograms are now scaled parallel the LIGO design spectrum between 1 and 10 Hz. The window length for these displacement spectrograms was 30 seconds (to get finer spectral resolution) and the window was again shifted 5 seconds each frame. The square root of the amplitudes was again taken and the contour plot generated at fixed levels for this set of plots. This maintains the same scale for the 1 to 12.5 Hz displacement spectrograms.

The reasons for calculating the displacement spectrograms was to investigate the temporal variation of the multiple spectral peaks that are observed in the spectra at the Corner site on Day 345 (see below), and to enhance the presentation of 6 a.m.to 7 a.m. traffic noise, at frequencies below 10 Hz which were not well-represented in the acceleration spectrograms. Figure 5-5 shows an example displacement spectrogram to illustrate the low frequency line spectra at the Corner. The set of displacement spectrograms illustrate systematic temporal variations in most of the line spectra, and the effect of traffic below 10 Hz can be observed. The displacement spectrograms for Day 345 are included in Appendix B.

Additional Spectrograms. Acceleration spectrograms were also used to analyze specific time periods when videotaping potential noise sources, such as construction activity and highway traffic. These observations provide correlative information about visible and audible phenomena and the noise signals. In addition, the spectrograms were also useful in evaluating the effect of wind speed as determined by the meteorological instruments. The spectrograms for these special periods of analysis are included as separate appendices to be described later.

6.0 Hourly Spectra

Amplitude spectra were prepared from one-hour segments of data for a 24-hour period at each of the three sites. Spectra were also prepared for the 6 a.m.to 7 a.m. time period for each day of recording unaffected by on-site construction/vehicle activity (excludes Day 342 and 343). The hourly plots for the three days (331,338, and 345) correspond to GMT hours 00 to 23, which is 4 p.m. Saturday to 4 p.m. Sunday at each of the three sites. Examples of the spectra for three one-hour periods are shown in Figures 6-1 to 6-5. Spectra of all three components are shown for the first time period. The spectra are in units of log-amplitude spectral density; they equal one-half the log-power spectral density. The 24-hour spectra are included in Appendix C.

The spectral plots for each day include periods when there were vehicles on site; these time periods include Day 331, Hours 03 and 23;Day 338, Hours 21 and 22, and Day 345, Hours 20 and 21. The spectra for these time periods are not representative of ambient conditions, because five of the six disturbed time periods were caused by data collection activities at the sites.

Spectra were also calculated for the microphone data to assist in identifying atmosphere-coupled versus earth-coupled noise. Seismic and acoustic spectra are included in Appendix F for the 6 a.m. to 7 a.m. hour periods, and are later used in special studies of various noise phenomena.

The amplitude spectra were calculated by averaging 39 180-s windows that overlapped the adjacent windows by 90 s. A 50% cosine taper was applied to each of the windows so that the effect of the overlap is practically compensated, and the windows have an effective length of approximately 90 s. Each window was first de-meaned prior to tapering, and scaled by the appropriate velocity transducer constant. The FFT was then taken of each window, and the result divided by 2*pi*f to obtain a displacement spectrum, and squared to produce a power spectrum. Corrections for the window length and taper were made, and the results saved to temporary files. Averaging is done in two ways: the simple mean of the power spectra is calculated frequency-by-frequency, and the mean of the logarithm of the power spectrum is similarly calculated. Claiming that the distribution of the power spectra is nearly log-normal, the latter provides a robust central estimate that should be close to the median of the distribution. The mean power spectrum is equivalent to the mean-squared amplitude spectrum. The spectra are presented on a log displacement amplitude scale. Therefore, the "median" estimate represents the median amplitude spectrum of a log-normal distribution of amplitude spectra, and the "mean" estimate represents the r.m.s. amplitude spectra.

The r.m.s. amplitude spectra are obviously affected by outliers, especially evident in the hours mentioned above that vehicles were operating at the site. A comparison of the individual amplitude spectra to the r.m.s amplitude spectrum indicates that the r.m.s spectra are exceeded by 1 to 3 of the individual spectra, suggesting an approximate interpretation as the 97th to 90th percentile (respectively) of the distribution of the 39 total spectra. The 90th-percentile approximation generally applies to those instances when the difference between mean and median is small, and the 97th-percentile approximation generally applies to those instances when the difference between mean and median is large (e.g., when a vehicle passed near the site creating the outlying spectra).

It is apparent in practically all of the spectral plots that the poor coupling of the seismometer to the sand is making the measurements inaccurate above 40 Hz, especially for the two horizontal components. The apparent amplification of noise now covers a wider range than was observed when the instruments were calibrated/compared on a solid concrete floor. When the noise levels above 40 Hz approach the 10^{-12} level (the lowest level shown in these spectra), the noise is actually approaching the noise floor of the seismometer as indicated by the seismometer difference spectra. Because of the coupling problem and the limited noise resolution at high frequency, the spectra have not been corrected for the amplitude roll-off of the seismometers' response, which would merely amplify these effects. The raw (uncorrected) spectra are accurate to within 10% for all frequencies between 0.1 and 30 Hz. At 50 Hz, the seismometer response is attenuated by 30%, but most spectra have reached the noise floor of the seismometer in this frequency range.

7.0 Hourly Histograms

Histograms of the signal amplitudes were prepared from one-hour segments of data for a 24-hour period at each of the three sites, excluding segments that were affected by vehicles travelling directly past the site (two segments for each of the sites). Histograms were also prepared for the 6 a.m.to 7 a.m. time period each day of recording unaffected by on-site construction/vehicle activity (excluding Days 342 and 343). The histograms for the three 24-hour periods and the daily 6 a.m.to 7 a.m. periods are included in Appendix D. Examples of the histograms are shown in Figures 7-6 and 7-7.

The histograms are derived from a set of band-pass filters that isolate the motions in the frequency bands 0.5-1 Hz, 1-2 Hz, 2-4 Hz, 4-8 Hz, and 8-16 Hz. The data were first filtered and decimated to 50 samples/s with the same anti-alias filter as is applied by the Reftek recorder. This filtering maintains the full signal amplitude to a frequency of 40 Hz. The data were then demeaned, a taper applied to the 0.36 seconds of the beginning and ending of the data (2/10,000 of the data was affected), and a high-pass, 8-pole Butterworth filter was applied at 0.5 Hz. The stronger filtering below 0.5 Hz was needed to reduce the rising amplitude of the low-frequency microseism noise. These time series were corrected by the appropriate velocity-transducer constants and integrated to produce displacement time series. A set of 4-pole Butterworth band-pass filters was then applied at the above frequency limits to produce separate displacement time series for each band (only a low-pass was needed for the lowest frequency band, having already applied the 8-pole high-pass at 0.5 Hz). The spectral amplitudes are reduced 3 dB (to 70%) at the upper and lower band limits by the Butterworth filters. The spectral effects of the different filters on an example signal are shown in Figures 7.1 to 7.5. The band-passed time series were then segmented into short time samples that corresponded to a single cycle of the lowest frequency represented in each band. This results in the time sampling shown below for each one-hour period.

Frequency Band (Hz)	Sample Length (s)	Number of Samples
0.5 - 1	2	1800
1 - 2	1	3600
2 - 4	0.5	7200
4 - 8	0.24	15000
8 - 16	0.12	30000

The r.m.s. amplitude was calculated in each sample, and a cumulative histogram of the number of times r.m.s. ground displacements exceeded levels spaced at logarithmic intervals of 0.05 units were calculated. See Figures 7-6 and 7-7 for examples of the histograms.

8.0 Special Studies of Noise Phenomena

8.1 Highway Traffic

Traffic on nearby highways was documented for several periods of time on video tape. Three segments of noise data taken during video documentation have been analyzed. One weekend period was videotaped along Highway 240 at its nearest location to the South-west End. The highway is approximately 1.9 km from the measurement site or the South-west End. A second period that was analyzed was also a weekend period at the Corner when traffic was so low that the video camera was left recording while a vehicle was driven back and forth on Route 10 past the LIGO entrance. These two periods of time occurred during the days selected for 24-hour analysis (Day 338, 20:30-21:20 GMT, and Day 345, 21:00-22:00 GMT, respectively, corresponding to 12:30-1:30 p.m. and 1-2 p.m. PST). A third period intermittently recorded evening rush hour on Day 347, 22:00 to Day 348, 01:00 (2-5 p.m. PST Tuesday, December 13), also at the Corner. The spectrograms, spectra, and histograms for these special analyses are included in Appendix E. A log of the video-taped activities in included as Appendix J.

The analysis of these data assisted in the identification of a number of phenomena in addition to traffic that were apparent on the spectrograms, and also led to the analysis of the 6 a.m. to 7 a.m. hourly spectra during morning rush hour. No rush hour videotaping was successfully made at either End site (due to high winds), but the traffic is heavy on all the nearby roads during morning rush hour. The spectrograms, spectra, and histograms for the 6 a.m. to 7 a.m. hour are included in Appendix F.

Highway 240 weekend video period. The vertical channel acceleration spectrogram for this period, during which the video camera was documenting traffic passing by the LIGO Southwest End, is used to select the segments for this analysis. The video-taped portion includes only the first 2320 seconds of the hour shown in Figure 8.1.1. Traffic was limited to one to 3 cars, pickups, or passenger vans at a time, passing at intervals of 1 to 3 minutes, nominally at speeds from 55 to 65 m.p.h. There was no observable effect of vehicle traffic at this site. The time period after 3000 seconds is affected by a vehicle being operated near the seismometer location. These data are not analyzed further for measurement of traffic effects, but other features of the high-frequency noise spectrum are evident here.

The principal phenomenon of interest in this data was the video camera microphone, the seismometers, and acoustic microphone all recorded the sound of a propeller-type airplane. For approximately 20 seconds at a time 300 s from the start of the spectrogram, the spectrogram shows a prominent "glide tone" at frequencies ranging from near 100 Hz to 50 Hz that reflects the Doppler shift as the plane flew past the site. This was the only such event detected on the video camera microphone during this period, but it is apparent that there were several other similar signals of lower strength during the first 2320 s when the video camera was recording.

A spectrogram of the acoustic channel of the infrasound microphone (Figure 8.1-2) shows the same pattern of "glide tones", but there is no observable effect of the vehicle operating

near the site in the last 600 seconds, demonstrating that traffic/vehicle noise is not dominantly transmitted acoustically to the site.

Route 10 weekend video period. The vertical channel acceleration spectrogram (Figure 8.1-3) for the period that the video camera was documenting traffic passing by the LIGO Corner is used to select the segments for this analysis. The video-taped portion begins 1280 s into the spectrogram and ends at 3000 s. Prior to 1280 s, movement of a single person collecting data from the nearby wind speed site creates impulsive, broad-band noise.

At 1320 s, a small propeller plane flew overhead, and at 2340 s, a jet plane was heard on the video camera microphone; these again correspond to two of the largest "glide tones" noticed in the previous section.

During the period 1650 s to 2940 s, a "Suburban" truck/van was driven away from the measurement site and made 9 passes on Route 10 past the entrance to the LIGO site that are clearly visible on the spectrogram. Afterwards, the vehicle was left running for a period before beginning final departure at 3240 s. In addition to the Suburban, a car passed by the site at 2040 s just prior to pass #3, and a van passed at 2760 s at the same time as pass #9; the former extending the duration of the apparent signal and the latter increasing the amplitude of the Suburban's signal slightly. For comparison, a patrol car passed the site prior to this experiment at 1280 s that is barely visible.

It is also apparent on the spectrogram that there is a band of noise below 10 Hz that is increasing in amplitude and to a slight degree in frequency that begins to interfere with the later passes of the Suburban.

Spectra and histograms for this period are calculated for 3 overlapping segments of data, each 360 s long. These cover the nine passes of the Suburban, 3 complete passes in each segment, but the central segment overlaps the first and last by 60 s each. Spectra and histograms are also calculated for a 360 s period from 1280-1640 s, prior to the Suburban passes, that included a single, smaller car passing during the entire period. Spectra are calculated from 39 overlapping windows each with a 50% taper resulting in an effective window length of 9 s. This analysis is identical to the hour-long spectra described earlier, with all time lengths scaled by 1/10.

The complete set of spectra and histograms for all components are included in Appendix E. Figures 8.1-4 and 8.1-5 compare spectra of the vertical channel from the 360-s period including the single car and the 360-s period containing the first three passes of the Suburban truck.

A very slight effect is observed by comparing the spectra from the single-car spectrum (segment 0) to the three-car spectra (segments 1-3), and only in the frequency range of 12 to 16 Hz. This effect can be observed by comparison of Figures 8.1-4 and 8.1-5 for the vertical channel. The main area where the LIGO design spectrum is exceeded is between 5 and 9 Hz and is unrelated to vehicle movement, as evidenced on the spectrogram for this time period Figure 8.1-3). The cause of this relatively wide-band noise is not identified.

Histograms of band-passed signals were also prepared for these same four segments and are shown in Appendix E. The effect of single vehicles is observable in the 8-16 Hz band. The time series for the 9 passes of the Suburban was band-pass filtered in a 12-16 Hz band, for comparison to the 8-16 Hz band-pass signals (see Appendix E). The 12-16 Hz band-pass signal shows the effect of the vehicle more clearly than the 8-16 Hz band-pass signal used for the histograms, as indicated on two time series plots included in Appendix E.

Route 10 weekday afternoon rush-hour video period. The vertical channel acceleration spectrograms for the period that the video camera was documenting traffic passing by the LIGO Corner (Figures 8.1-6 to 8.1-8) are used to select the segments for this analysis. Video taping documented traffic and other noise sources from 2:26 to 3:13 p.m. PST (1560 s into the 2 p.m. spectrogram to 780 s into the 3 p.m. spectrogram), and again from 3:43 to 4:30 p.m. (2580 s into the 3 p.m. spectrogram to 1800 s into the 4 p.m. spectrogram). Between these two segments, the engine of the observers' vehicle was running.

An unsuccessful attempt was made to identify individual vehicles in the noise spectrogram. What is apparent is that as rush hour intensified from a few vehicles passing every minute or so at the start of taping to a continuous stream of cars and small trucks by the time video taping was stopped at 4:30, the spectrogram indicates a significant noise increase in the frequency range of 7 to 30 Hz.

Audible aircraft were noted, including a small airplane at 2 p.m. + 2820 s, a jet airplane at 3 p.m. + 240 s, and additional small airplanes at 3 p.m. + 2580 s and + 2700 s. The first two small airplanes (propeller) are clearly evident in the spectrograms at the respective times. It is noted that there are many more of these "glide tones" during the period of heavy traffic from 4:10 to 4:30, and these others are not noted on the video tape log. As demonstrated earlier, these signals are acoustically transmitted, but the audible jet aircraft signal appears to have a different characteristic (the doppler shift is not obvious).

Data selected for calculating spectra and histograms included three continuous 360-s segments from 4:12 p.m. to 4:30 p.m. (720 to 1800 s on the 4 p.m. spectrogram). This represents a period when traffic was essentially continuous, when the observers were stationary, and where the spectrogram has few impulsive events below 40 Hz. An earlier segment, just prior to the arrival of the observers was selected from 680 to 1040 s on the 2 p.m. spectrogram, for comparison to the rush hour traffic segments.

A comparison of the noise spectra in the control segment 0 to the rush hour traffic segments 1-3 indicates that rush hour traffic increases ground noise in the frequency range from 6 to over 30 Hz. Figures 8.1-9 and 8.1-10 illustrate the effect of traffic on the vertical signal during segments 0 and 1, respectively. The effect is strongest just above 10 Hz, reaching levels that are up to a factor of 10 higher than the control segment. The rush hour spectra exceed the LIGO design spectrum from 6-16 Hz by approximately a factor of two for the r.m.s. spectra (the higher of the two plotted spectra). At frequencies between 2 and 5 Hz, it is observed that noise was actually higher prior to rush hour, but the cause of this is unknown and inconsistent with the observed flow of traffic. These observations apply

equally well to the other time segments and components whose spectra are included in Appendix E.

A comparison of the noise histograms in Appendix E illustrates the same conclusion. Only the 8-16 Hz band-pass signal is significantly affected; this band is normally the lowest of the five plotted, as is the case for the control segment. For the rush hour segments, this band is generally the second or third highest of the five bands.

Morning traffic 6 to 7 a.m. at all three locations. As described in a previous section, a one-hour segment of data was chosen to represent morning rush hour traffic at the Northwest end due to traffic on Route 4 South, at the Southwest end due to traffic on Highway 240, and at the Corner due to traffic on Route 10. Spectrograms, one-hour spectra, and one-hour histograms were all generated for the three components of motion for each day of data taken except Days 342 and 343 (an early arriving vehicle passed the Corner site these two days). The spectrograms, spectra, and histograms are all included in Appendix F.

Based on a comparison to the spectrograms of the video-taped sections of traffic effects, it is apparent that no significant morning-traffic effects were observed over the Thanksgiving Holiday, Days 328-331, at the Northwest End, but traffic-like effects are observable for the weekday periods at this station for Days 332-335. Note that this hour on Day 334 was windy with winds in the 10 m/s range, and the noise in this spectrogram is significantly higher in several frequency bands (wind speed effects are analyzed in a later section and wind speed measurements for the entire period are included in Appendix H). Traffic-like signals are not continuous as observed at the Corner but include a few relatively strong episodes mixed with a number of minor ones at low frequency. In addition, there are bands of continuous noise present in some of these work-week early morning periods.

The Southwest End was extremely quiet over the weekend (Days 337-338), but weekday traffic-like signals are apparent on the spectrograms for the work-week mornings, Day 336 and Days 339-341. On Friday (Day 336), wind speeds during this hour (14:00 GMT) are relatively high, around 7 m/s; the rest of the morning hour segments had wind speeds below 5 m/s. Monday, (Day 339) has a significant amount of high-frequency noise that cannot be attributed to the wind (wind speeds were below 5 m/s)

At the Corner, the spectrograms again indicate higher amplitude line spectra, even over the weekend (Days 344-345), and several vehicle-like signals per hour. The work-week samples (Days 346, 347 and 348) are quite similar to the evening rush hour documented above at this site. Wind speeds were always below 5 m/s at this hour when the Corner station was occupied.

Low-frequency (1-12.5 Hz) displacement spectrograms were also generated for the 6 a.m. to 7 a.m. windows to provide better resolution of the temporal variation in noise below 10 Hz. These spectrograms (included in Appendix F) also reveal the effect of traffic-like signals, and also reveal the continuous vs. intermittent line noise sources at these frequencies.

Acoustic pressure spectra were also calculated for the 6 a.m. to 7 a.m. period. These spectra can be compared to the seismic spectra for the corresponding times, all are included in

Appendix F. The line spectra are clearly evident on the acoustic pressure signals, as well as the effect of wind. Although wind speeds were measured to be relatively low on Day 339, the microphone signals appear similar to those taken during a windier period (e.g. Day 336). Some of the quietest acoustic measurements are observed for the low-wind period of operation (Days 348-349, the microphone was disconnected for the earlier days) at the Corner.

The largest effect of traffic is observed at the Corner, which is closest to any of the heavily-travelled roads in the area. The Northwest End is 2.3 km from Route 4 South, the Southwest end is 1.9 km from Highway 240, and the Corner is 0.6 km from Route 10. Figures 8.1-11 to 8.1-13 show the spectra at the Corner for the three components of motion for the 6 a.m. to 7 a.m. period on Day 347, when wind speeds were below 2 m/s. Figure 8.1-14 shows the spectra for the acoustic pressure signal, illustrating the set of high-amplitude line spectra common to the seismic channels. The low-frequency "microbarom" spectral peak that is analogous to the "microseism" peak in the seismic signals at frequencies near 0.15 Hz is particularly well-resolved in this example.

8.2 Construction Activity

Construction activity was documented for several periods of time on video tape. Two segments of noise data taken during video documentation have been analyzed. The first was at a temporary site approximately 300 m from a rock-laying operation involving two front-end loaders and a backhoe. The second was when multiple front-end loaders, a backhoe, dump trucks, and a vibrating packer were operating near the Corner while seismic measurements were being made at the Northwest End. Spectrograms, spectra, and histograms are included in Appendix G. The video tape logs are included in Appendix J.

Four short segments of data, each 360 s long, were selected from each of the two periods. Spectrograms were scaled independently to illustrate the principal phenomena. Spectra were calculated by dividing these into 39 overlapping, tapered windows in the exact same manner as the hourly spectra, but with all time lengths now scaled by 1/10. Thus the effective length of the windows is now 9 s. Similarly, the histograms were normalized to the appropriate number of samples available in these 360-s segments, keeping the window lengths for the calculation of r.m.s. amplitude the same as previously done for the one-hour histograms. The histograms for these segments are again scaled in exactly the same way as the hourly histograms, but the scale has been shifted one unit larger to accommodate the construction noise.

Noise at 300 m. The four segments selected were from 1100-1460 s, 1500-1860 s, 2240-2600 s, and 2800-3160s as measured on the corresponding spectrogram in Appendix G. The large event at the beginning of the spectrogram is the last dump truck to leave the site at the end of the day. Pickup trucks travelled past the site at 2100, 2650, 3300, and 3350 s. The second window includes a line in the spectrogram at approximately 28 Hz.

The spectra for the four segments are all approximately a factor of 10 above the LIGO design spectrum from 1 Hz to 30 Hz for all three components. It appears that the construction activity has increased the noise out to above 30 Hz relative to the quiet periods ana-

lyzed hour-by-hour. But the noise at 1 Hz and below does not appear to be significantly affected by the activity. Figures 8.2-1 to 8.2-3 show examples of the spectra from the first noise segment analyzed for the three components of motion recorded at the temporary site.

Noise at 4 km. The four segments selected were from 600-960, 960-1320, 2340-2700, and 2700-3060 s as measured on the corresponding spectrogram in Appendix G. During this period of time, several additional phenomena were occurring, including air shocks from the anti-tank weapons at the Yakima Training Center, which appear as the short-duration 5-35 Hz signals. There is also an intermittent narrow line spectrum at approximately 13 Hz and a somewhat wider one at approximately 26 Hz. Also, there are two prominent glide tones at high frequency, the first at around 800 s, and a second, multiple-sweep one at around 3100 s. The videotaped segment extends from 540 to 2700 s on the spectrogram, but there was no note of the first glide tone being correlated with an audible aircraft. The first three segments all include one of the Yakima Training Center acoustic signals. The fourth segment was included as a check on the influence of these interfering signals, but was just after the video taping was turned off.

The spectra measured for these four noise segments show that the construction activities 4 km distant significantly increase the noise in the 1 - 10 Hz range. Figures 8.2-4 to 8.2-6 show examples of the spectra for the three components measured during Segment 2 at the Northwest End. During the construction 4 km distant, the spectra are a factor of 3 or more larger than the LIGO design spectrum in this frequency range for the horizontal components. The vertical component noise spectrum also exceeds the design spectrum, but to a lesser degree and for a narrower frequency band.

8.3 Wind Speed

Interpretation of some of the morning traffic spectra above has mentioned some of the wind measurements as a means of explaining noise periods inconsistent with a simple correlation with nearby highway traffic. This section analyzes the effect of wind speed on the measurements in a more controlled way. The wind speed data in Appendix H was examined for periods of time when the wind speed varied significantly during late evening and early morning hours. The two periods selected were from 06:00 to 14:00 GMT (10 p.m. to 6 a.m. PST) on Day 335 at the Northwest End site, and from 03:00 to 11:00 GMT (7 p.m. to 3 a.m. PST) on Day 343 at the Corner site.

Two segments of data recorded at each of these two sites with low mean wind speeds (approximately 1-2 m/s) were selected for spectral analysis. Two additional segments of data from each site during periods of moderate winds (approximately 6-8 m/s) were also selected. Two additional periods of data during high winds (10 m/s and greater) at the Corner (Day 343) were selected for comparison to the moderate-wind segments. The segments were 360 s long and the calculation of spectra is exactly the same as conducted for traffic and construction noise.Wind speed plots, spectrograms, and spectra are included in Appendix H for these two time periods.

Description of wind noise, Day 335, 06:00 to 14:00 GMT. Wind speeds increase from approximately 5 m/s to 10 m/s within the first hour of this period, and then drop rapidly just prior to 9:00. A comparison of the hourly spectrograms and hourly plots of wind speed (Appendix H) for the first several hours of this period shows a strong correlation of wind speed and noise amplitudes. When mean wind speeds increase to approximately 5 m/s, a narrow band of noise becomes visible between 26-28 Hz, and a second narrow band between 75-80 Hz becomes visible as mean wind speed increases above approximately 7 m/s. Further increases in mean wind speed (up to 10 m/s) tend to broaden the detectable noise around these two frequencies. The lower-frequency noise band tends to extend to lower frequencies as wind speeds increase.

Figure 8.3-1 shows the one-minute mean and one-minute peak wind speed at the Northwest End for a one hour period of moderate winds.The spectrogram for this hour, shown in Figure 8.3-2, gives an example of the seismic noise correlation with wind speed. A later period of low wind speed and the corresponding spectrogram are shown in Figures 8.3-3 and 8.3-4. (Note that these spectrograms also include aircraft noise and artillery noise bursts). Figures 8.3-5 and 8.3-6 show the spectra for the vertical channel for two 6-minute samples from these two hours, illustrating the change in noise spectra due to moderate wind. Similar effects for the other components and analysis segments are observed in the set of plots in Appendix H.

Description of wind noise, Day 343, 03:00 to 11:00 GMT. Wind speeds during this period increase rapidly from 2 m/s to above 10 m/s within the first hour, and then gradually decrease to very low speeds. The spectrograms (Appendix H) show the noise band between 26-28 Hz is observed again at this site, but a wide band from 55-65 Hz is observed at mean wind speeds above approximately 7 m/s. This band of noise also appears to have three peaks within it at approximately 55, 60, and 65 Hz. Another very broad band of noise between 80 and 110 Hz also appears when mean wind speeds exceed approximately 7 m/s. These three band broaden significantly and merge with one another when mean wind speeds exceed 9-10 m/s.

Figure 8.3-7 shows the wind speed measured at the Corner for a period of high wind, and Figure 8.3-8 shows how the rapid increase in wind speed affects the noise as represented by a spectrogram. Figures 8.3-9 and 8.3-10 show a later time period with low wind speed. (Note that the low-wind spectrogram in Figure 8.3-10 is dominated by a few aircraft and the periodic noise of the recorder's disk drive.). Figures 8.3-11 and 8.3-12 show the spectra for a 6-minute sample at high and low wind speeds, respectively. The high wind spectrum shows that winds increase the noise signal across a broad frequency range.

The high-frequency spectral peaks excited by the wind at the Corner in Figure 8.3-11 are somewhat different than those observed at the Northwest End (see Figure 8.3-5), and are probably related to subtle differences in the installation and coupling of the seismometer. Moderate winds seem to have a greater effect at the Corner compared to the Northwest End. Moderate winds (6-8 m/s) appear to generate noise at the Corner that slightly exceeds the LIGO design spectrum, but lower noise is observed at the Northwest End for similar wind speeds. Higher wind speeds observed at the Corner (over 10 m/s) do not appear to generate significantly higher seismic noise compared to moderate wind speed at

this site. Wind-generated noise exceeds the ambient noise conditions at these sites at frequencies higher than 4-5 Hz.

8.4 Acoustic Phenomena

Line spectra. Line spectra are represented by very narrow peaks in the sets of 24-hour spectral plots, and their short-term temporal variability is evident on the 24-hour spectrograms of the vertical channels and acoustic channel. There is a set of narrow spectral peaks at multiples of approximately 18.5 Hz (18.5, 37, 55.5, 74, 92.5, and even 111 Hz), and less frequently a second set at approximately 23, 46, 69, and (again) 92 Hz. Line spectra are least prominent at the Northwest End (Day 331), and most prominent at the Southwest End (Day 338) and Corner (Day 345). A set of spectrograms for the Southwest End was generated for the acoustic channel, for comparison to those from the vertical seismic channel. Although the scales are different, these spectrograms indicate that acoustic transmission of these low-frequency sound waves into the near-surface soil is fairly efficient. The amplitudes vary temporally, suggesting that the source of this noise varies with time, or that the meteorological conditions change. It is unlikely that the temperature profile changes rapidly, and there is no obvious diurnal dependence. A cursory examination of wind speed and direction changes being correlated with changes in the amplitude of the acoustic noise was negative. Figure 8.4-1 shows an example where one of the two line sets described above persists while another disappears. An obvious example of the source changes is found on the acoustic spectrogram in Figure 8.4-2, when the line spectra waver in parallel, then disappear. It is not known which of the surrounding facilities are the sources for these acoustic signals.

Aircraft "Glide Tones". Numerous signals were observed on the spectrograms that are identified as aircraft acoustic signals (see Figure 8.4-1 and 8.4-2 for examples). These narrow-band signals evolve with time from a high frequency (100 Hz and above) to a lower frequency (as low as 40 Hz) consistent with a Doppler shift. During several periods of video tape documentation, nearby aircraft could usually be detected by the observer or by the microphone recording on the video camera that would correlate with the strongest of these noise signals. These acoustic signals are directly correlated with the seismic signals (compare Figures 8.1-1 and 8.1-2). They appear to occur most frequently during daylight hours, but it is difficult to understand why these signals occur so frequently. This noise source can observably increase seismic noise levels at the measurement site during quiet periods, but have a relatively minor effect compared to highway traffic, and their effect is limited to high frequencies.

Yakima Training Center Activity. One of the acoustic phenomena that was recognized from regional seismic array experience was the occurrence of acoustic signals from the Yakima Training Center tank-artillery exercises within roughly 50 miles northwest of the LIGO site. These signals are characterized on the seismic spectrograms by short duration impulsive signals in the frequency band from approximately 5 Hz to over 30 Hz (see Figure 8.3-4 for example). The artillery signals were particularly evident at the Northwest End on Day 331. A comparison between the spectra and spectrograms for this day shows that the acoustic signals raise the r.m.s. hourly spectrum to the level of the LIGO design spectrum at approximately 10 hz for all three components, and generally increase the

r.m.s. spectral amplitudes at frequencies up to 30 Hz for the horizontal components. The median spectrum is affected much less by these short, transient events. Figures 8.4-3 to 8.4-5 show an example of the effect of the artillery acoustic signals on the hourly spectra at the Northwest End site.

9.0 Wind Effects on a Large Structure: Moses Lake, WA

Seismic vibration, acoustic, and wind speed measurements were made at the Japan Air Lines (JAL) aircraft hangar at the Grant County Airport in Moses Lake, WA (Figure 9-1), located approximately 90 miles north of the Hanford LIGO site, from August 25 to August 30, 1994. The JAL hangar measures 370' by 268' and is 66' high. It is constructed of riveted steel truss-work and corrugated steel siding with approximately 2" of fiber-board insulation lining the walls. It contains three concrete-block enclosures between 15 and 25 feet tall that are coupled to the roof with steel truss and concrete pillars. The JAL hangar is the last building on the flight line, so that the only buildings that could obstruct the wind are located to the west in about a 60 degree arc. The remaining 300 degrees of surrounding land is flat, level airport property.

The Grant County airport was closed for the month of August, so that activity in the area was at a minimum. However, daily activities generated significant noise and so only the late evening and early morning hours were considered for analysis. The CMG-3T seismometer was used to make these measurements, because the CMG-40T had not yet been received. Based upon the cross-calibration results comparing this CMG-3T to the CMG-40T used to make the LIGO site measurements, it is considered to be equivalent in the range 0.1-50 Hz. The seismometer was set on the concrete floor near the middle of the building with the horizontal North axis perpendicular to the long east-west dimension of the building and close to true North. The insulated 55-gallon barrel described in Section 3.2 was used to provide acoustic shielding and temperature isolation.

Data were recorded at 125 samples/s on the Reftek recorder at Moses Lake because the CMG-3T seismometer has a high-cut 50 Hz filter. The gain was set at 32, which was lower by a factor of 4 compared to the LIGO measurements or the cross-calibration. This would not be expected to affect the results because of this instrument's low noise floor.

Results. After five days of operation, wind speeds only approached 10 m/s for one half-hour period on the first night of operation. Although data were collected continuously, only the time period from 8 p.m. until 6 a.m. avoided interference from human activities. Two 360-s segments when the wind speed was in the range of 7-8 m/s were selected that avoided periodic noise in the building from mechanical sources (Hour 1, beginning 2000 and 2640 s into the hour).A comparative pair of samples was also selected when the wind speeds were in the range of 2-3 m/s (Hour 4, beginning 2540 and 3140 s into the hour). Plots of the wind speed, seismic signal spectrograms, and spectra of the segments described above are all found in Appendix I.

Figure 9-2 shows the wind speeds for one of the low-wind periods, and the corresponding spectrogram is shown in Figure 9-3. Figures 9-4 to 9-6 show the spectra for the three com-

ponents of the seismic signal. Figure 9-7 and 9-8 show the wind speed and spectrogram for a moderate wind period, and Figures 9-9 to 9-11 show the spectra for this period.

The spectra of noise during moderate wind speeds is comparable to that found for similar wind speeds in the open desert at the LIGO site; the presence of the building does not observably amplify wind-induced noise. The LIGO design spectrum is generally higher than the noise spectrum from 1-10 Hz, except at 3-4 Hz, but this peak in the noise spectrum is not entirely wind-induced. Above 10 Hz, there is little change in the noise spectrum between low and moderate wind conditions. High-frequency noise (apparently anthropogenic) is higher overall than found at the LIGO site for quiet conditions, but noise in the mid-frequency range (1-10 Hz) is reasonably low at the Moses Lake site.

It is also interesting to note that the amplitude of the "microseismic noise" from 0.1 to 1 Hz is significantly lower in these spectra compared to the LIGO site spectra. Because the Moses Lake measurements were made in August, this could be caused by reduced seasonal ocean storm intensities that generate this prominent noise peak.

10.0 Conclusion

In summary, it was found that the original LIGO design spectrum is a close approximation to the ambient ground vibrations measured at the site. The design spectrum below 1 Hz is usually slightly lower than the observed "microseism peak" during the period of the measurements. From 1 to 10 Hz, several transient phenomena including rush hour traffic, heavy equipment operations within 4 km, and wind speeds in excess of 10 m/s are observed to increase ground vibration to levels above the design spectrum. Above 10 Hz, the design spectrum nearly always envelops the observed ground vibration.

The seismometer selected for these measurements, and it's method of installation, limited the reliability of the measurements above 30-40 Hz. This "coupling" problem could possibly be reduced by a re-design of the emplacement. However, this single instrument strongly indicates that there are no significant noise sources above 30 Hz and so has served its purpose.

Acknowledgment. Donna McAlister-Myers and Jennifer Topping provided substantial support in the collection of this data set. Brenda Draper and Janie Treadway helped in many administrative ways. I also acknowledge the support of the LIGO Project, Caltech, and especially Lisa Sievers and Fred Asiri.

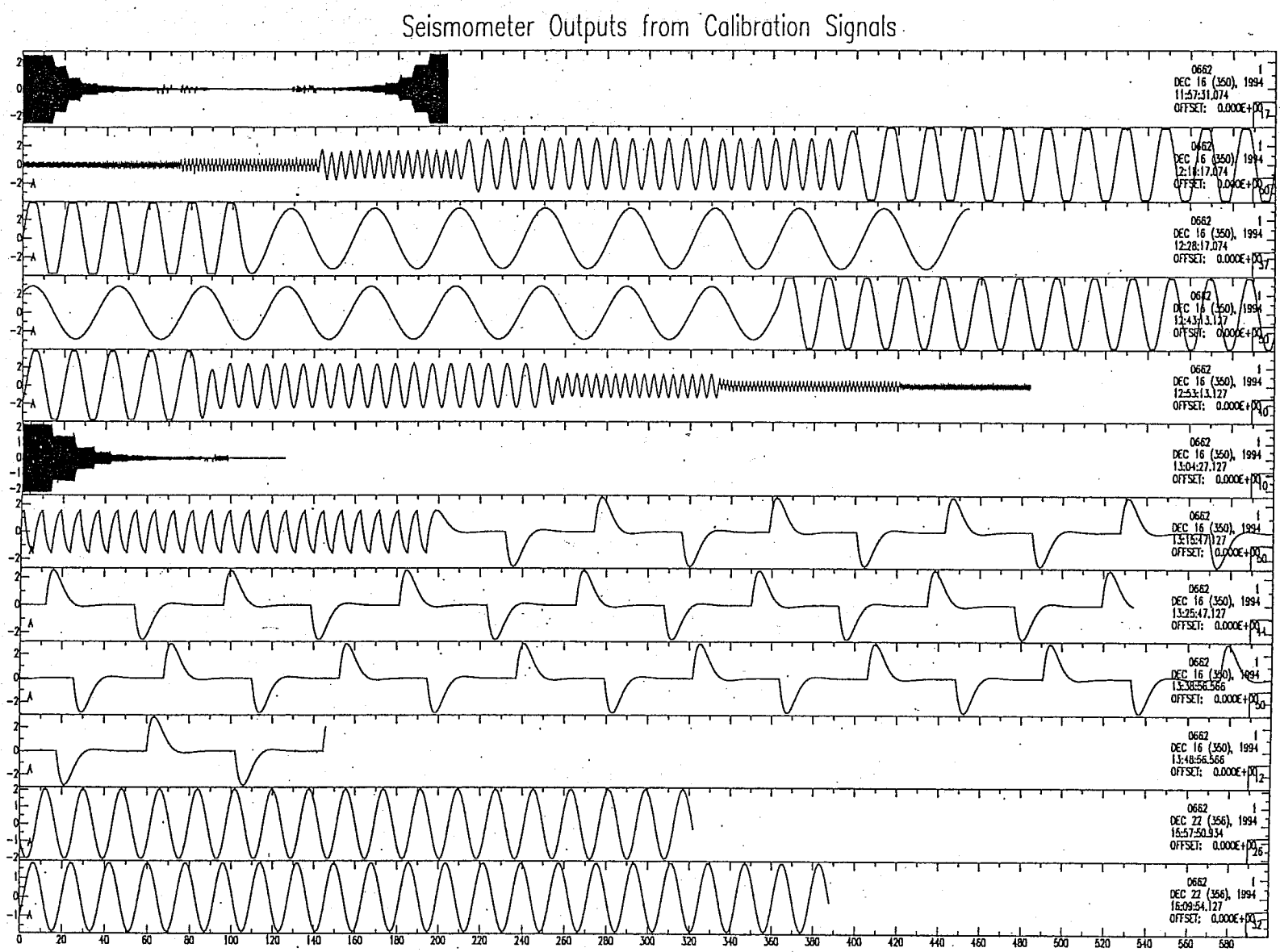

Figure 3-1: Examples of vertical channel output from two CMG-40T seismometers.

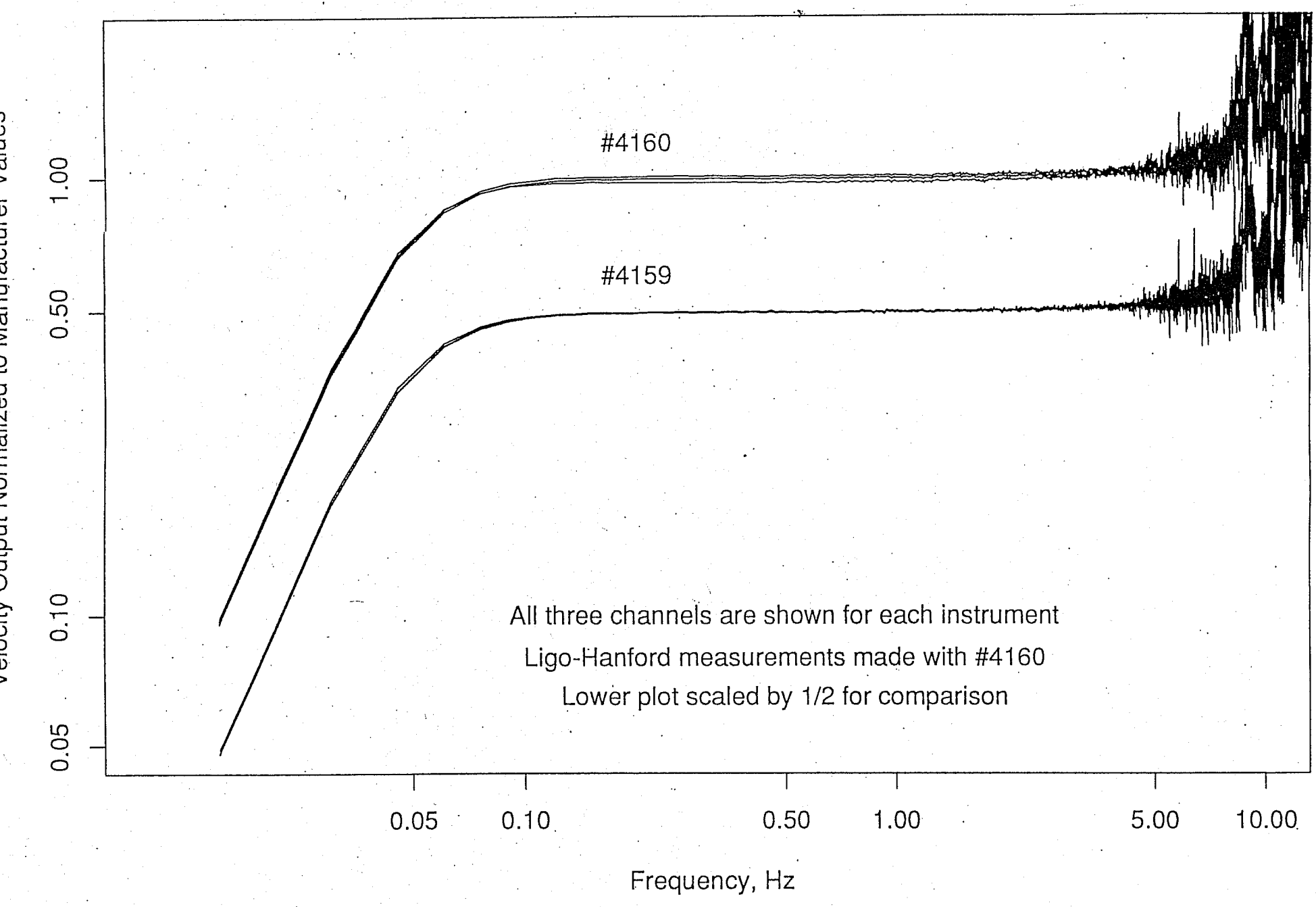

Figure 3-2: CMG-40T velocity response to 16 step inputs. Data is normalized to the velocity transduction constants provided by Gurlap Systems, Ltd.

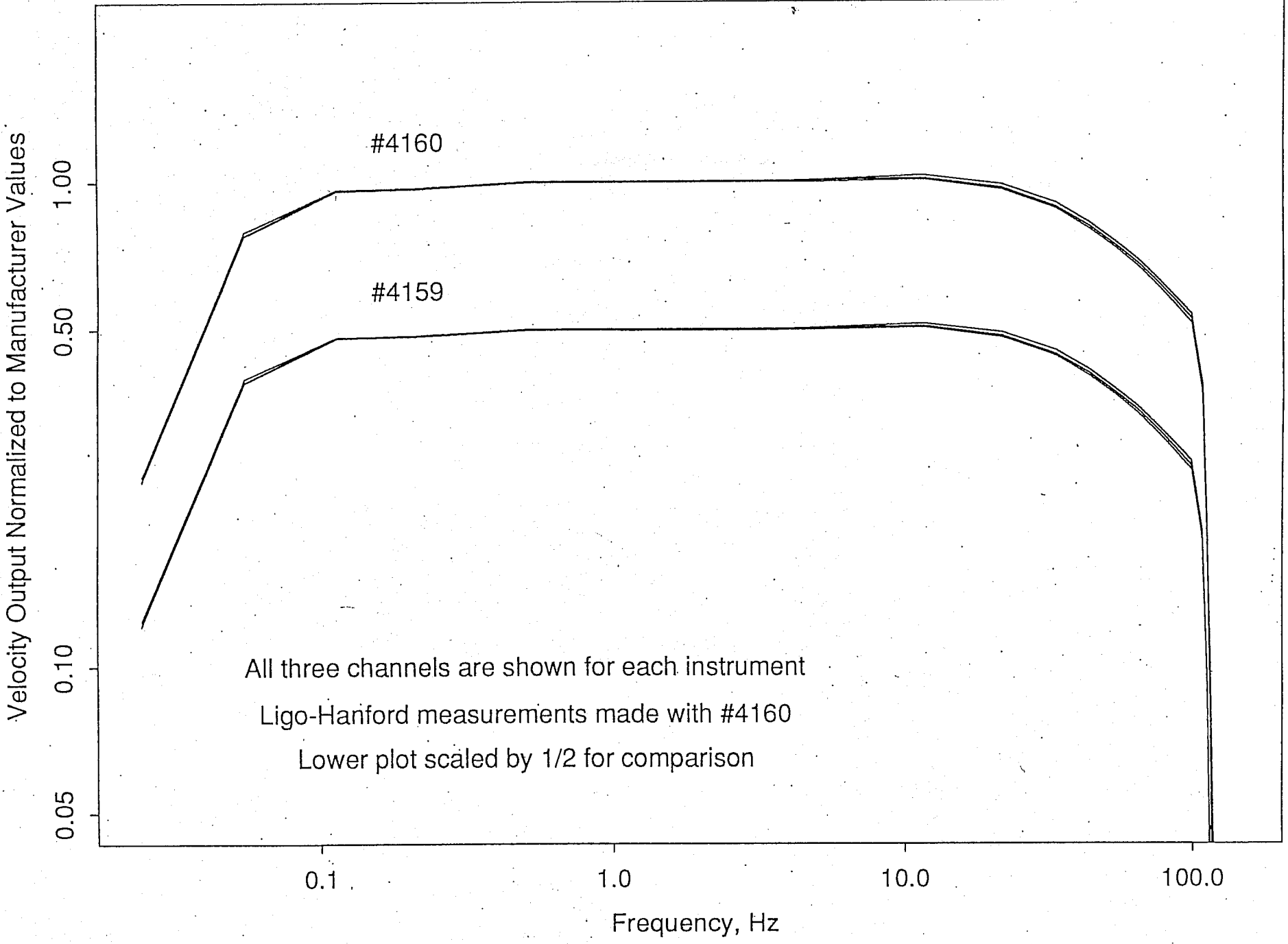

Figure 3-3: CMG-40T velocity response to sinusoidal inputs. Data is normalized to the velocity transduction constants provided by Gurlap Systems, Ltd.

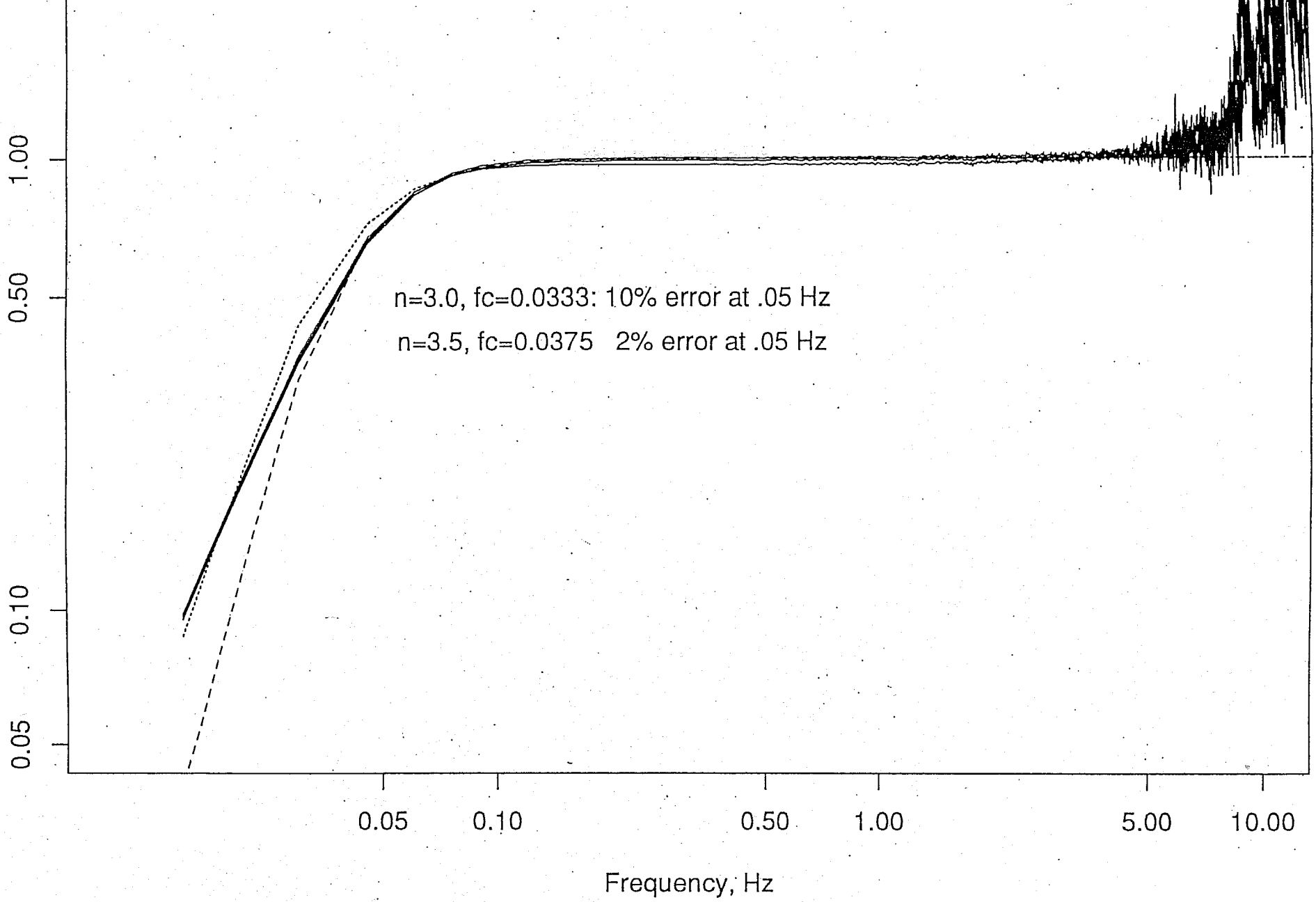

Figure 3-4: Low-frequency spectrum correction using form 1/(1+(fc/f)^n)

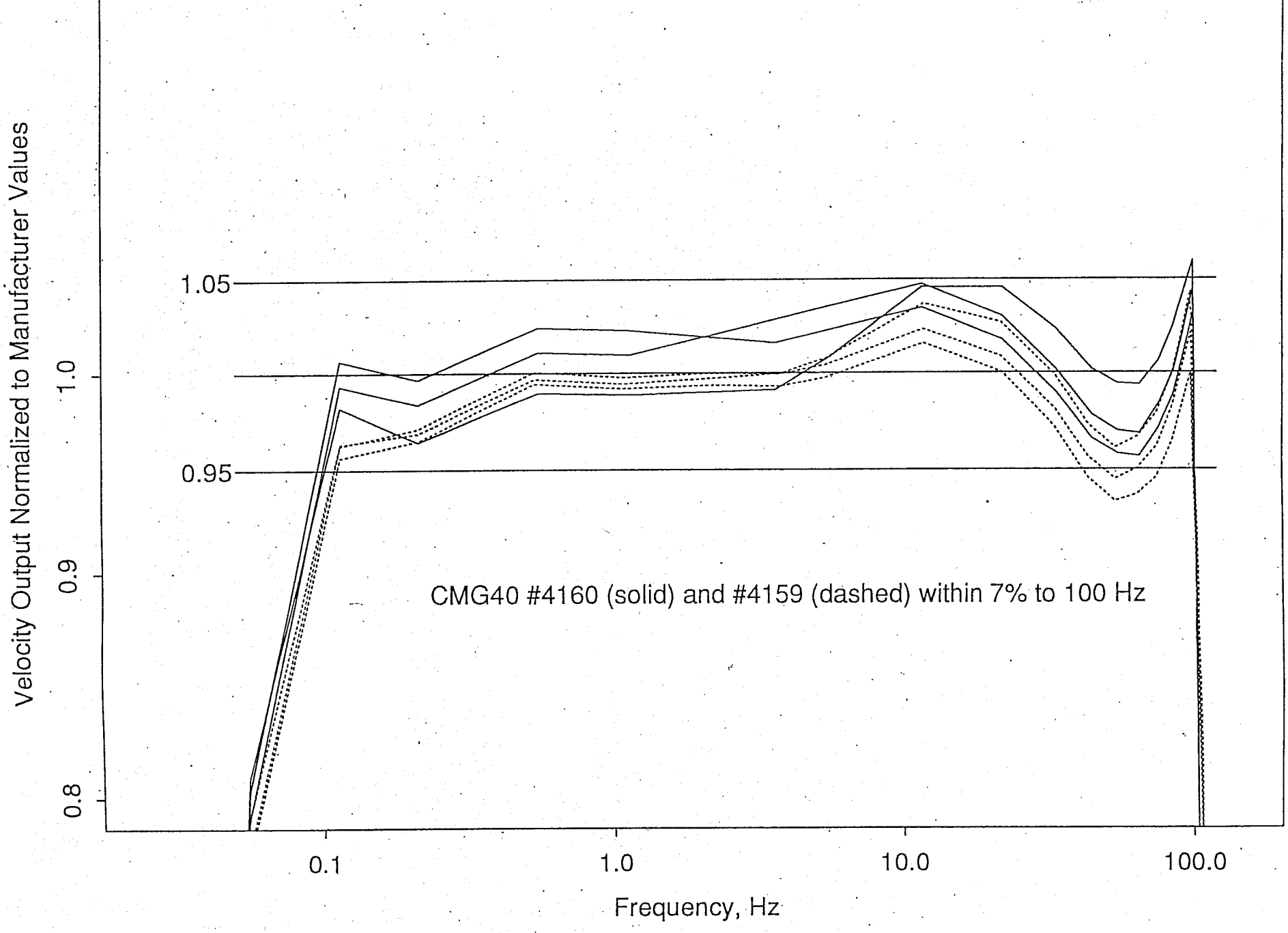

Figure 3-5: High-frequency correction using form 1/(1+(f/100)^2)

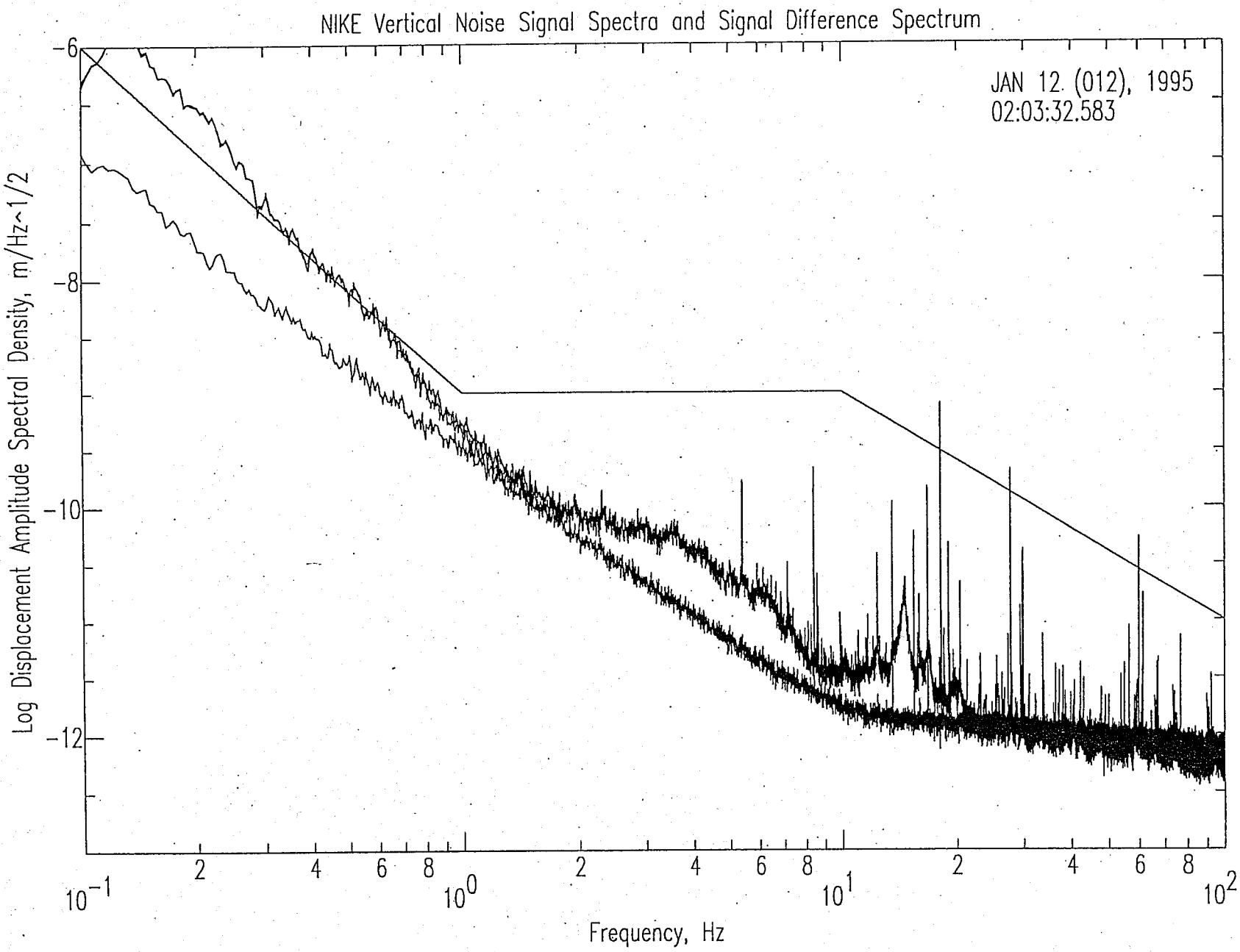

Figure 3-6: Vertical noise signal and signal-difference spectra from two CMG-40T seismometers located at the Nike missile bunker

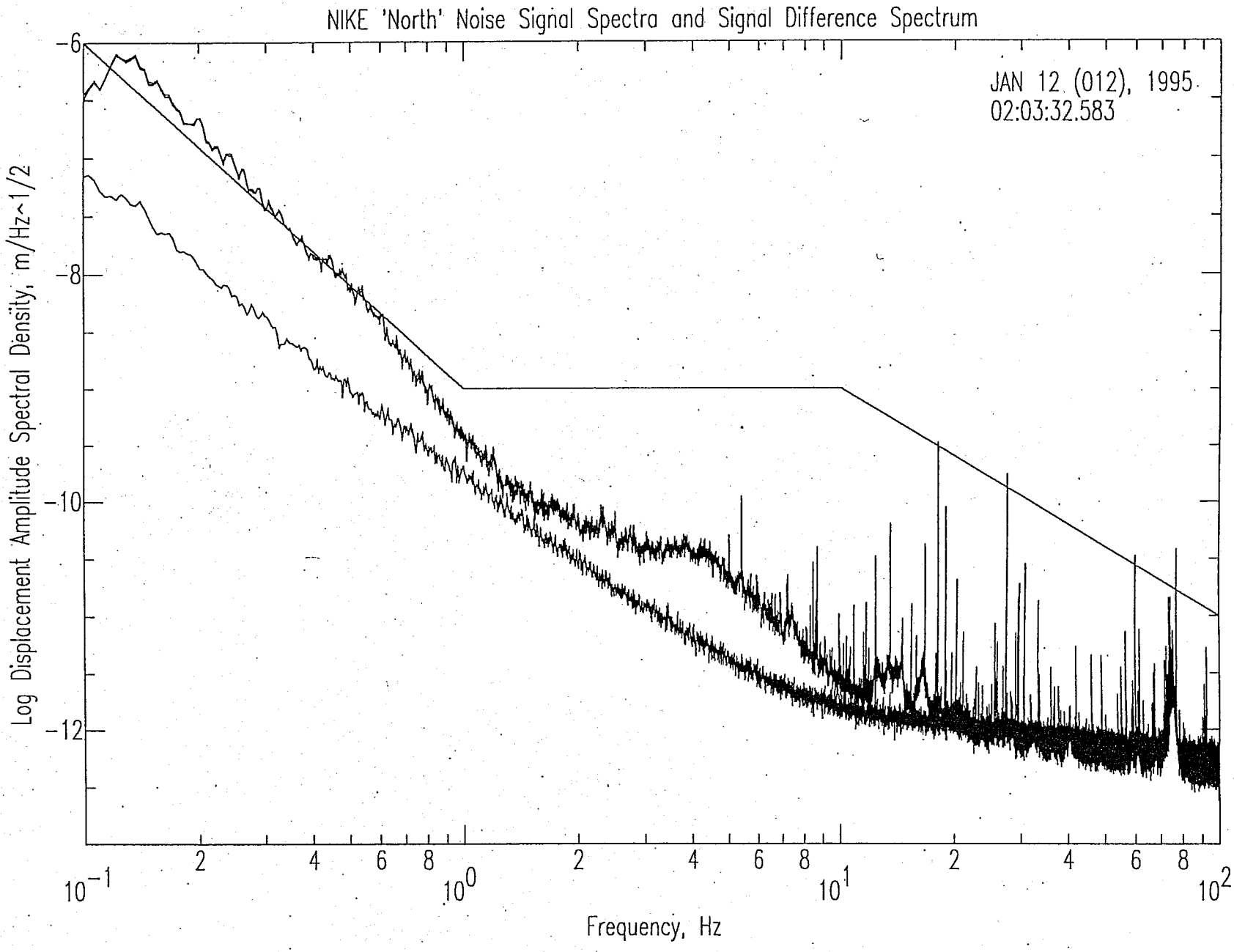

Figure 3-7: "North" noise signal and signal-difference spectra from two CMG-40T seismometers located at the Nike missile bunker

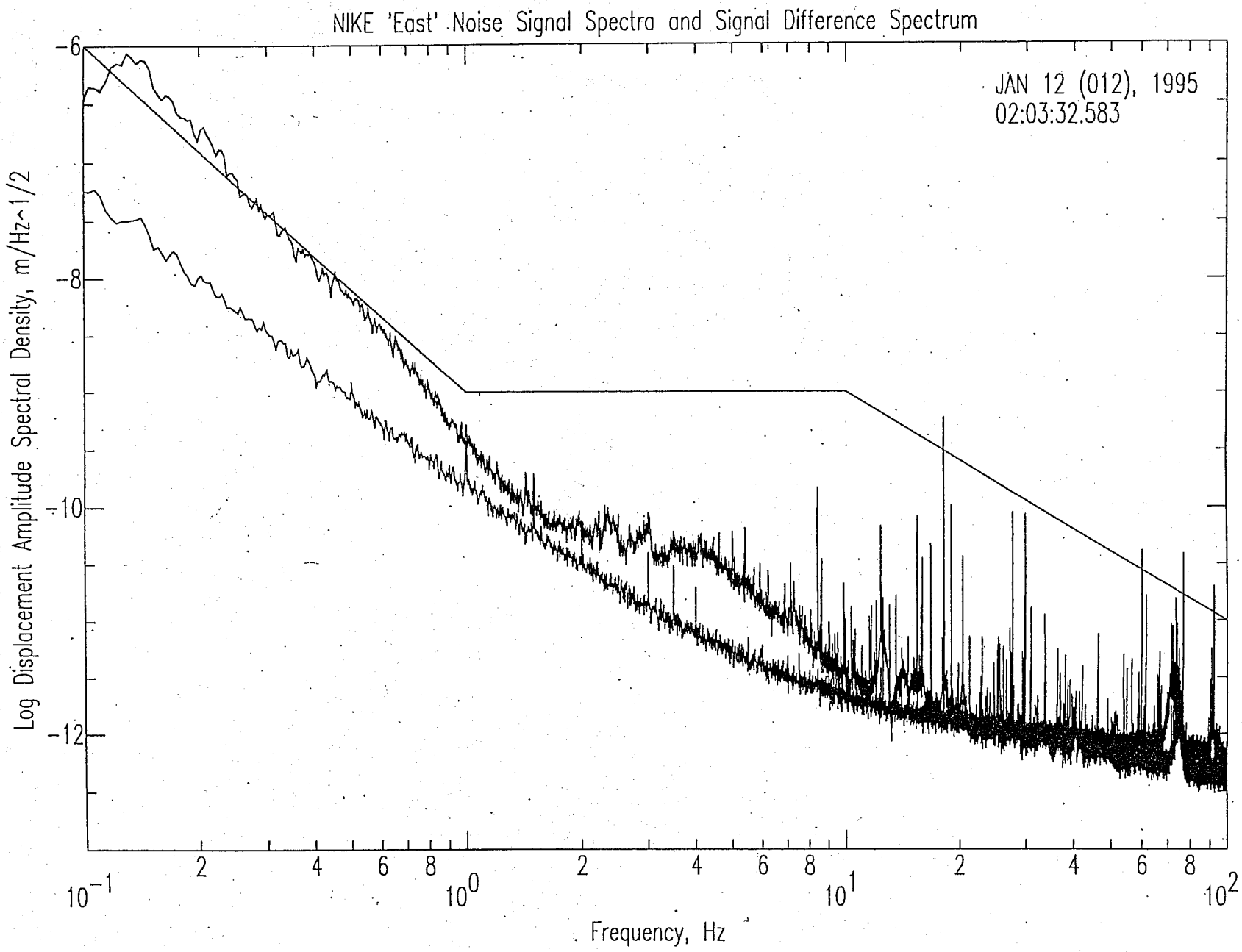

Figure 3-8: "East" noise signal and signal-difference spectra from two CMG-40T seismometers located at the Nike missile bunker

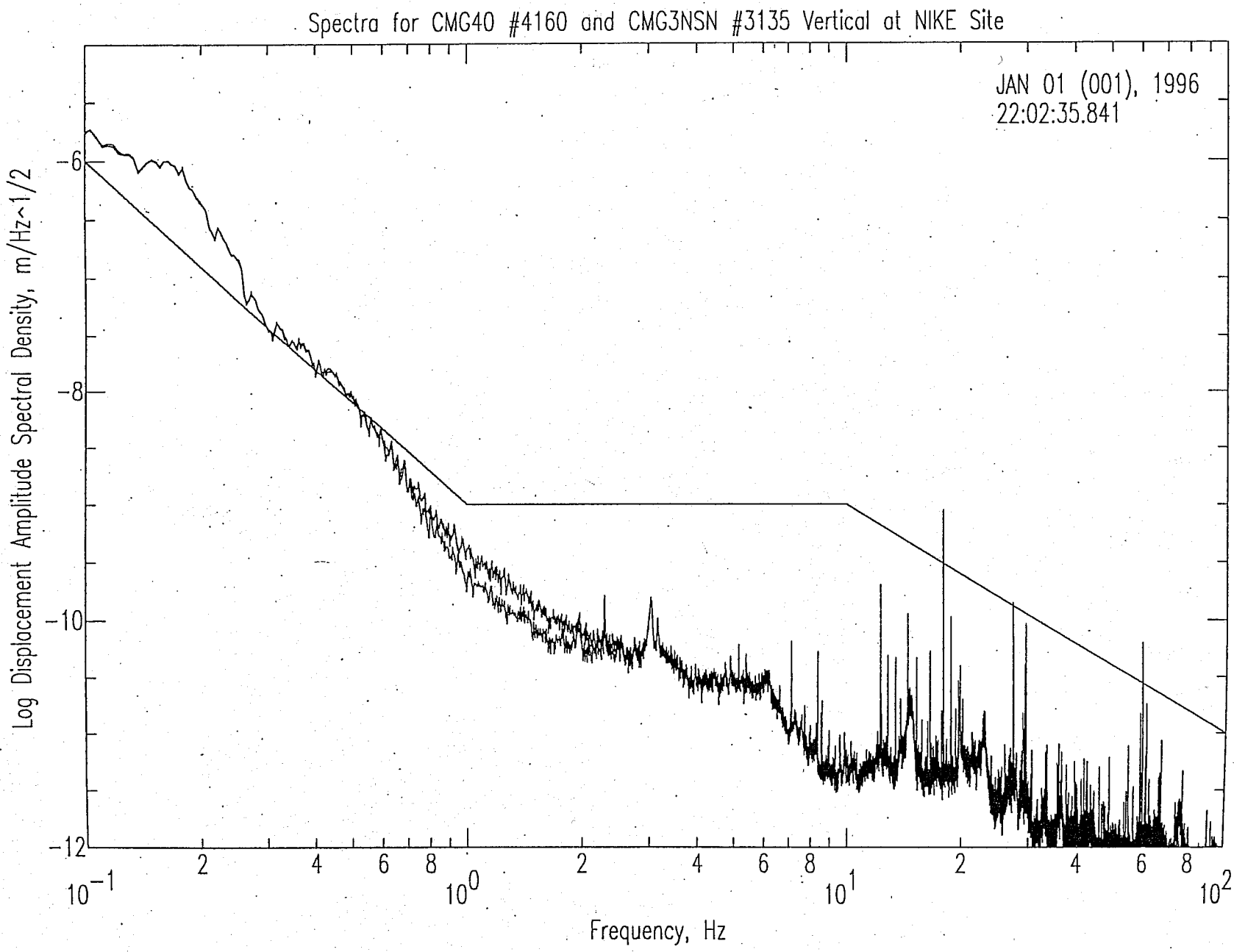

Figure 3-9: One-hour vertical noise spectra for seismometers CMG-40T (#4160) and CMG-3 (#3135) located at the Nike missile bunker. CMG-3 noise resolution is better at frequencies near 1 Hz.

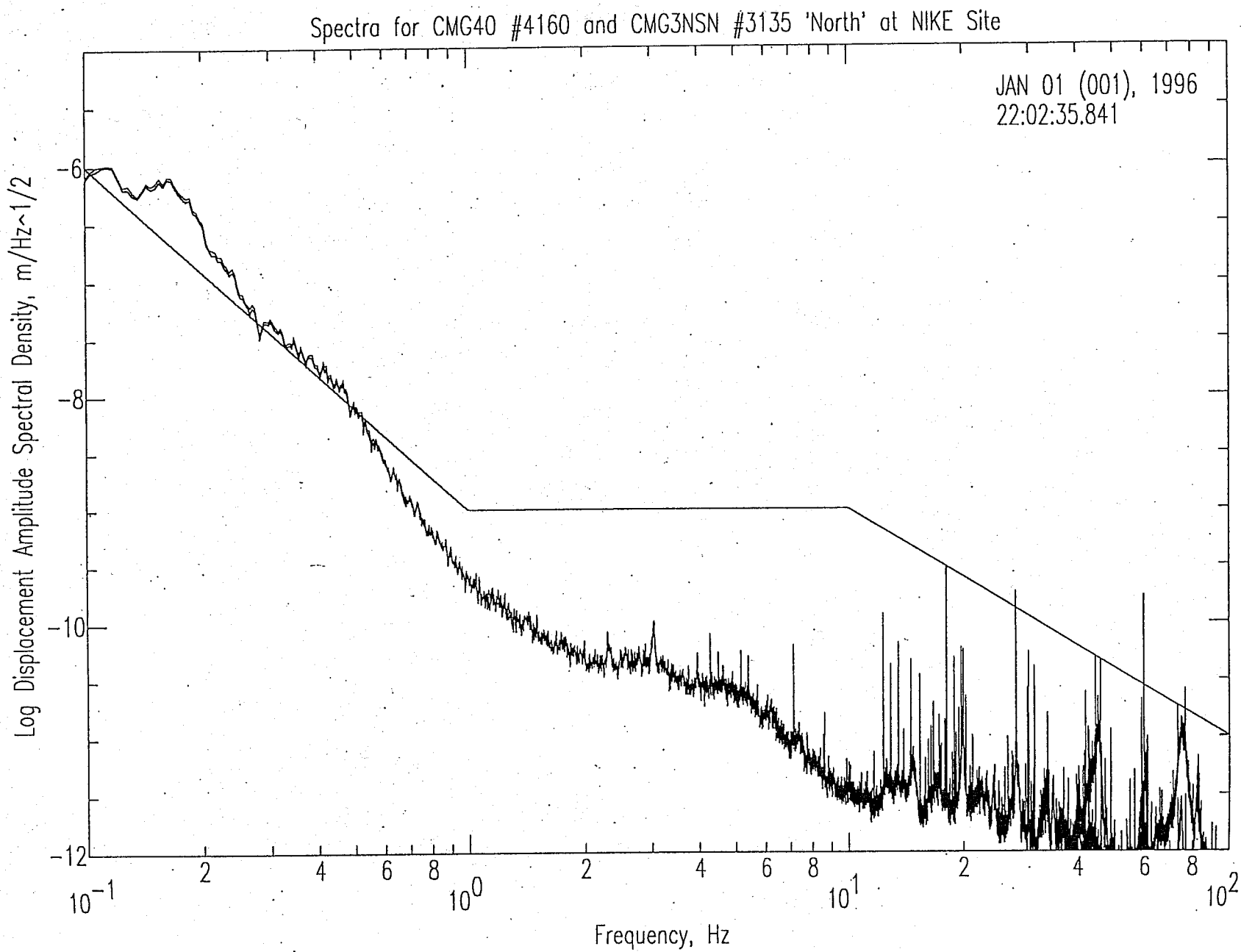

Figure 3-10: One-hour "north" noise spectra for seismometers CMG-40T (#4160) and CMG-3 (#3135) located at the Nike missile bunker. CMG-40T appears to resolve noise at this site throughout the frequency range shown.

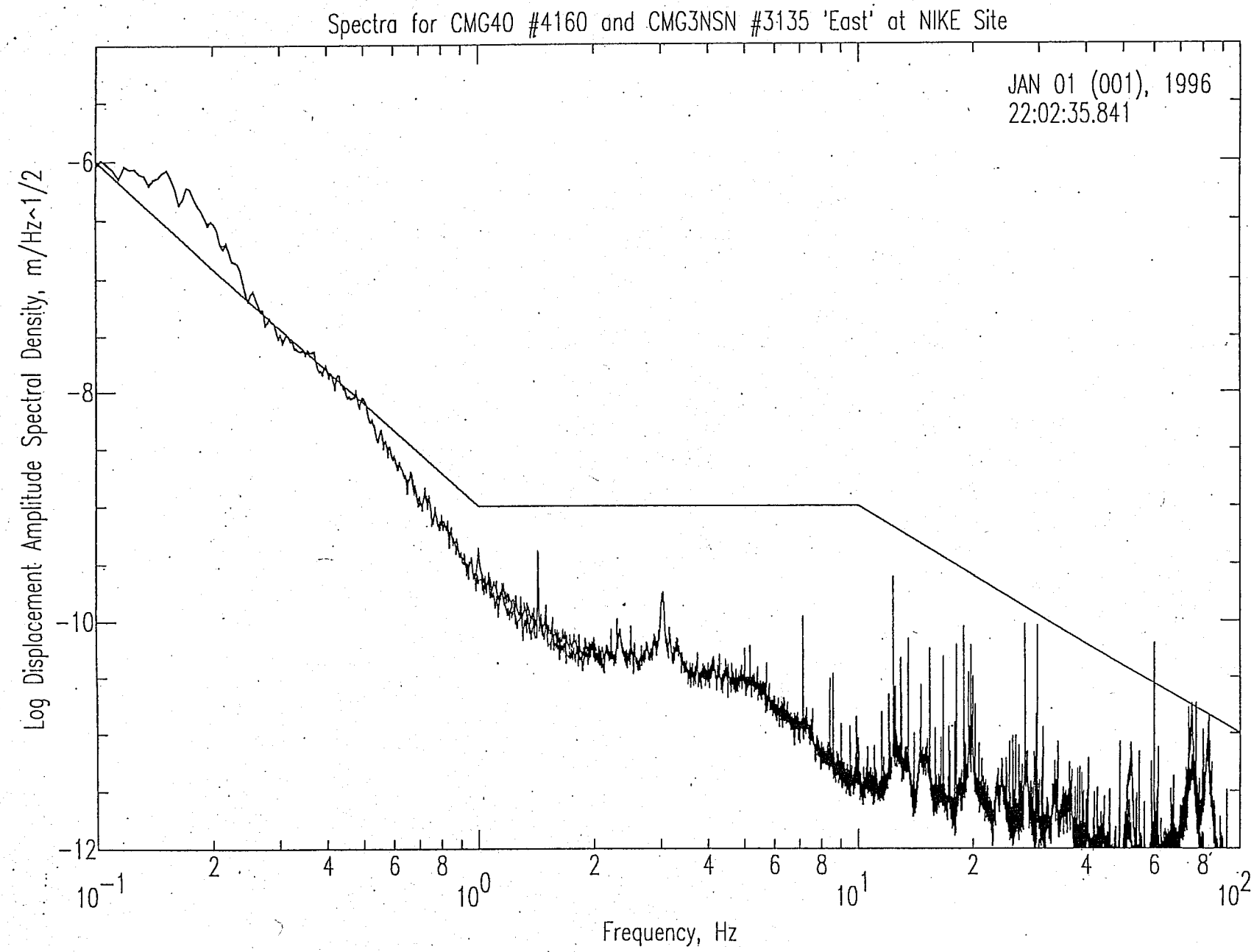

Figure 3-11: One-hour "east" noise spectra for seismometers CMG-40T (#4160) and CMG-3 (#3135) located at the Nike missile bunker.

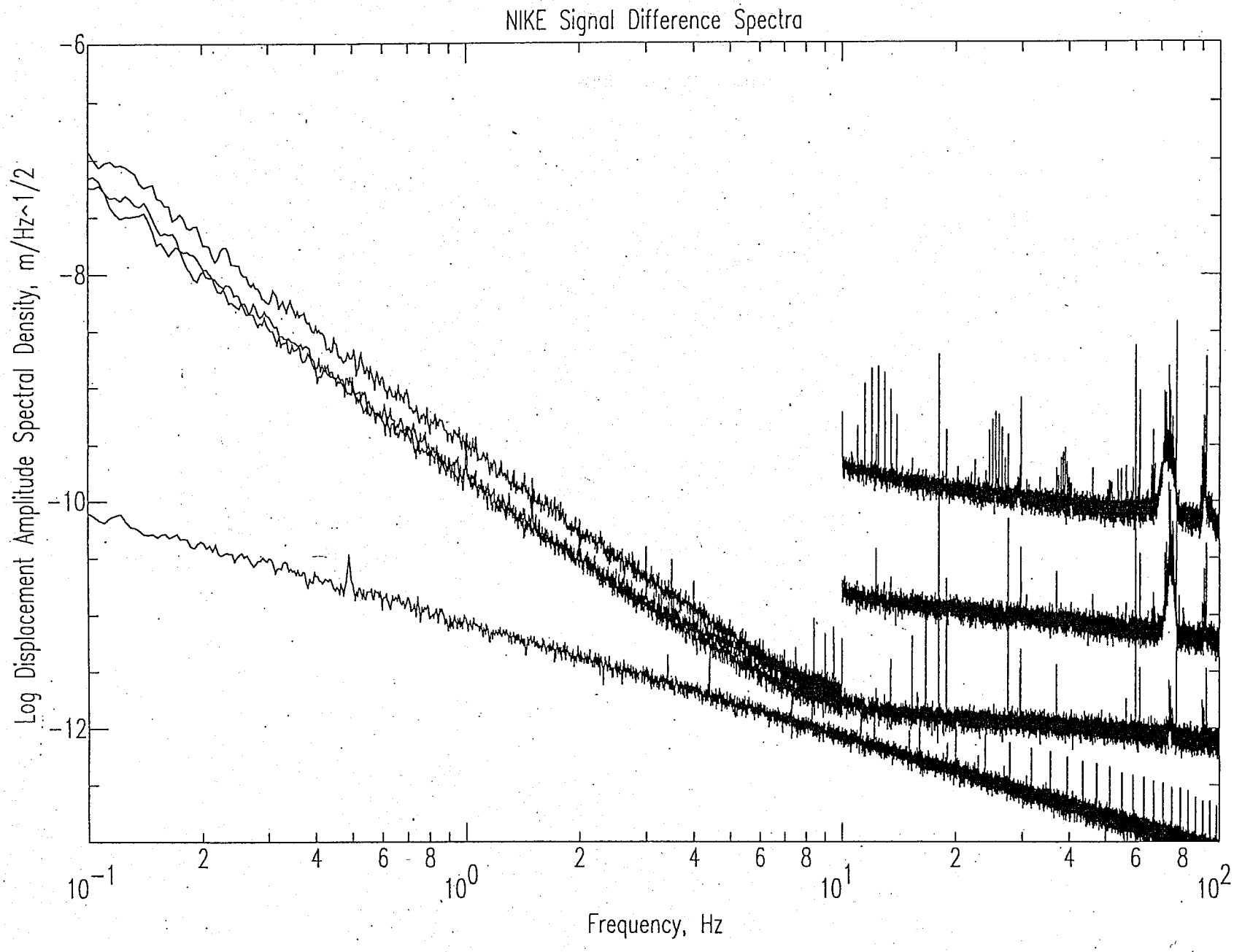

Figure 3-12: Comparison of CMG-40T signal spectra difference for all three channels (vertical, north, and east). The lower curve represents the estimated digital recorder noise. The two horizontal channel spectra are offset by a factor of 10 above 10 Hz for clarity.

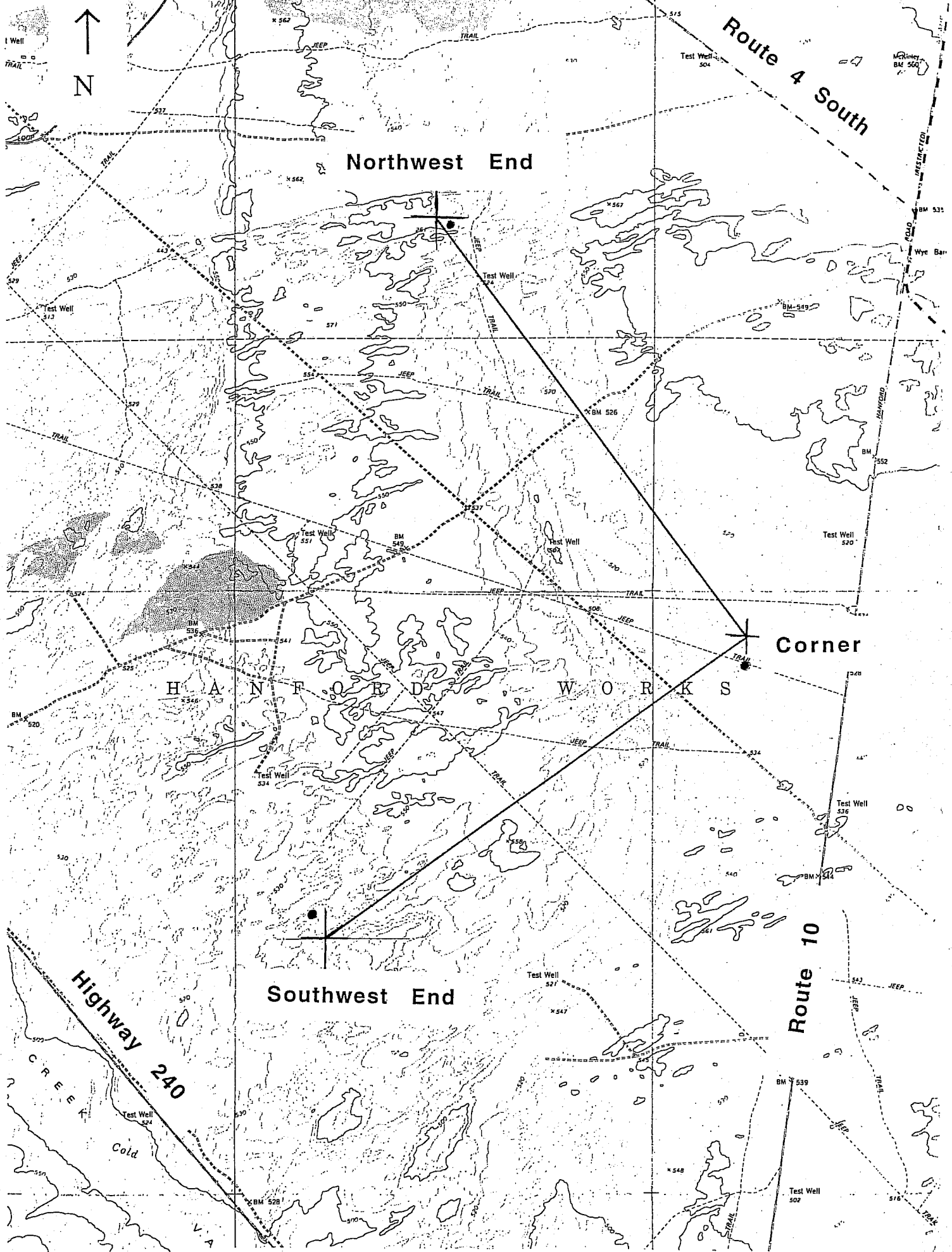

Figure 4-1: Locations of LIGO site seismic measurements

LIGO-C950572-02-O

Figure 4-2: 55-gallon open-bottomed drum emplaced in hole dug in sandy soil. Barrel contains the Reftek data acquisition system and batteries that supply power to the system.

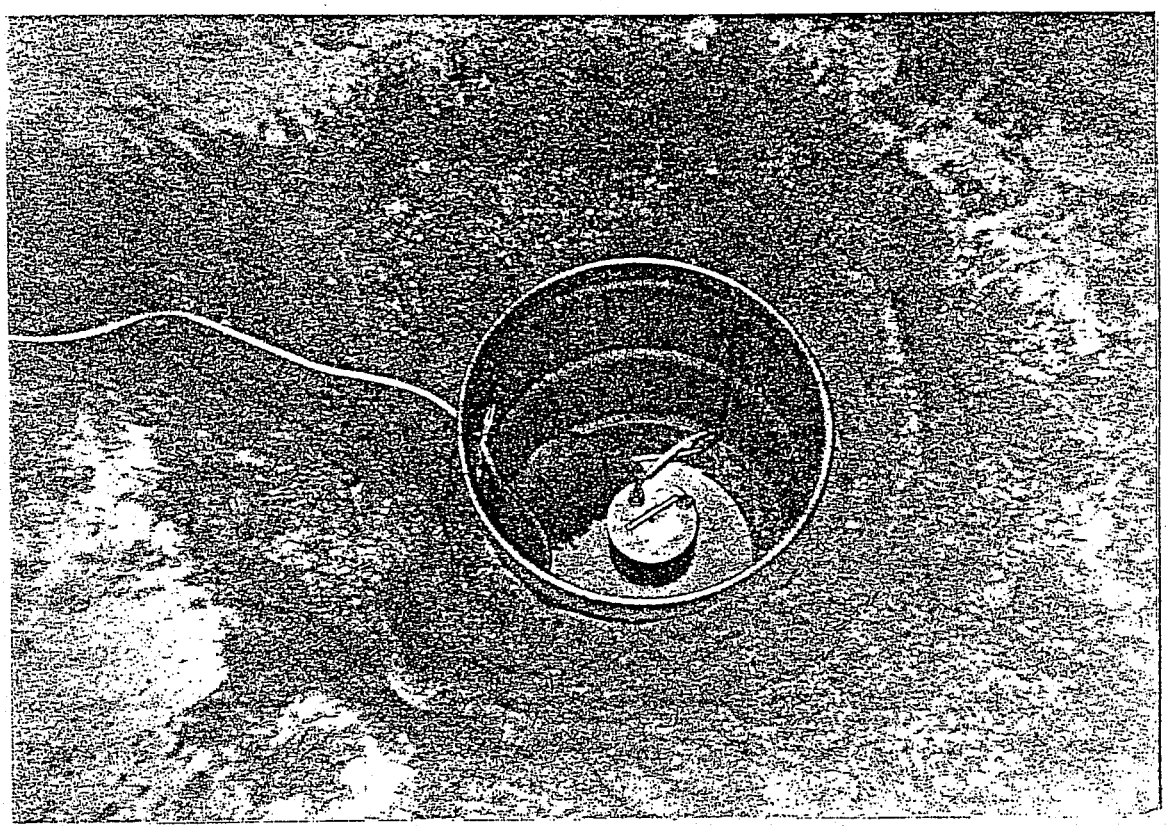

Figure 4-3: Seismometer placed on levelled paving stone at the bottom of 55-gallon drum. Drum is placed approximately 1 ft below grade in sandy soil (seismometer is approximately 4 ft below grade).

Figure 4-4: View of barrels containing the data acquisition system and seismometer prior to covering of barrels to help dampen acoustic noise.

Figure 4-5: View of in-place data acquisition system. Square patch is the pegboard covering the acoustic microphone.

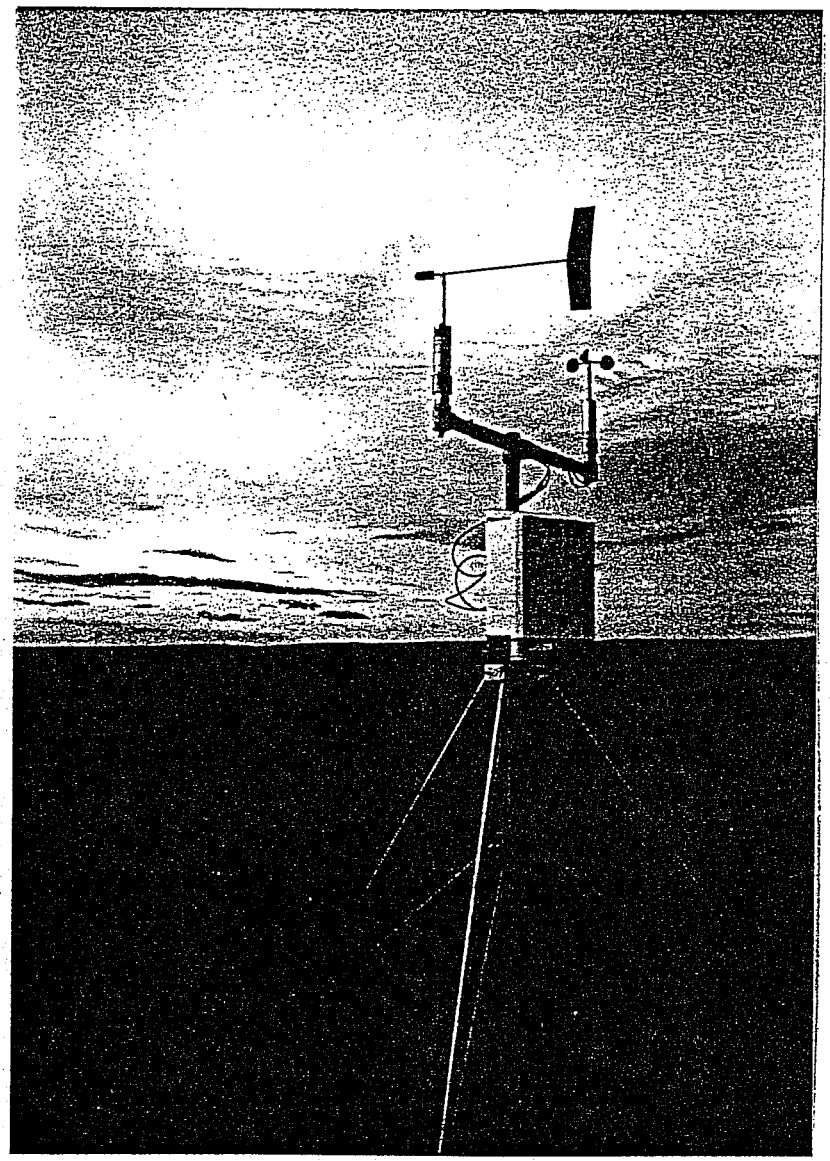

Figure 4-6: View of cup anemometer and wind vane attached to 1 m arm on tripod assembly. Box contains Campbell 21X data logger.

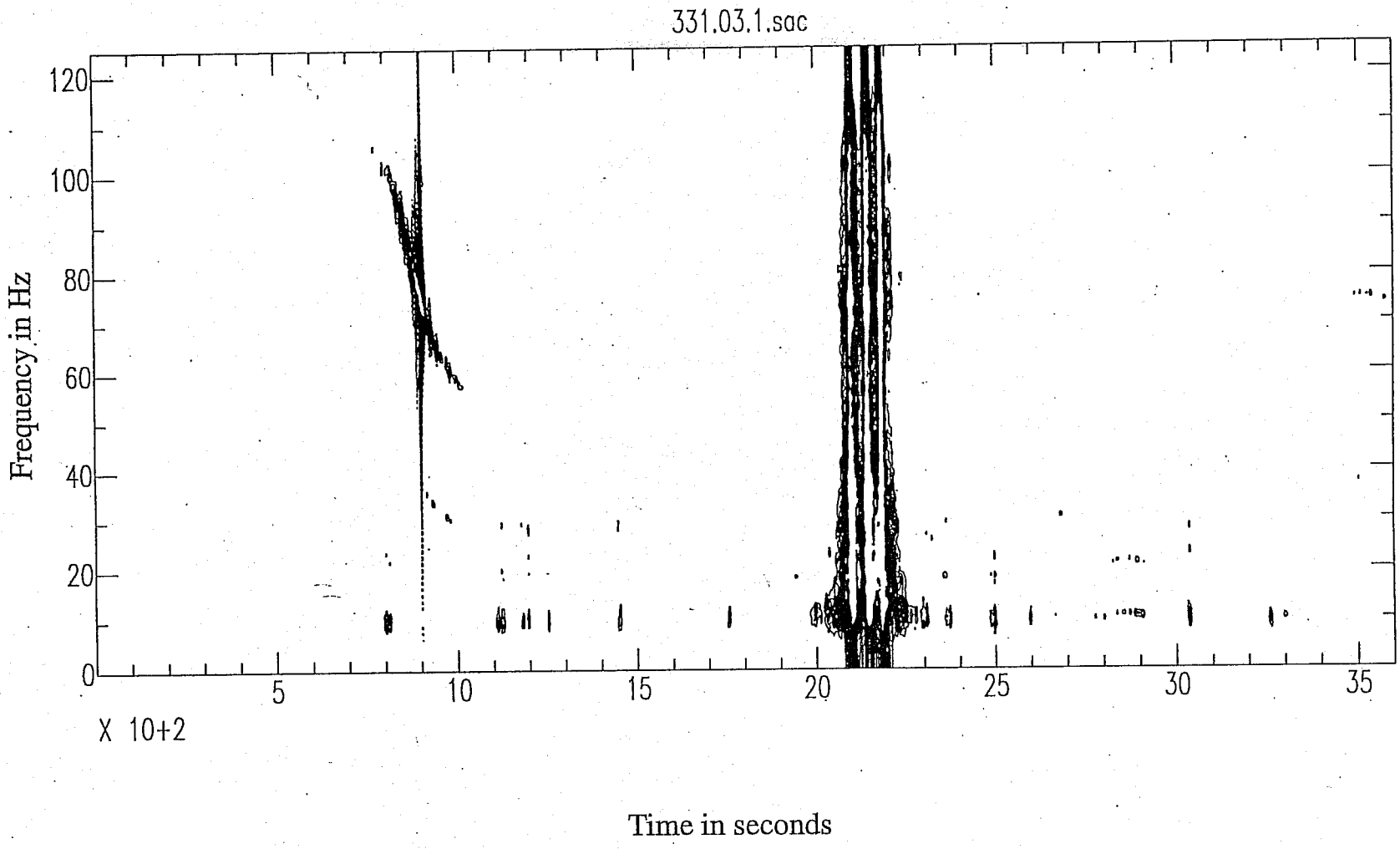

Figure 5-1: Spectrogram of the vertical component signal at the Northwest End, Day 331, GMT hour 03 (7 p.m. - 8 p.m. PST). At 900 s, an aircraft passes overhead and at 2000-2300 s, there is a vehicle driving past the site. The short-duration noise bursts at 10 Hz are from acoustic signals from artillery practice at the Yakima Training Center.

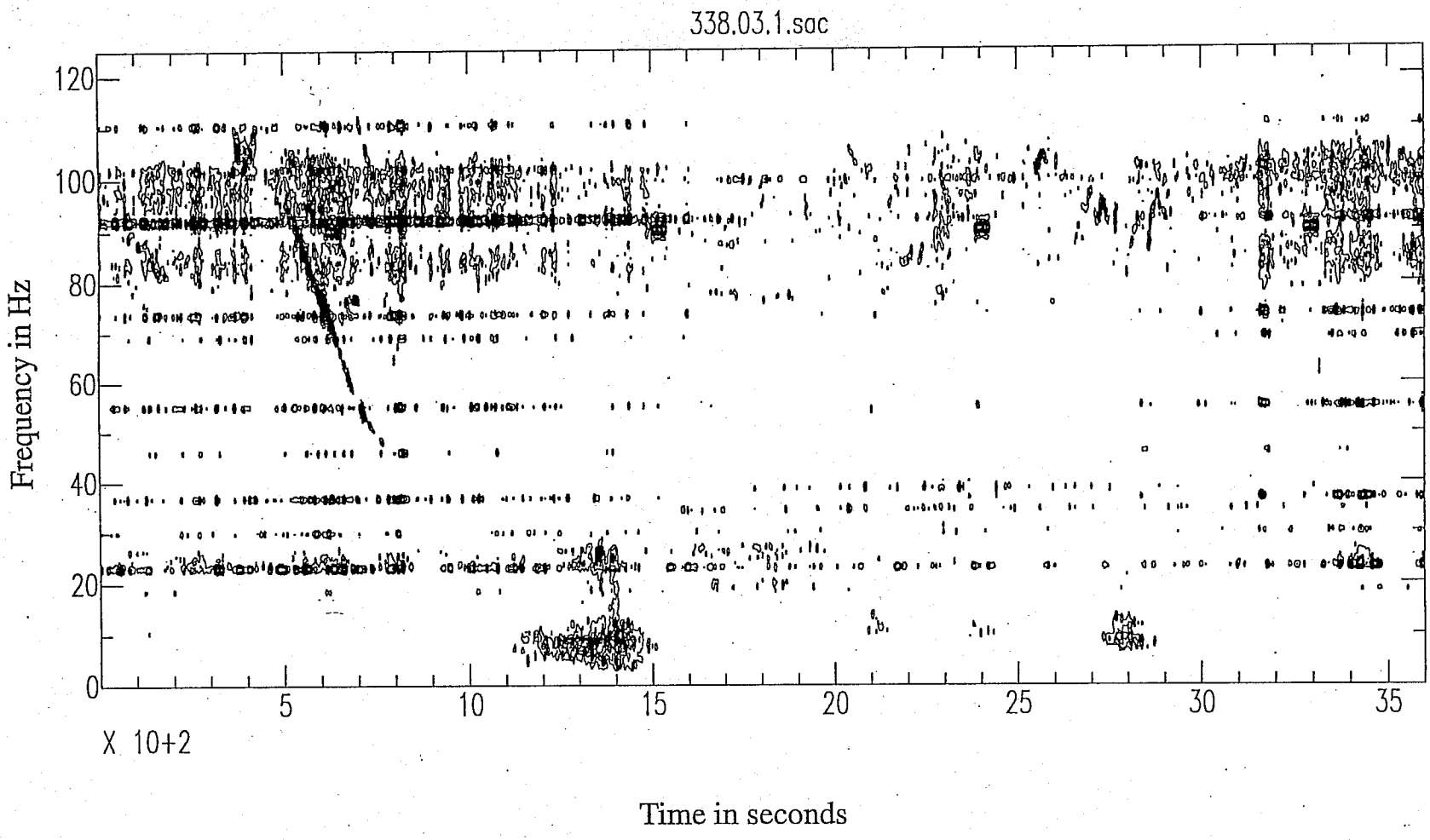

Figure 5-2: Spectrogram of the vertical component signal at the Southwest End, Day 338, GMT hour 03 (7 p.m. - 8 p.m. PST). The "glide tone" or frequency sweep signal from 500-800 s is due to aircraft. The set of narrow-band semi-continuous ("line spectra") noise is due to the operation of nearby industrial machinery (unidentified). The two periods of noise around 10 Hz from 1100-1500 and 2200-2400 s have a similar appearance to vehicle noise.

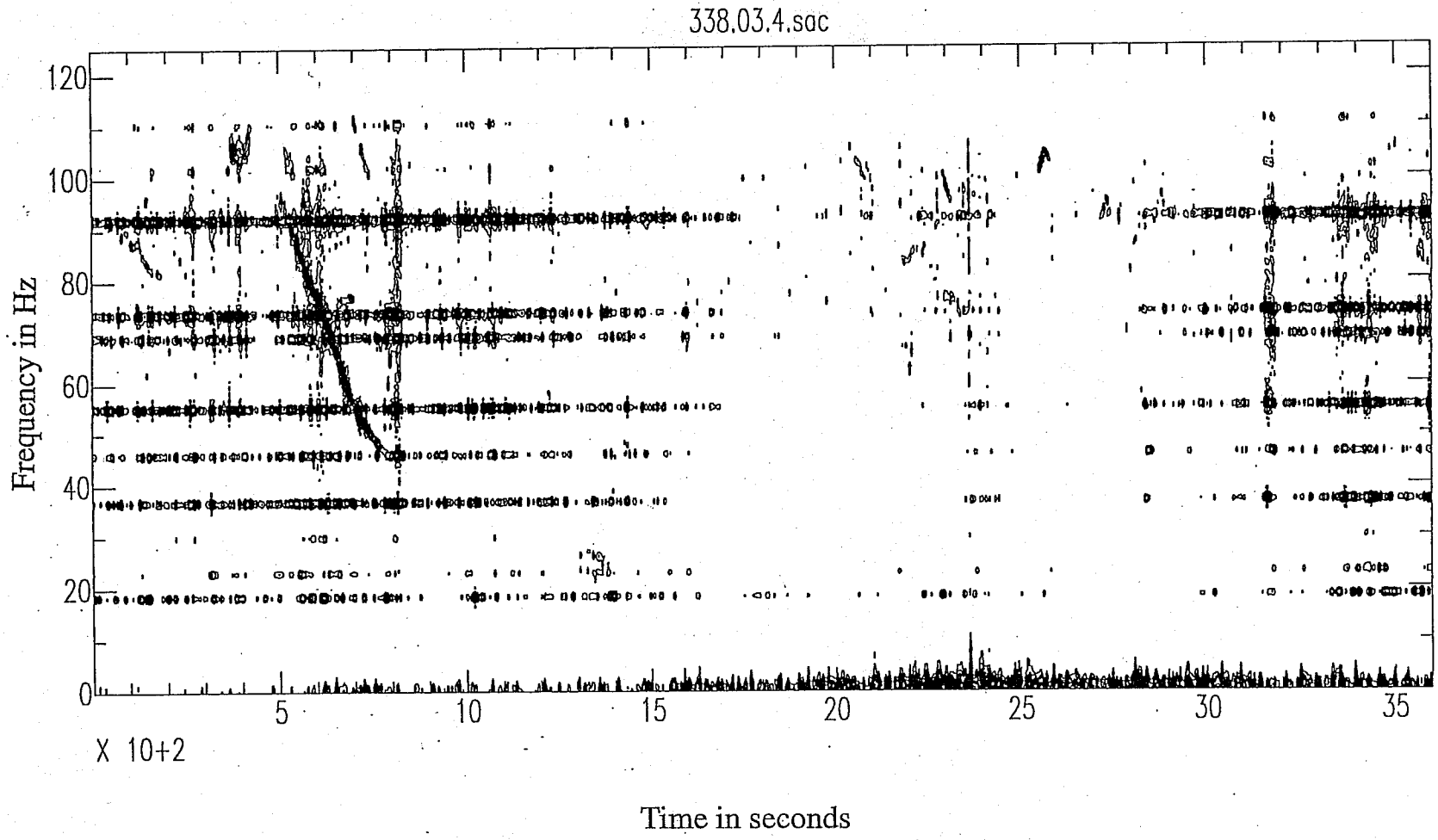

Figure 5-3: Spectrogram of the microphone signal for the time period shown in Figure 5-2. The aircraft glide tone from 500-800 s and the line spectra are temporally correlated with those found on the seismic signals, indicating that these are acoustic pressure signals being transmitted into the soil. Note the absence of the two periods of vehicle noise compared to Figure 5-2, indicating that these lower-frequency signals are transmitted to the site through the earth.

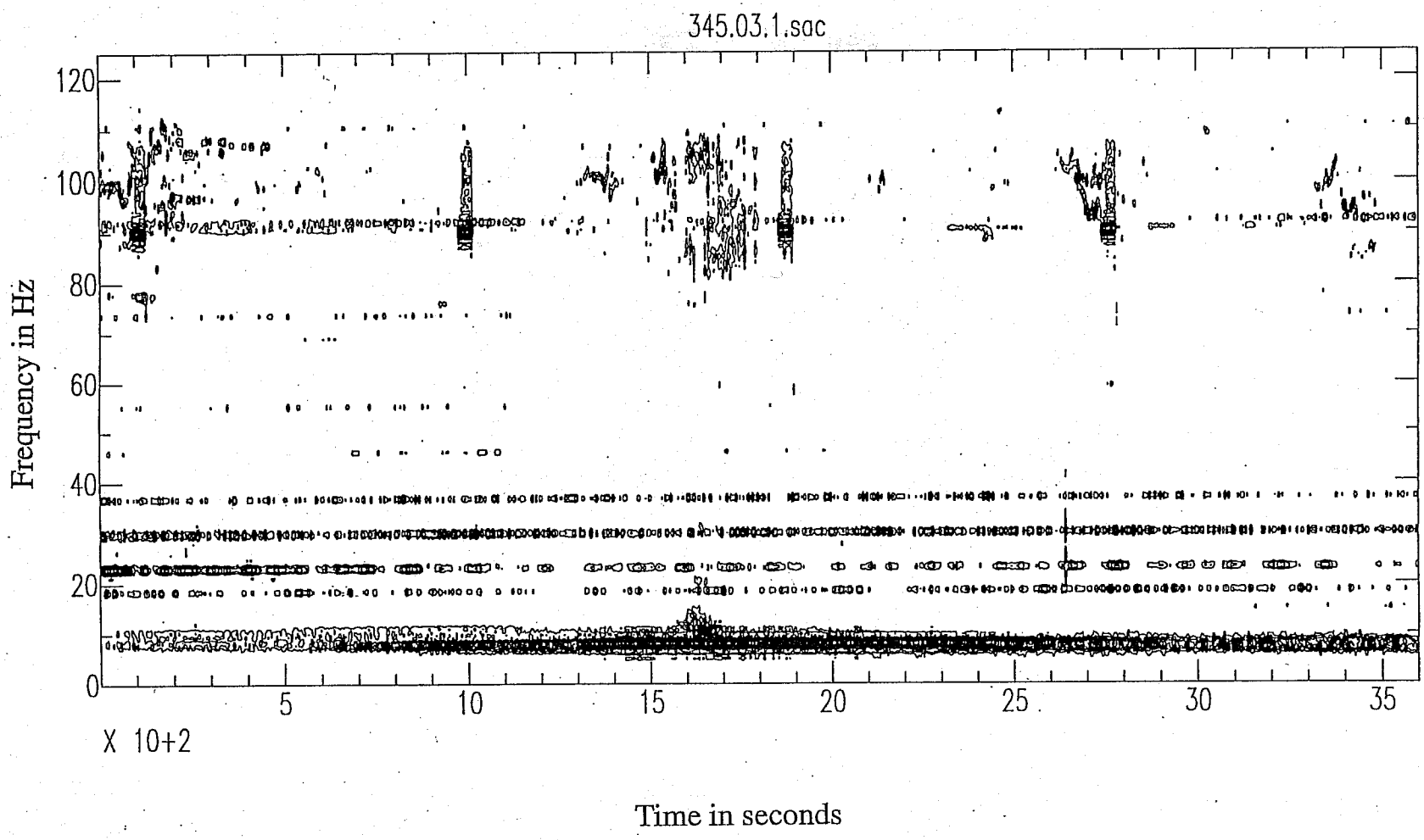

Figure 5-4: Spectrogram of the vertical seismic signal at the Corner, Day 345, GMT hour 03 (7 p.m. - 8 p.m. PST). During this time period at this site, line spectra are stronger at a lower set of frequencies, but the set of frequencies is generally the same compared to those observed at the Southwest End location (Figure 5-2). The periodic noise at 90-100 Hz is caused by the recording equipment and is not a characteristic of the site.

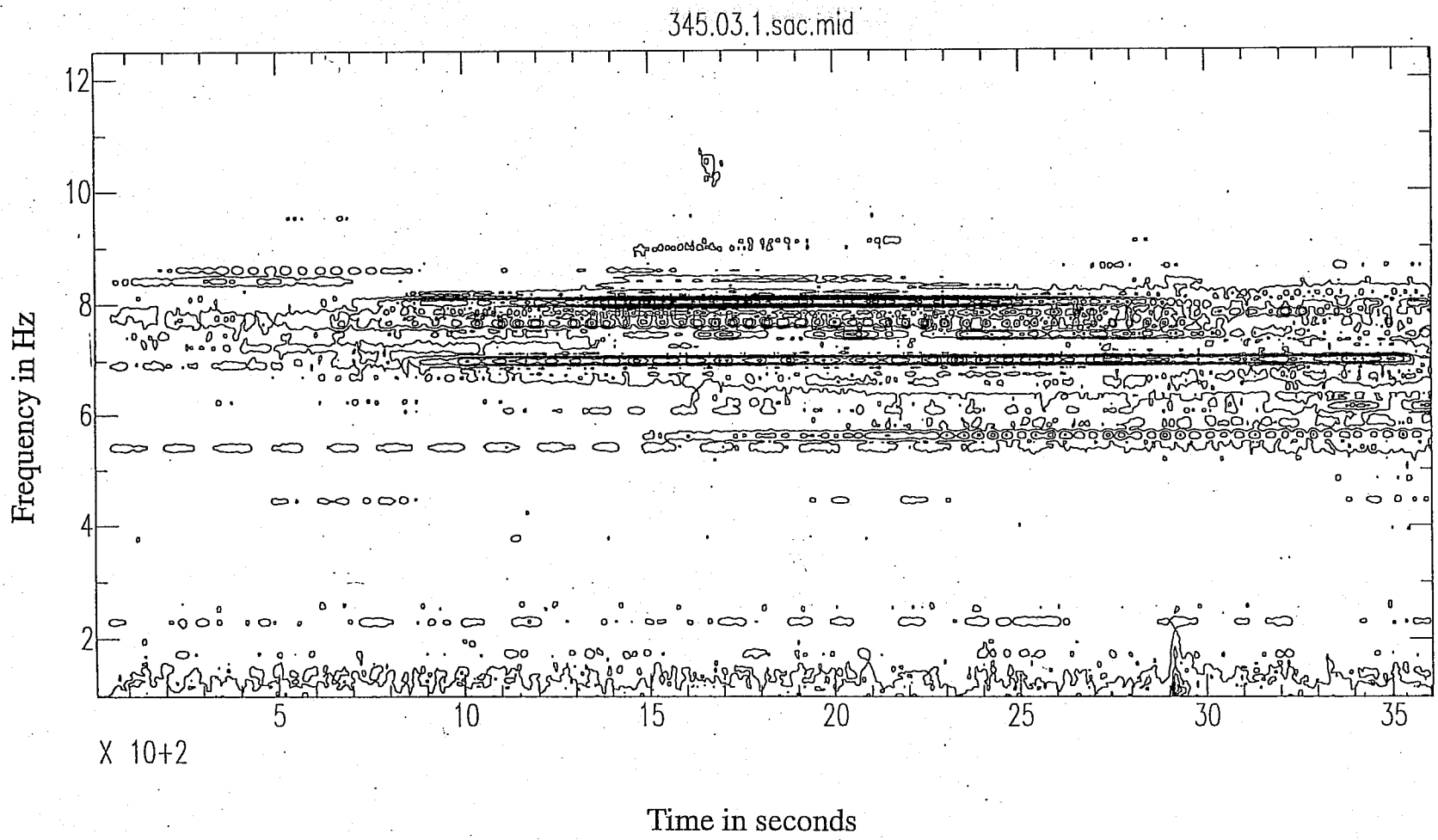

Figure 5-5: Displacement (low-frequency) spectrogram for the same signal as used in Figure 5-4, showing increased resolution of the line spectra below 10 Hz.

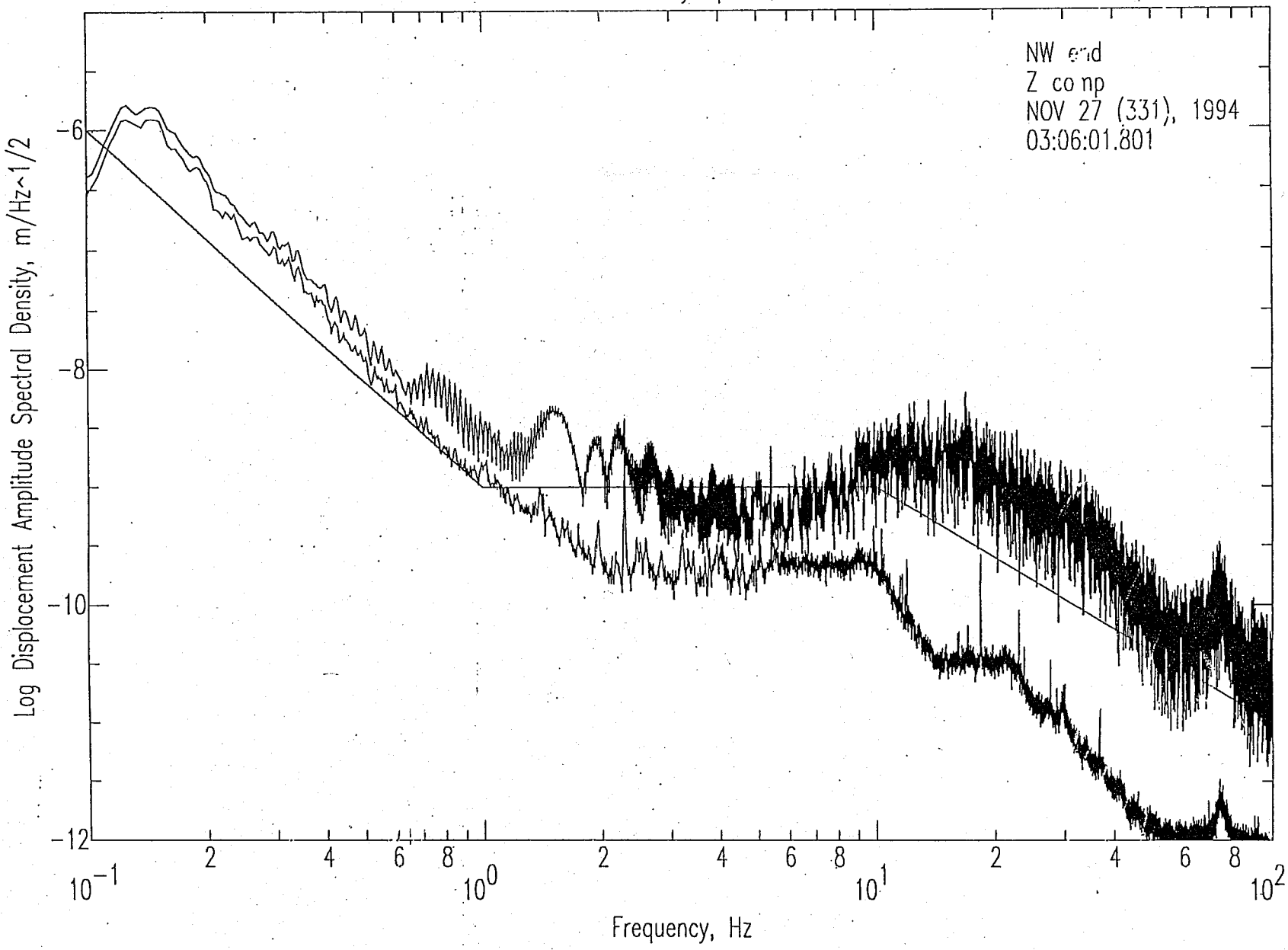

Figure 6-1: Vertical-component median and r.m.s. amplitude spectra for the one-hour time period, Day 331, GMT hour 03 (7 p.m. - 8 p.m. PST) at the Northwest End. The spectrogram for this time period was shown in Figure 5-1. The effect of a vehicle passing the site strongly affects the r.m.s. spectrum, but the median spectrum is robust to outliers. The signal exceeded the range of the recorder, creating the scalloping at some frequencies of the r.m.s. spectrum.

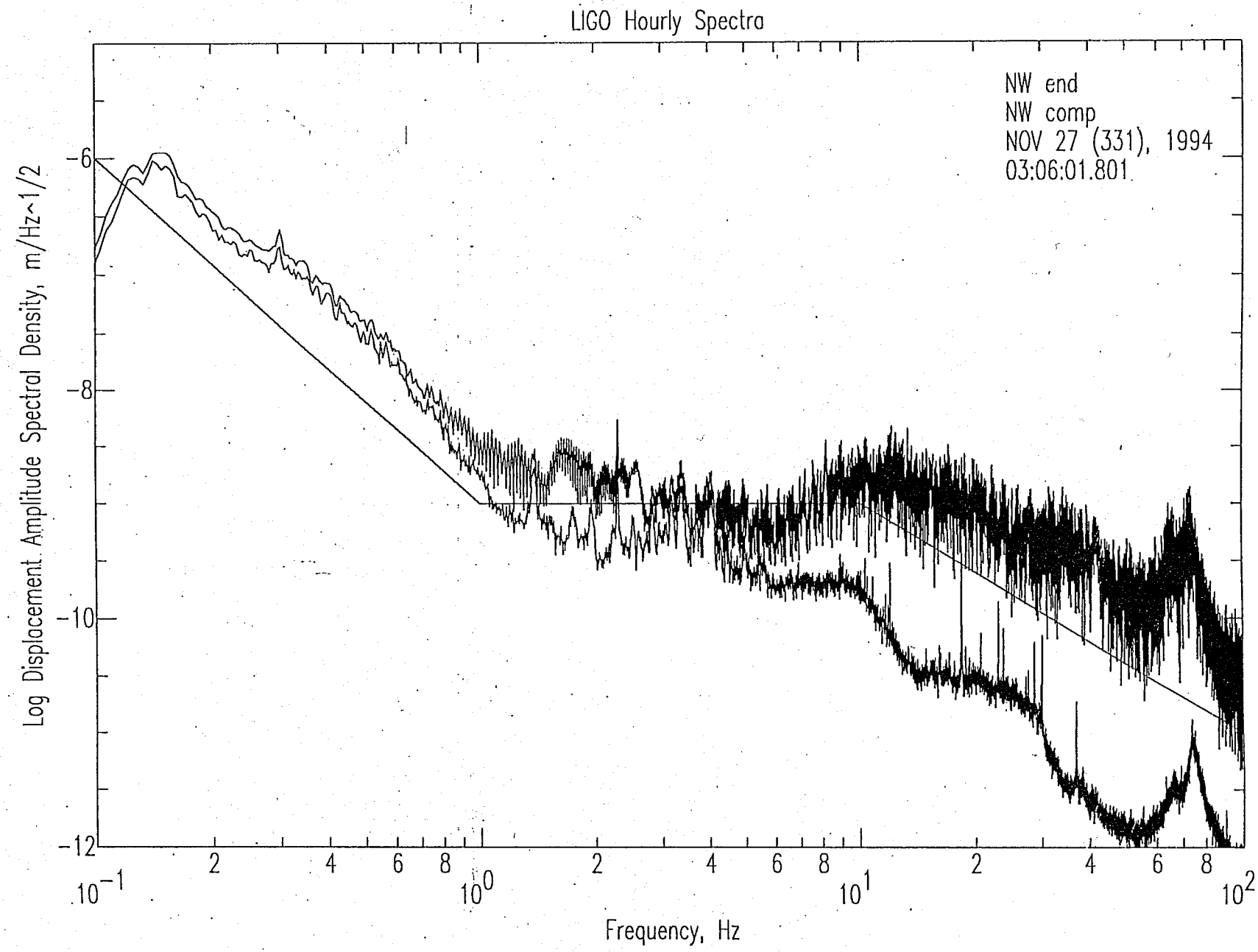

Figure 6-2: Northwest-component median and r.m.s. amplitude spectra corresponding to Figure 5-1. Note the resonance peak from 50 - 90 Hz is excited/amplified by the vehicle noise.

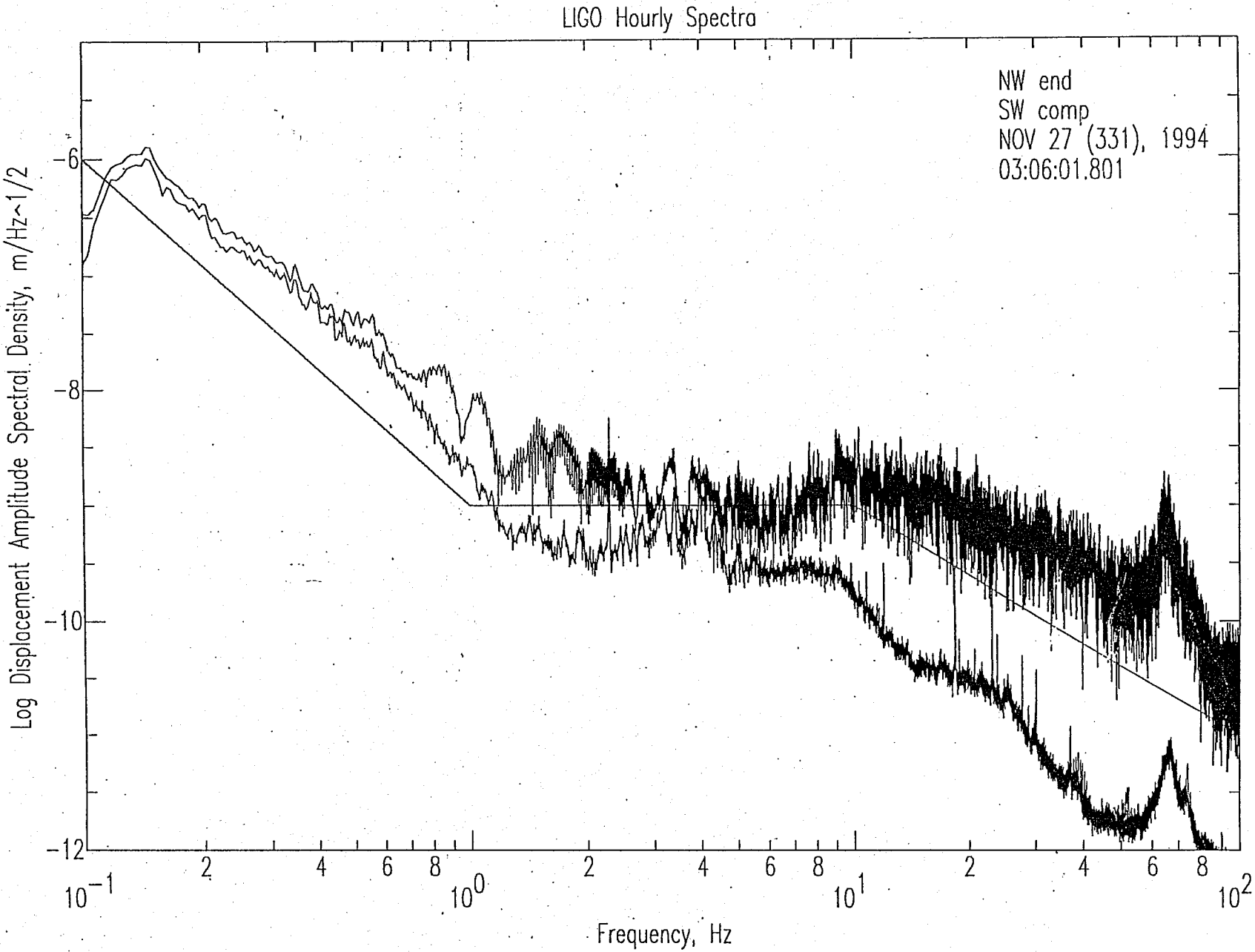

Figure 6-3: Southwest-component median and r.m.s. amplitude spectra corresponding to Figure 5-1. Note the resonance peak from 50 - 90 Hz is excited/amplified by the vehicle noise.

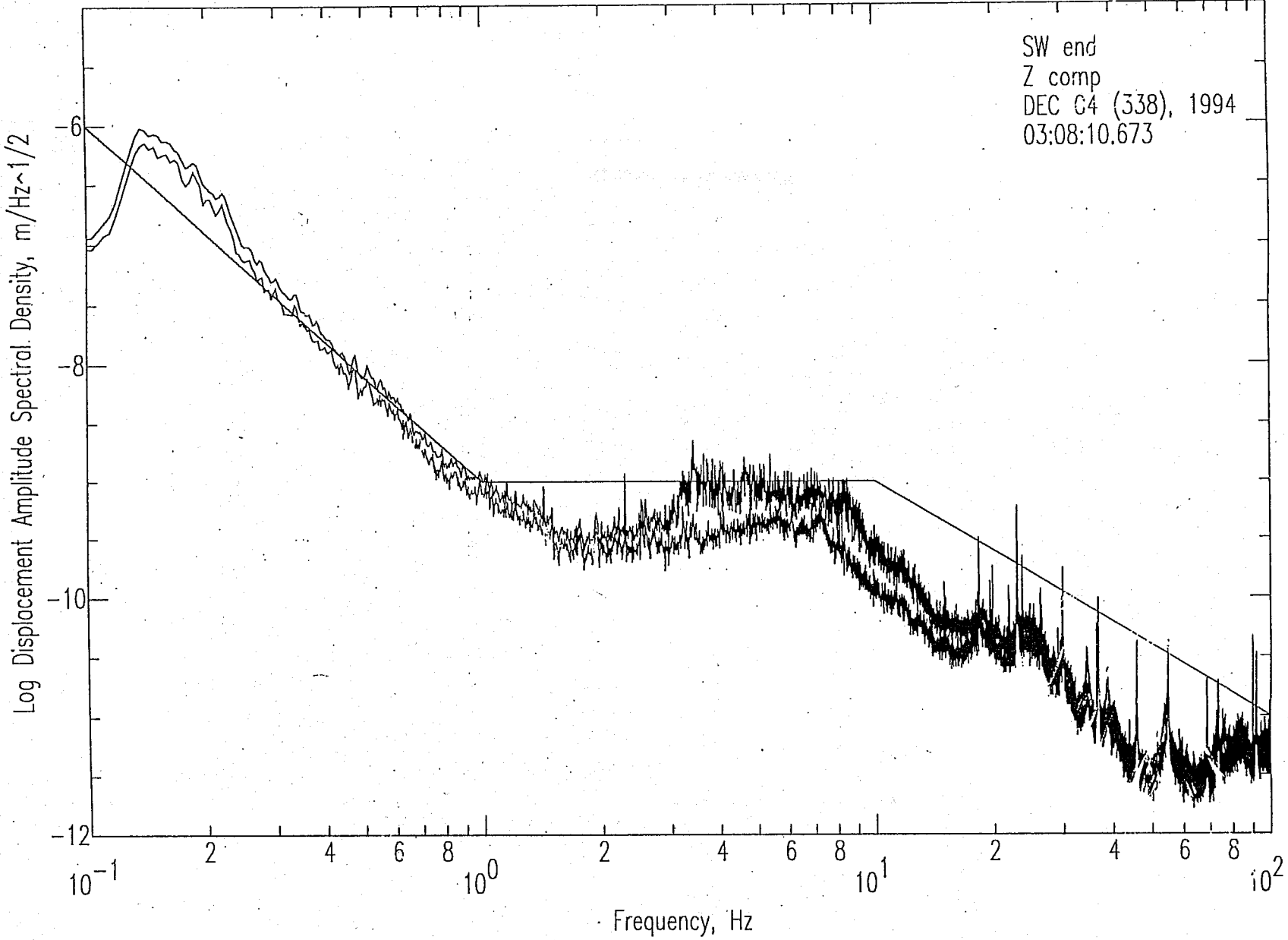

Figure 6-4: Vertical-component median and r.m.s. amplitude spectra for the one-hour time period, Day 338, GMT hour 03 (7 p.m. - 8 p.m. PST) at the Southwest End. The spectrograms for this time period were shown in Figure 5-2 and 5-3. Note the presence of the set of "line spectra", and the effect of the two instances of "traffic" noise at mid-frequencies (3 - 10 Hz).

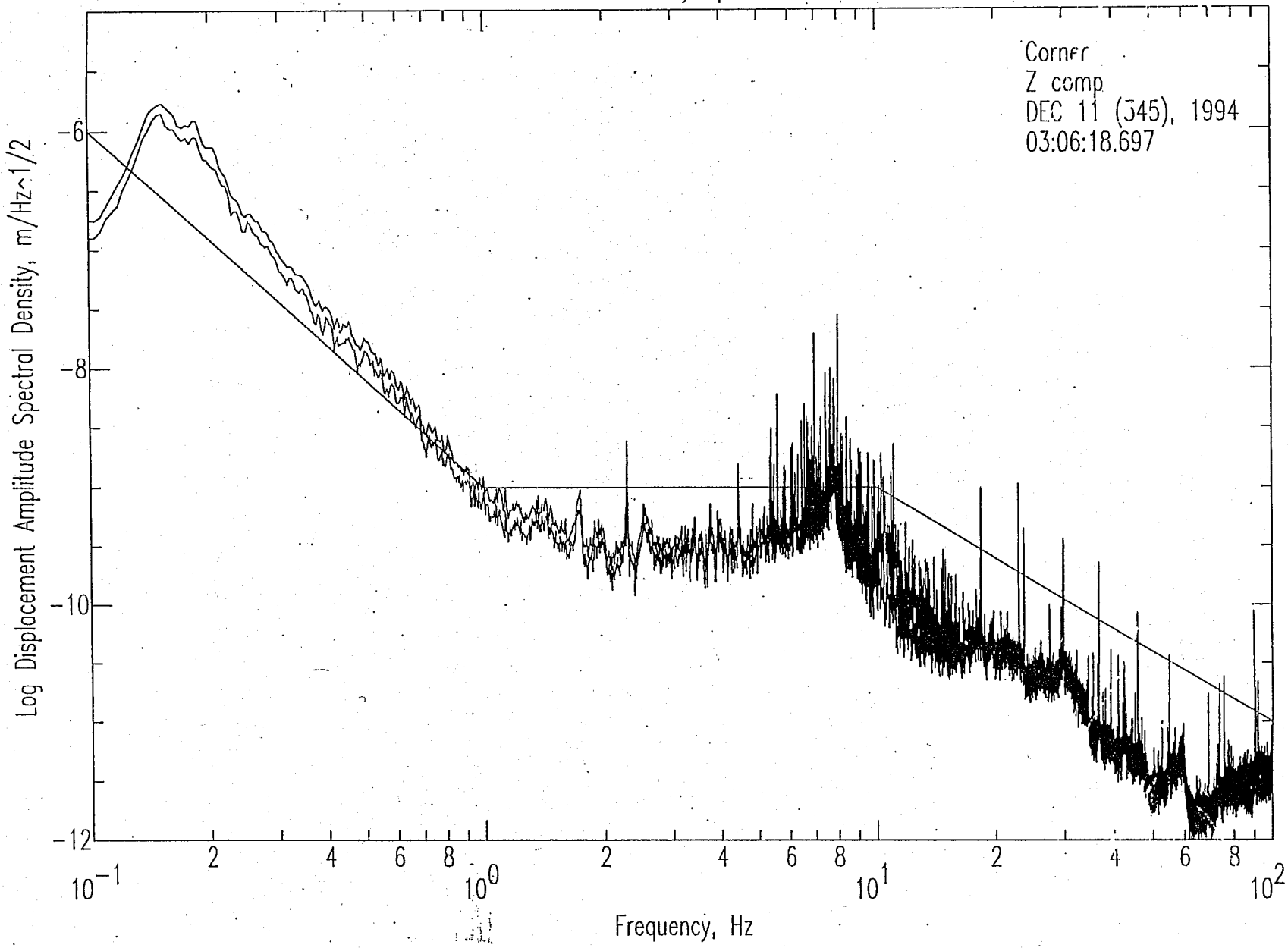

Figure 6-5: Vertical-component median and r.m.s. amplitude spectra for the one-hour time period, Day 345, GMT hour 03 (7 p.m. - 8 p.m. PST) at the Corner. The spectrograms for this time period were shown in Figure 5-4 and 5-5. The line spectra occur at many of the same frequencies as shown in Figure 6-4 for the Southwest End, but there are higher spectral amplitudes near 8 Hz (shown in detail on the displacement spectrogram in Figure 5-5).

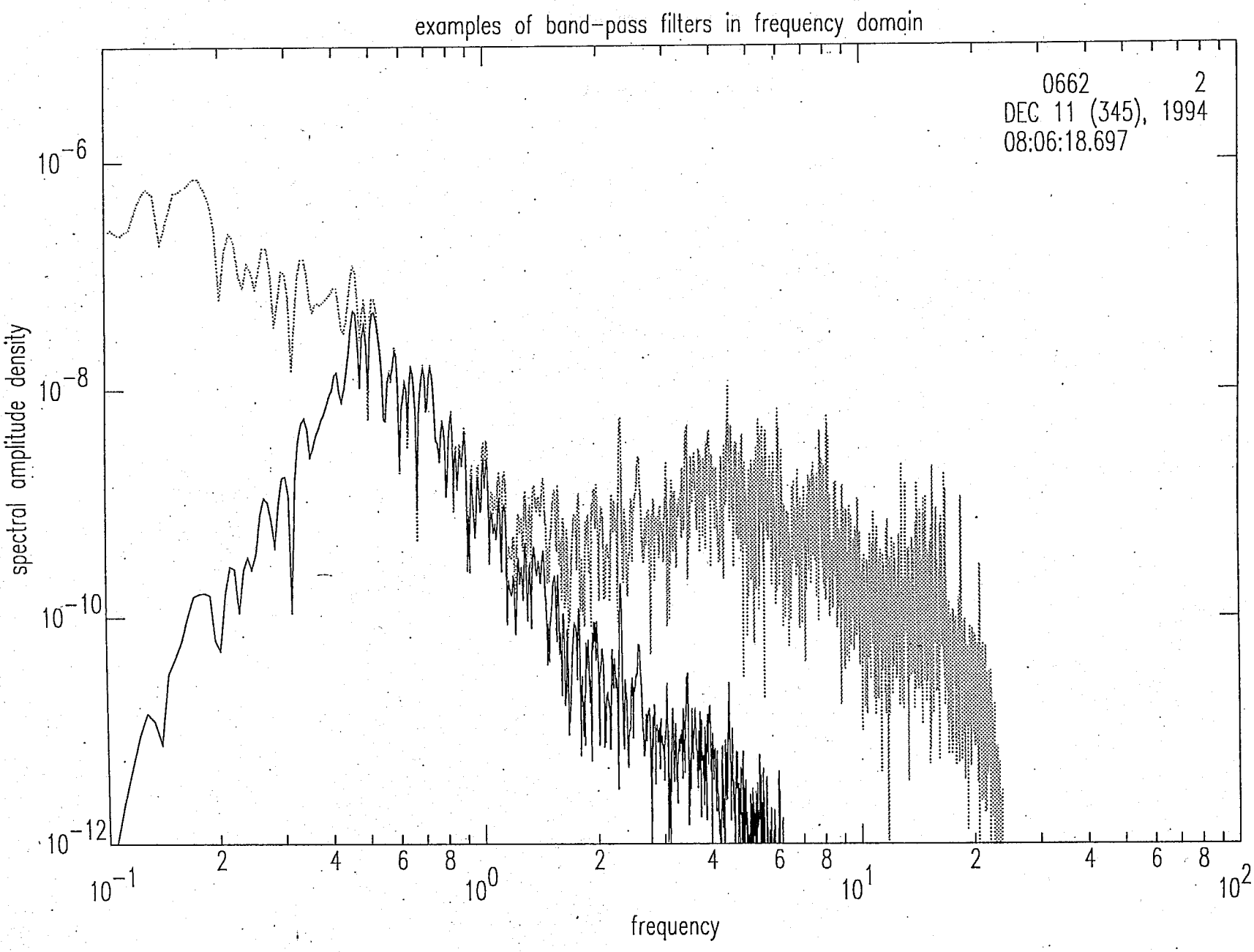

Figure 7-1: Effect of band-pass filtering 0.5 - 1.0 Hz. An 8-pole Butterworth filter is applied at 0.5 Hz, and a 4-pole Butterworth high-cut filter is applied at 1.0 Hz.

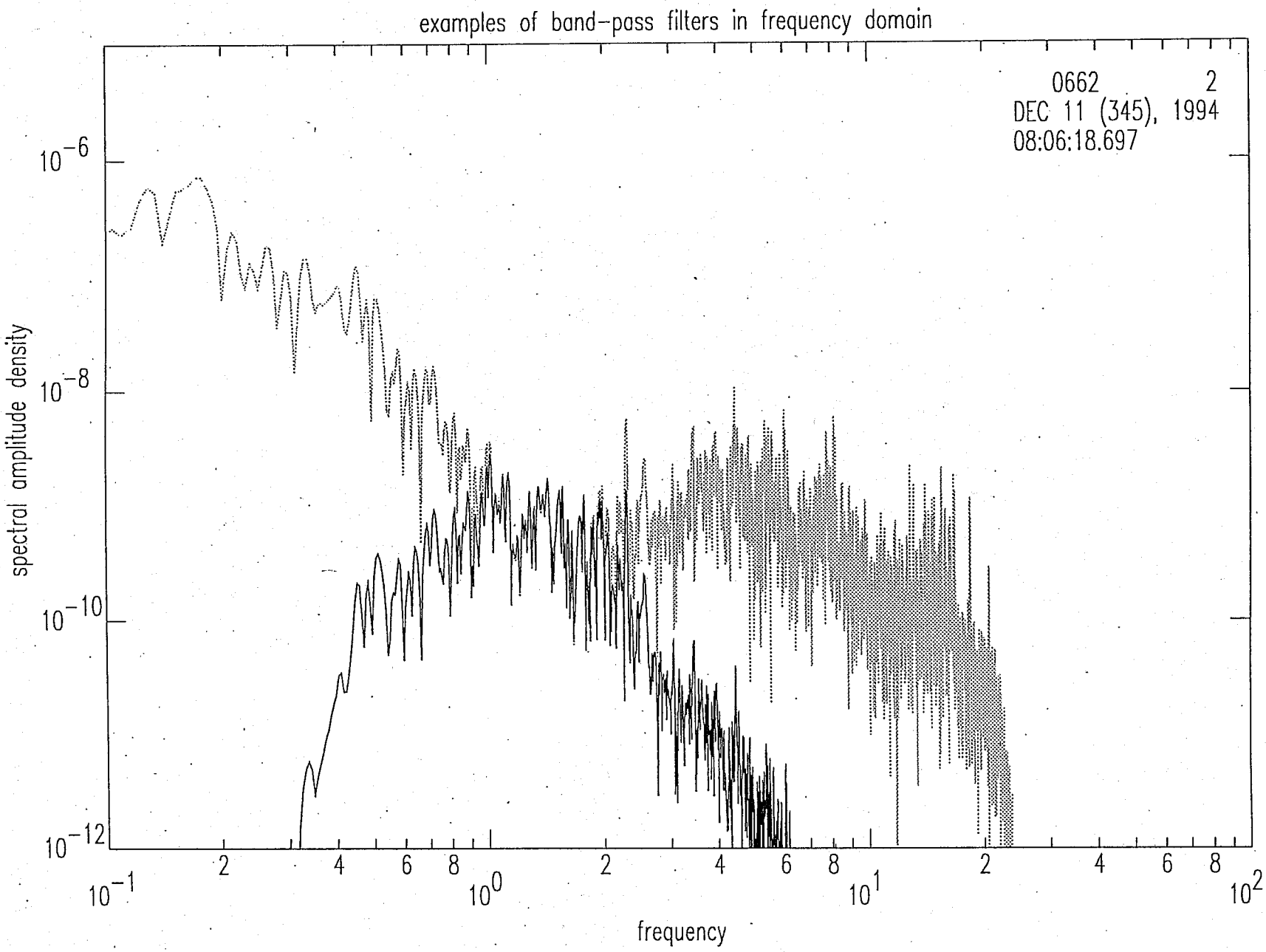

Figure 7-2: Effect of band-pass filtering 1.0 - 2.0 Hz. 4-pole Butterworth filters are used at 1.0 and 2.0 Hz. The effect of previous filtering at 0.5 Hz is still evident in this plot.

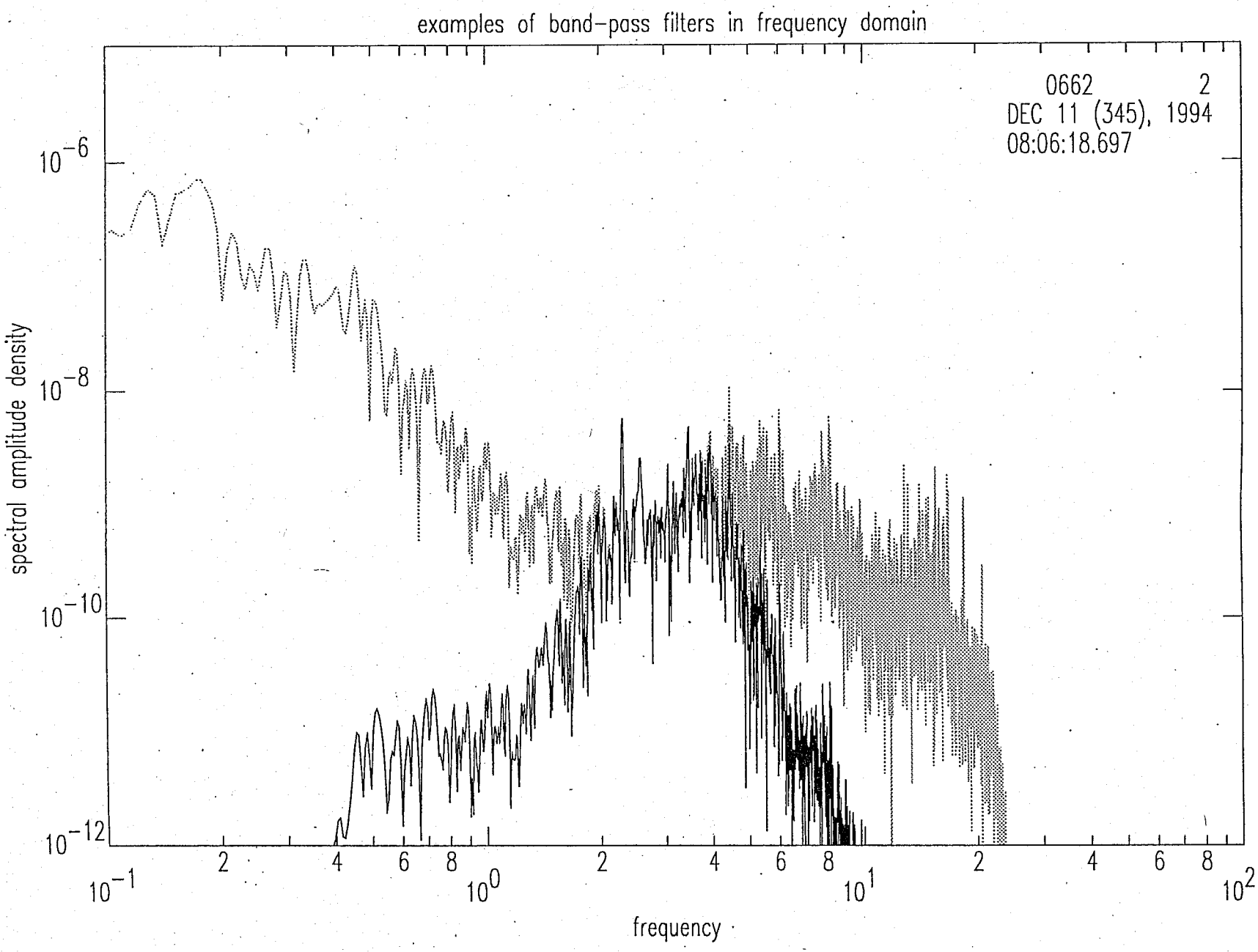

Figure 7-3: Effect of band-pass filtering 2.0 - 4.0 Hz. 4-pole Butterworth filters are used at 2.0 and 4.0 Hz. The effect of previous filtering at 0.5 Hz is still evident in this plot.

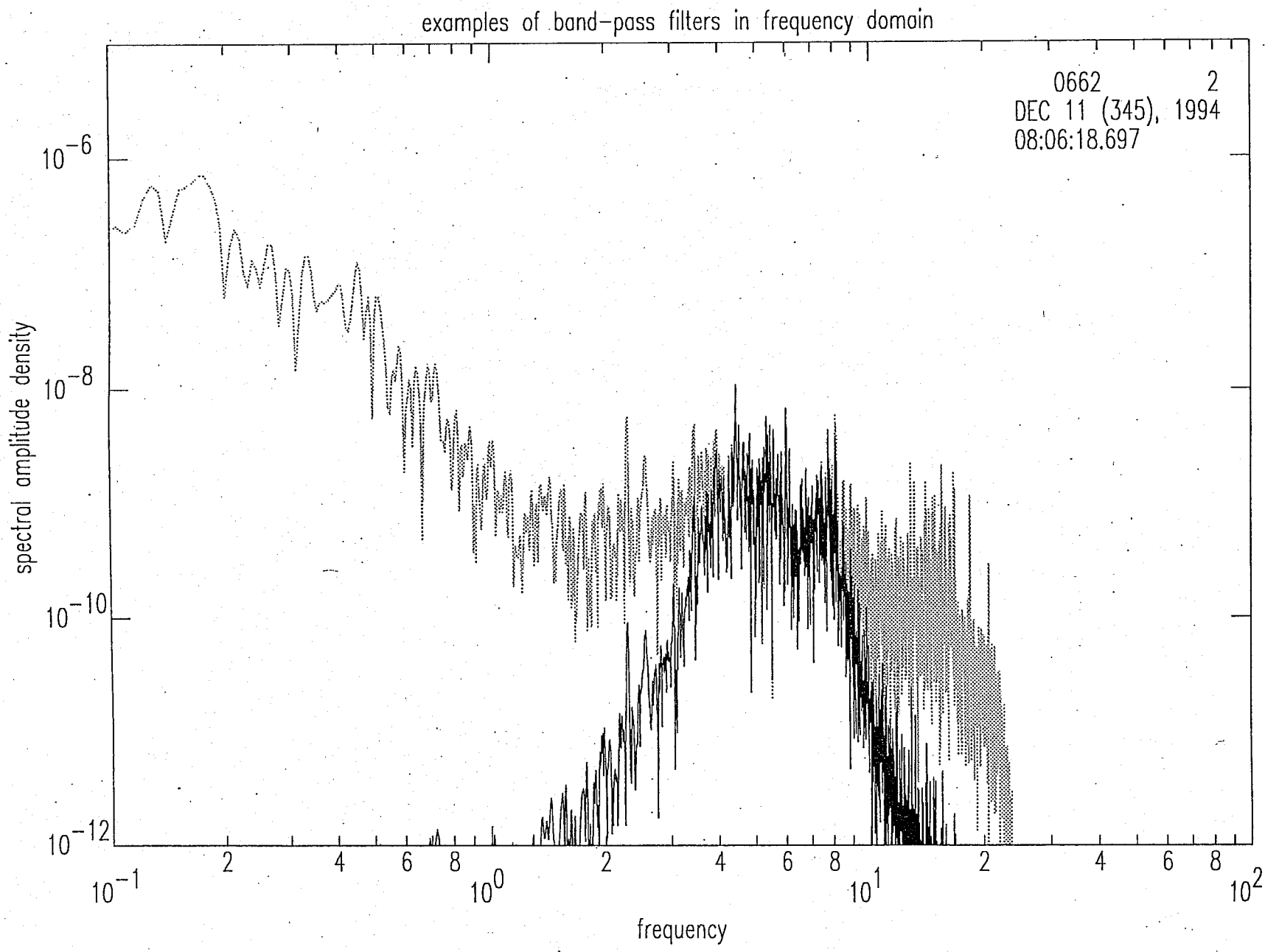

Figure 7-4: Effect of band-pass filtering 4.0 - 8.0 Hz. 4-pole Butterworth filters are used.

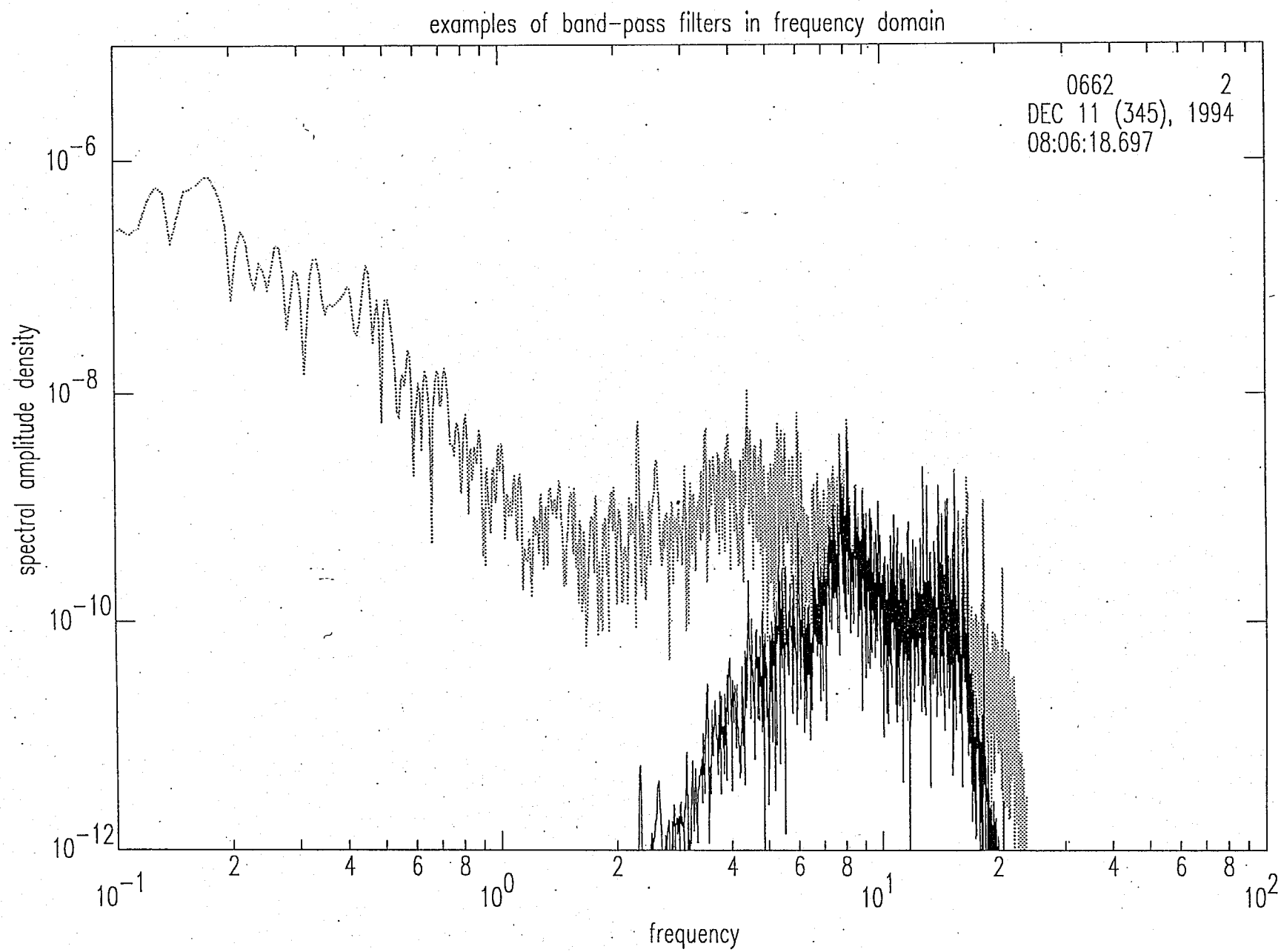

Figure 7-5: Effect of band-pass filtering 8.0 - 16.0 Hz. 4-pole Butterworth filters are used.

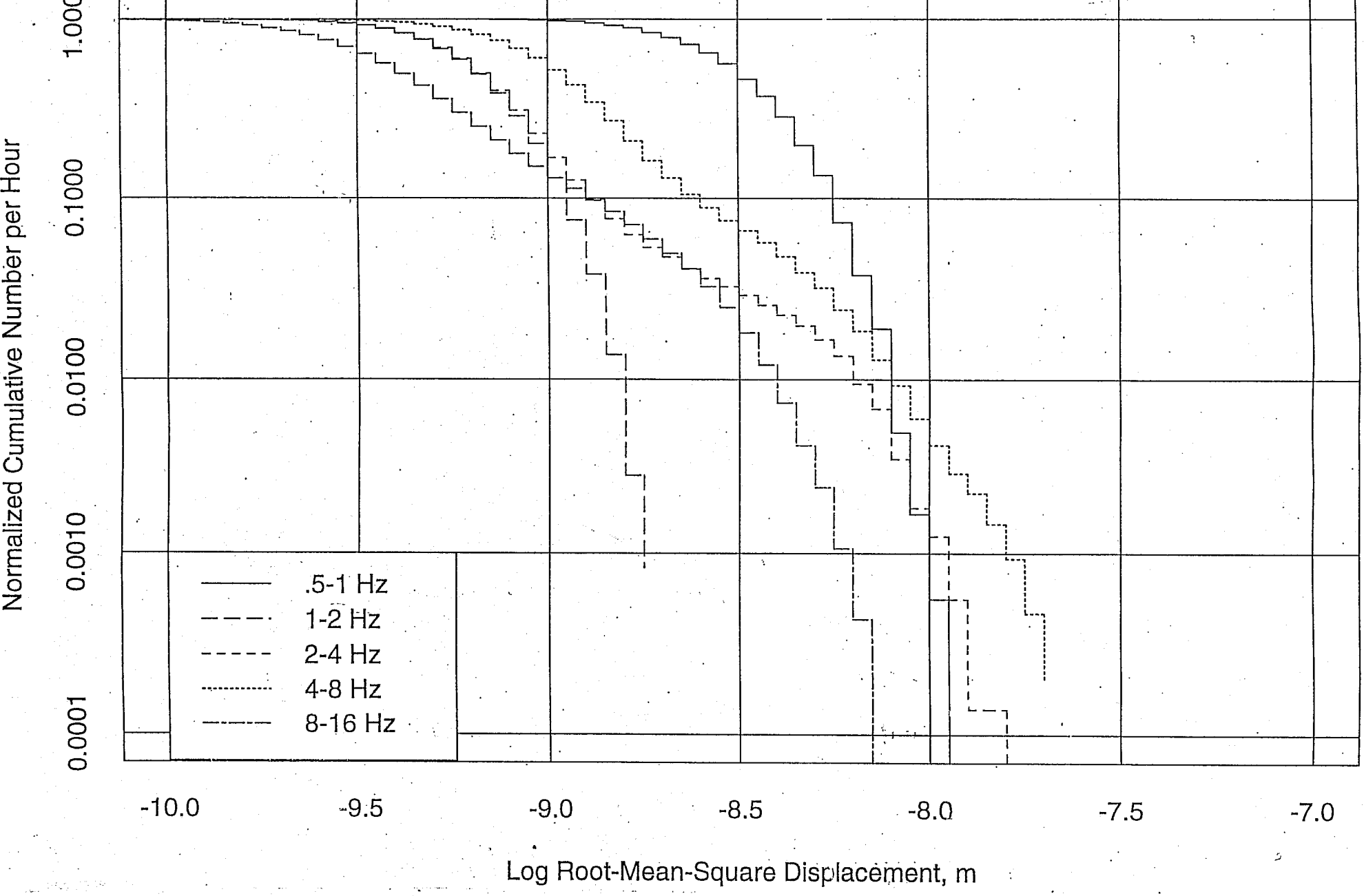

Figure 7-6: Vertical displacement histogram for the five frequency ranges for Day 338, Hour 03 at the Southwest End. As an example, the r.m.s. displacement for the frequency band 0.5 - 1.0 Hz exceeds 10^{-9} m 100% of the one-hour period, and exceeds $10^{-8.25}$ m 10% of the period. This time period corresponds to the spectrogram shown in Figure 5-2, and the amplitude spectrum shown in Figure 6-4.

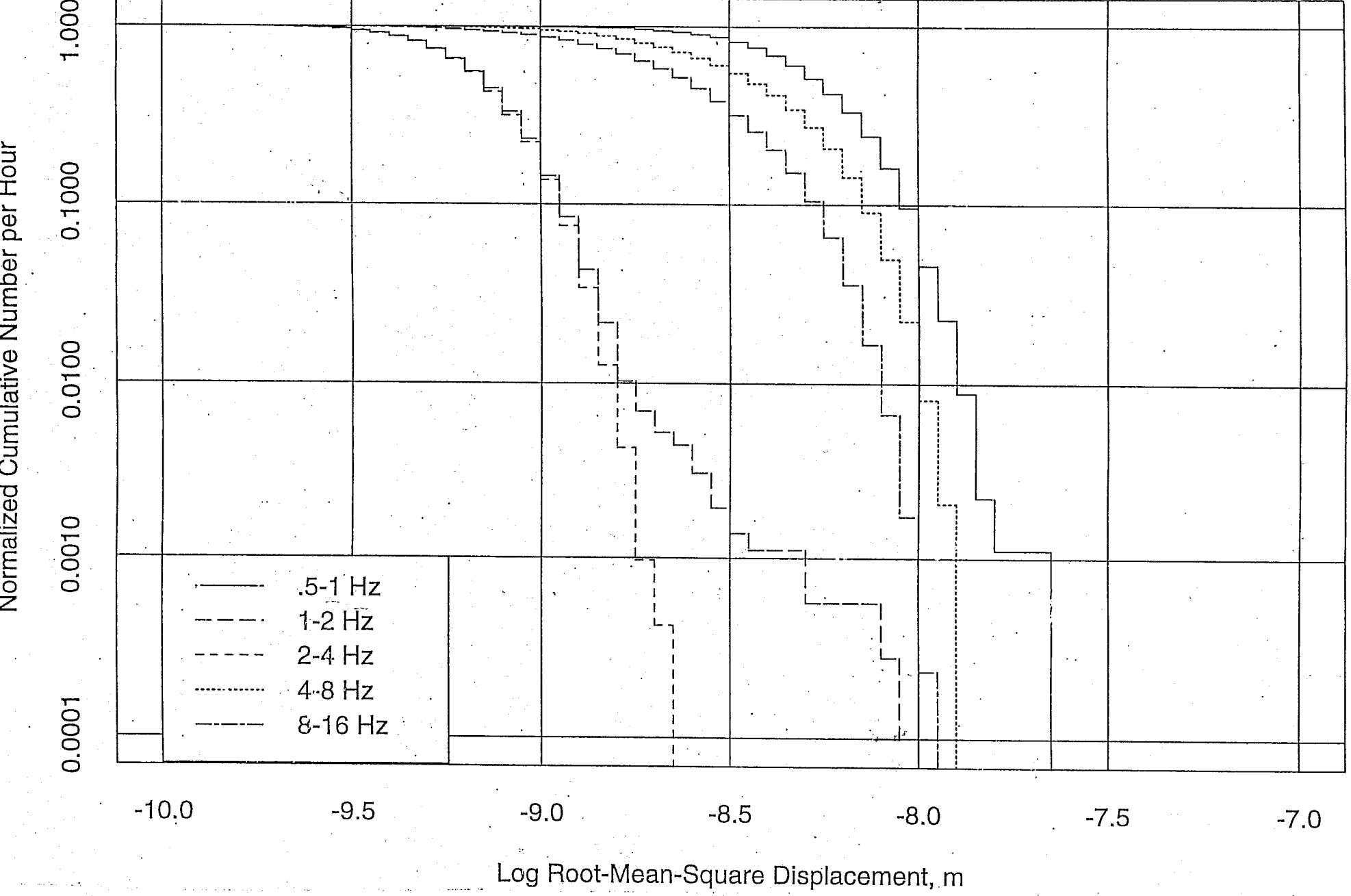

Figure 7-7: Vertical displacement histogram for Day 345, Hour 03 at the Corner. Larger displacements are observed more frequently in the 4.0 - 8.0 Hz frequency band compared to Figure 7-6. This time period corresponds to the spectrograms shown in Figure 5-4 and 5-5, and the amplitude spectra shown in Figure 6-5. This time period at the Corner station is characterized by higher-amplitude noise at frequencies around 8 Hz.

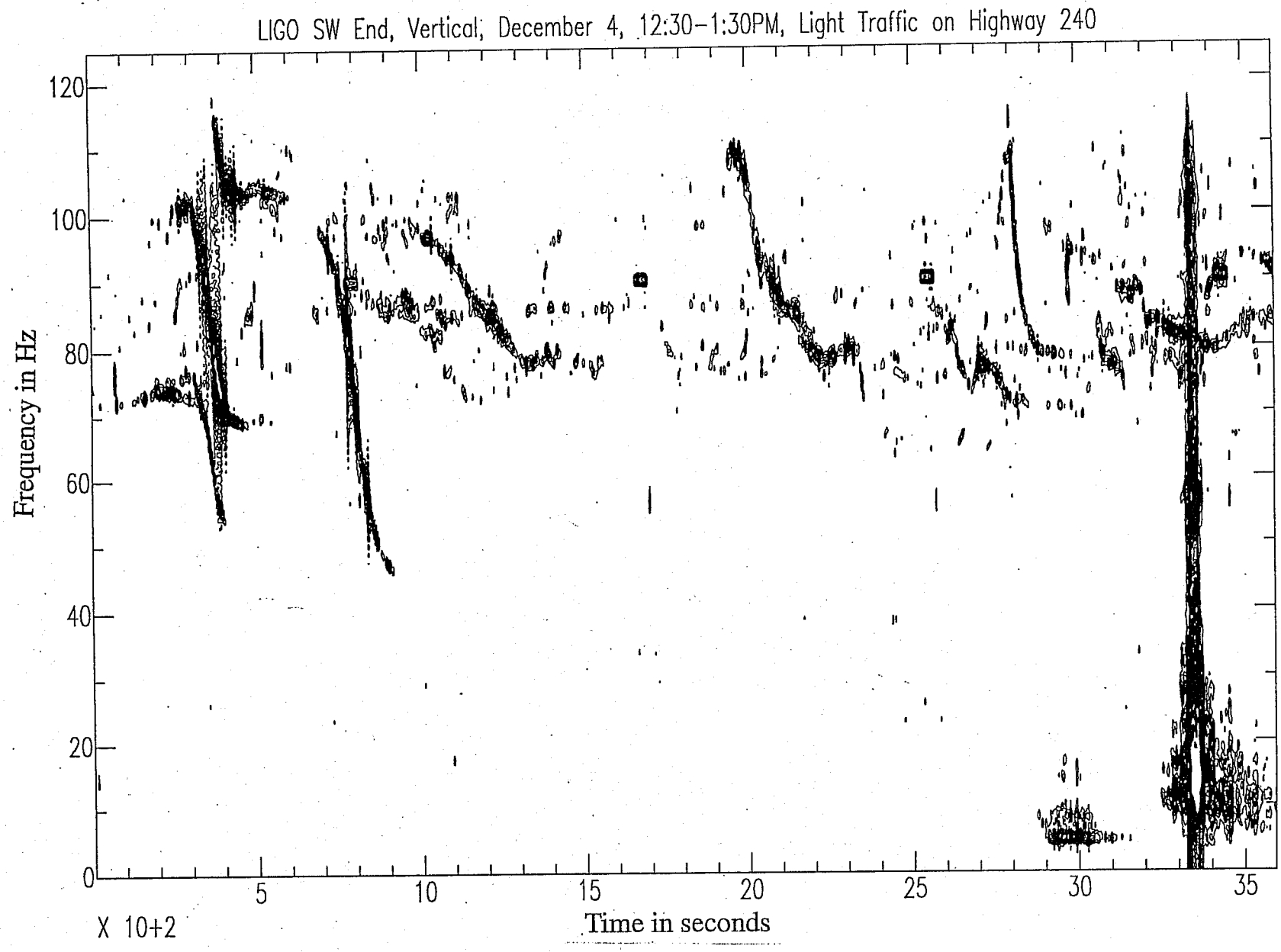

Figure 8.1-1: Spectrogram of vertical seismic signal from Southwest End during videotape of light traffic on Highway 240. Note the dominant presence of "glide tones" attributed to aircraft. The noise at low frequency at 3000 to 3350 s is from a vehicle being driven past, and later to the recording site.

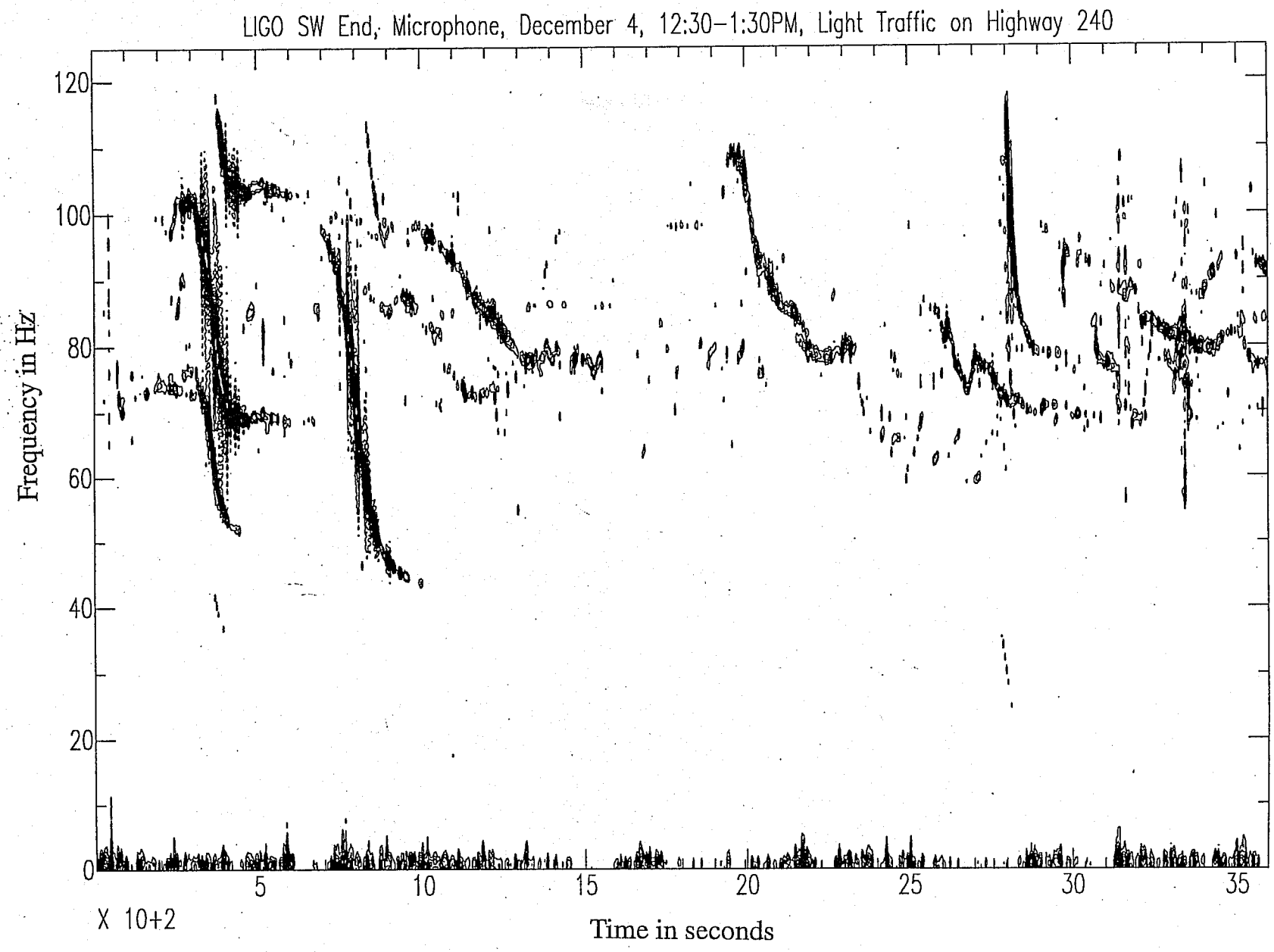

Figure 8.1-2: Spectrogram of microphone signal corresponding to the seismic signal in Figure 8.1-1. Note that the "glide tones" are acoustically transmitted from aircraft (only the first was audible on the videotape). Also note that the vehicle operating after 3000 s has virtually no acoustic signal.

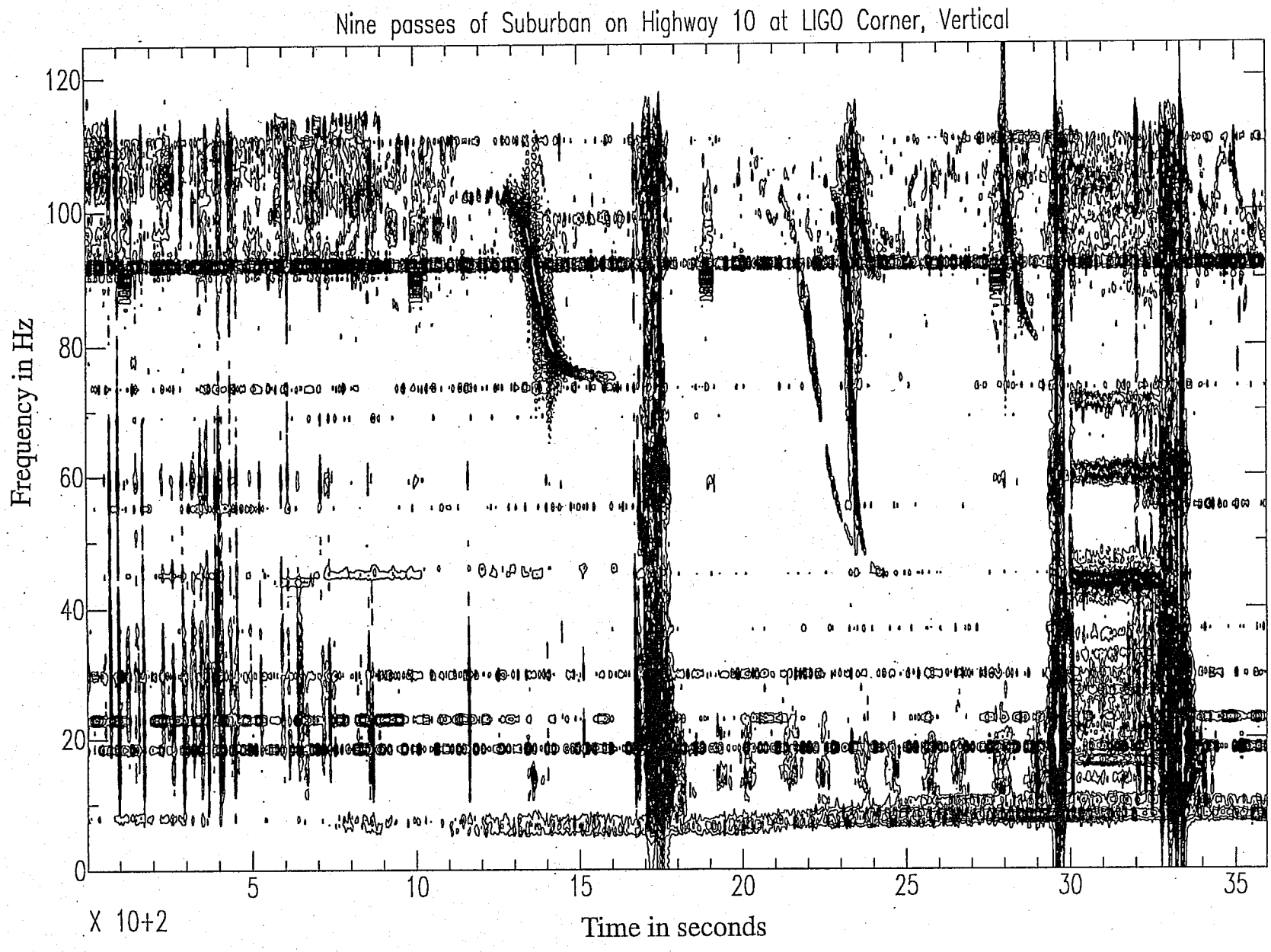

Figure 8.1-3: Spectrogram for vertical component at the Corner during light traffic on Route 10.

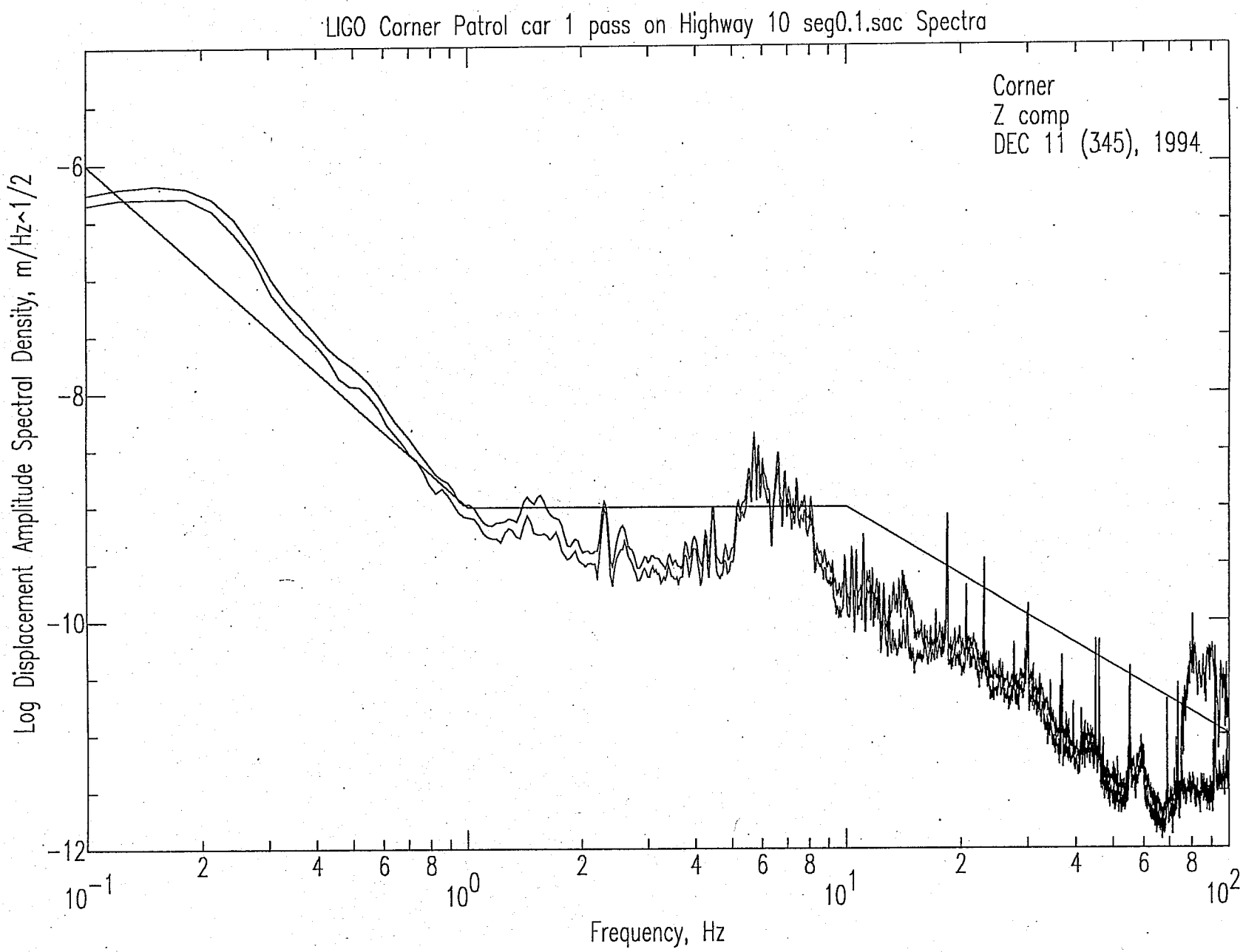

Figure 8.1-4: Amplitude spectra (median and r.m.s.) for the passing patrol car on Route 10 as observed on the vertical component at the Corner.

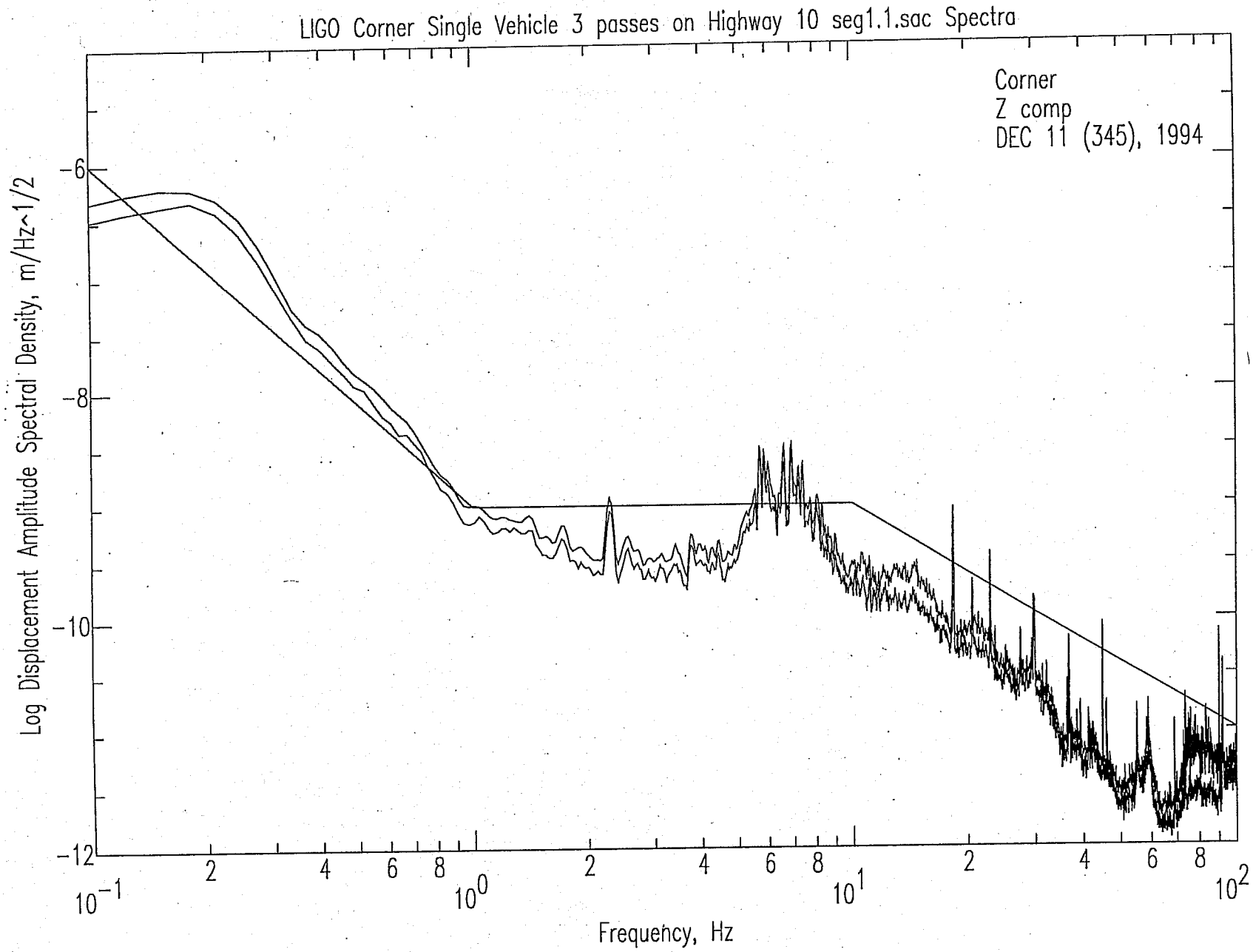

Figure 8.1-5: Amplitude spectra (median and r.m.s.) for three passsings of the Chevrolet Suburban on Route 10 as observed on the vertical component at the Corner. Only a slight increase in noise amplitude can be detected from 12.0 - 16.0 Hz, compared to Figure 8.1-4.

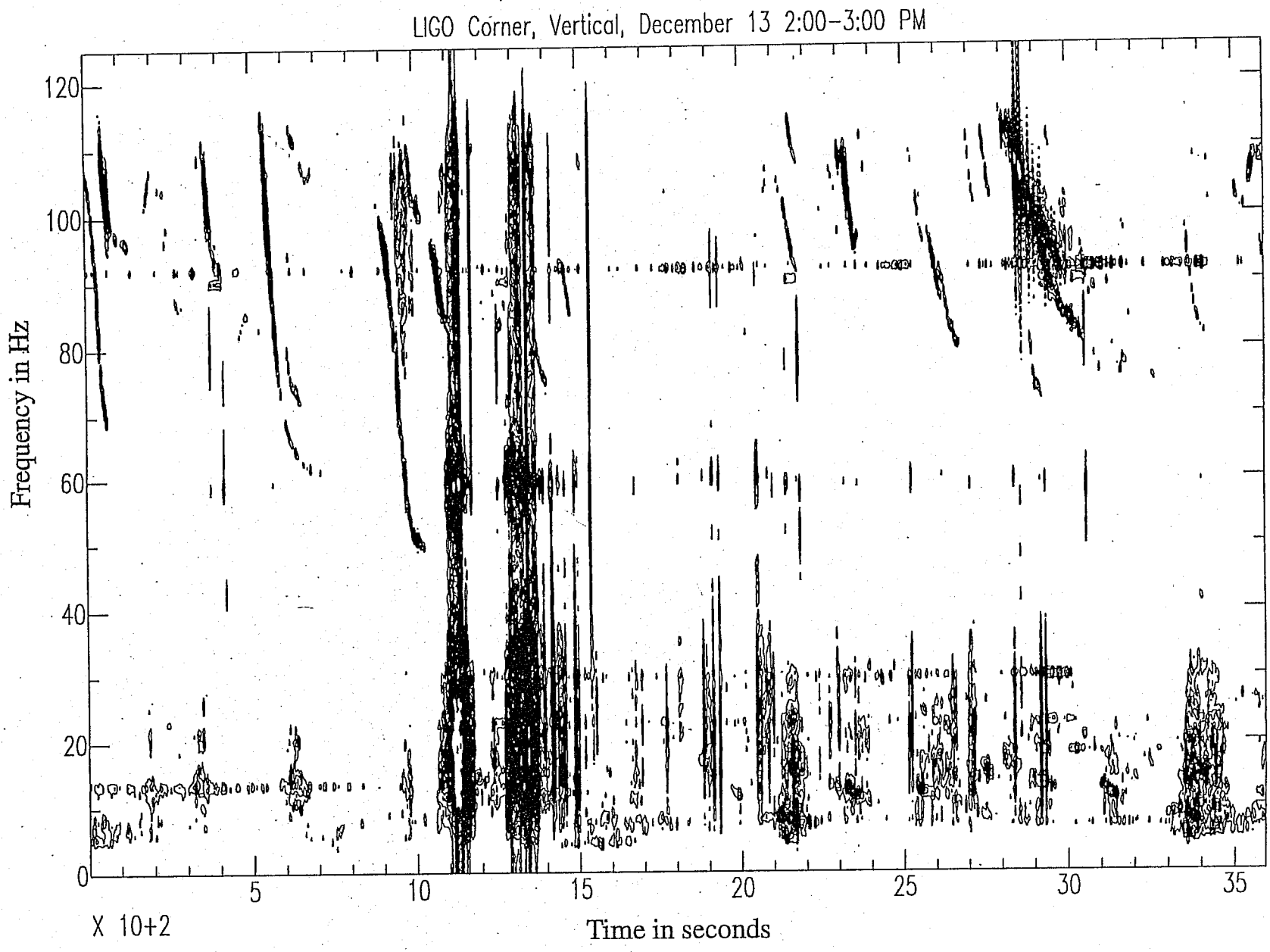

Figure 8.1-6: Vertical component spectrogram during videotaped weekday afternoon traffic at the Corner from 2 - 3 p.m. PST.

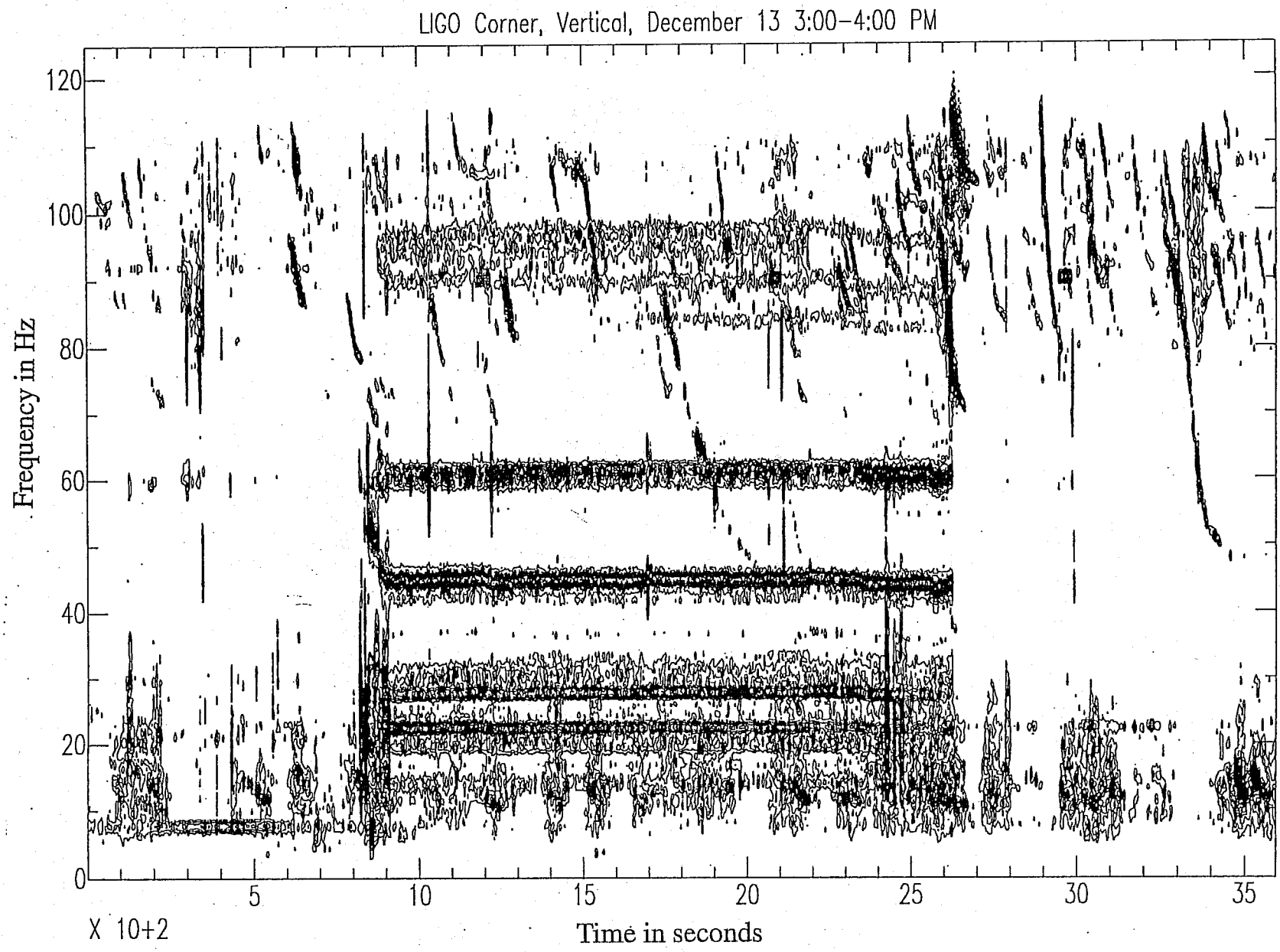

Figure 8.1-7: Vertical component spectrogram during videotaped weekday afternoon traffic at the Corner from 3 - 4 p.m. PST.

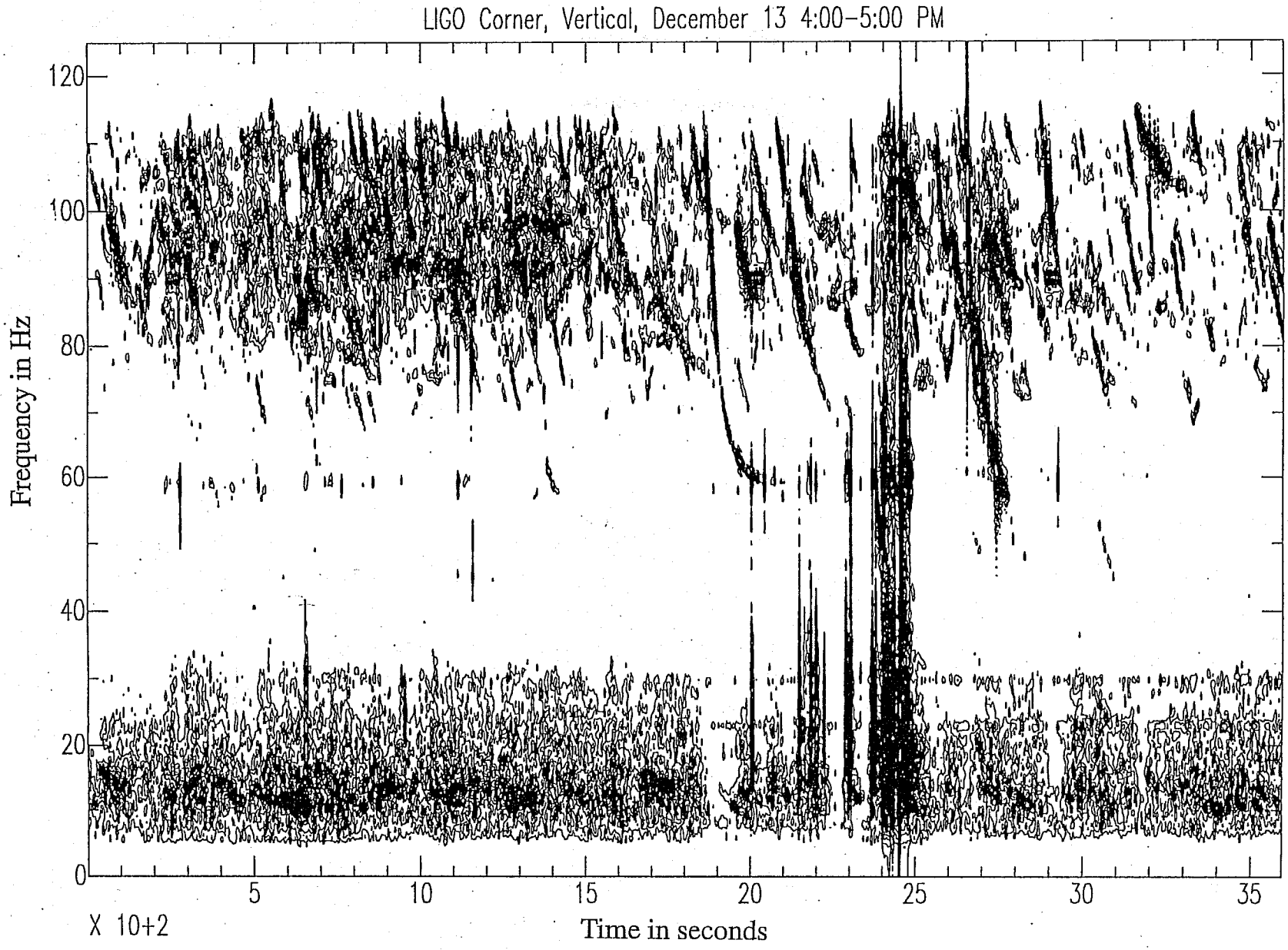

Figure 8.1-8: Vertical component spectrogram during videotaped weekday afternoon traffic at the Corner from 4 - 5 p.m. PST.

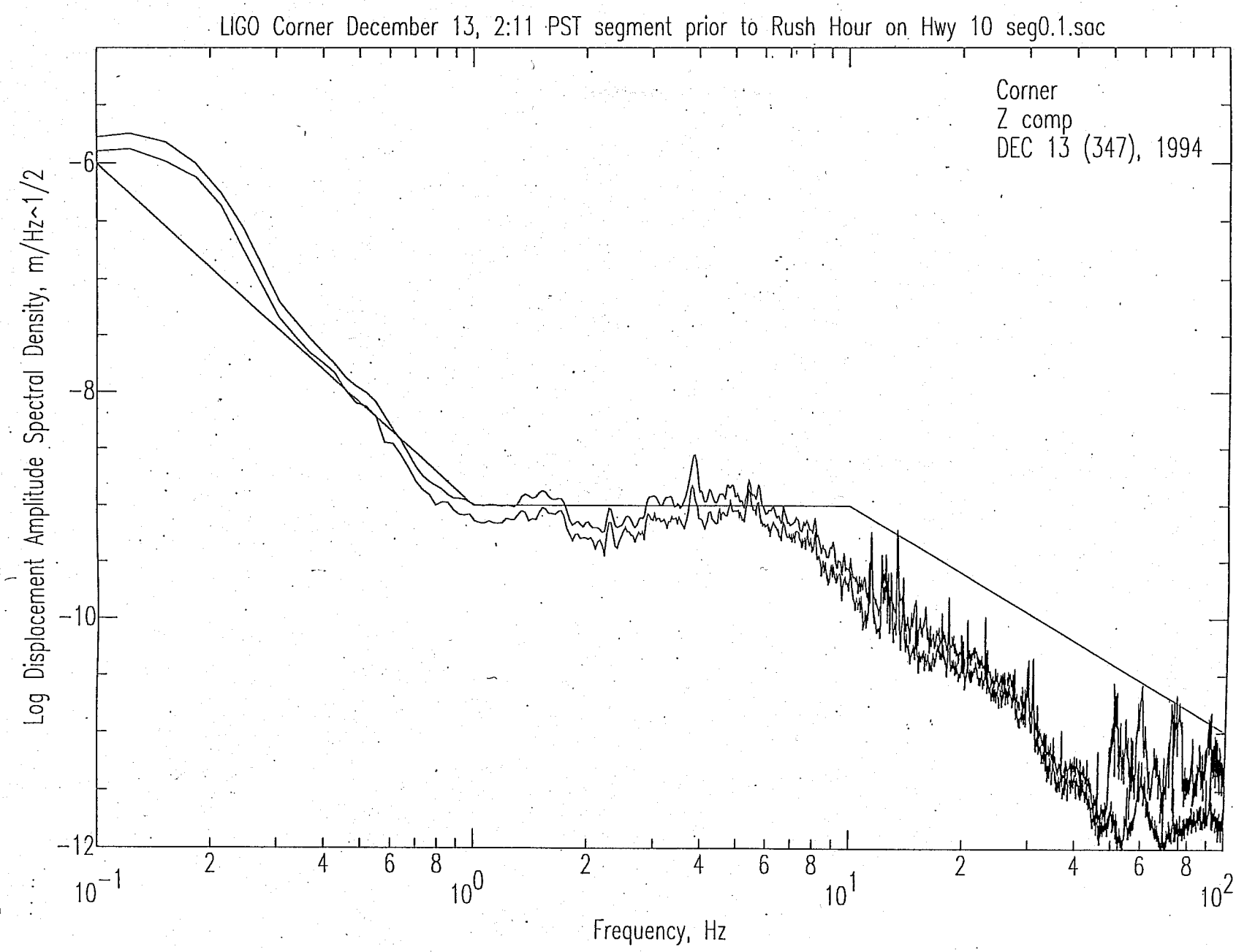

Figure 8.1-9: Vertical component amplitude spectra at the Corner on weekday afternoon prior to rush hour traffic. This time period corresponds to 680 - 1040 s on the 2 p.m. spectrogram in Figure 8.1-6.

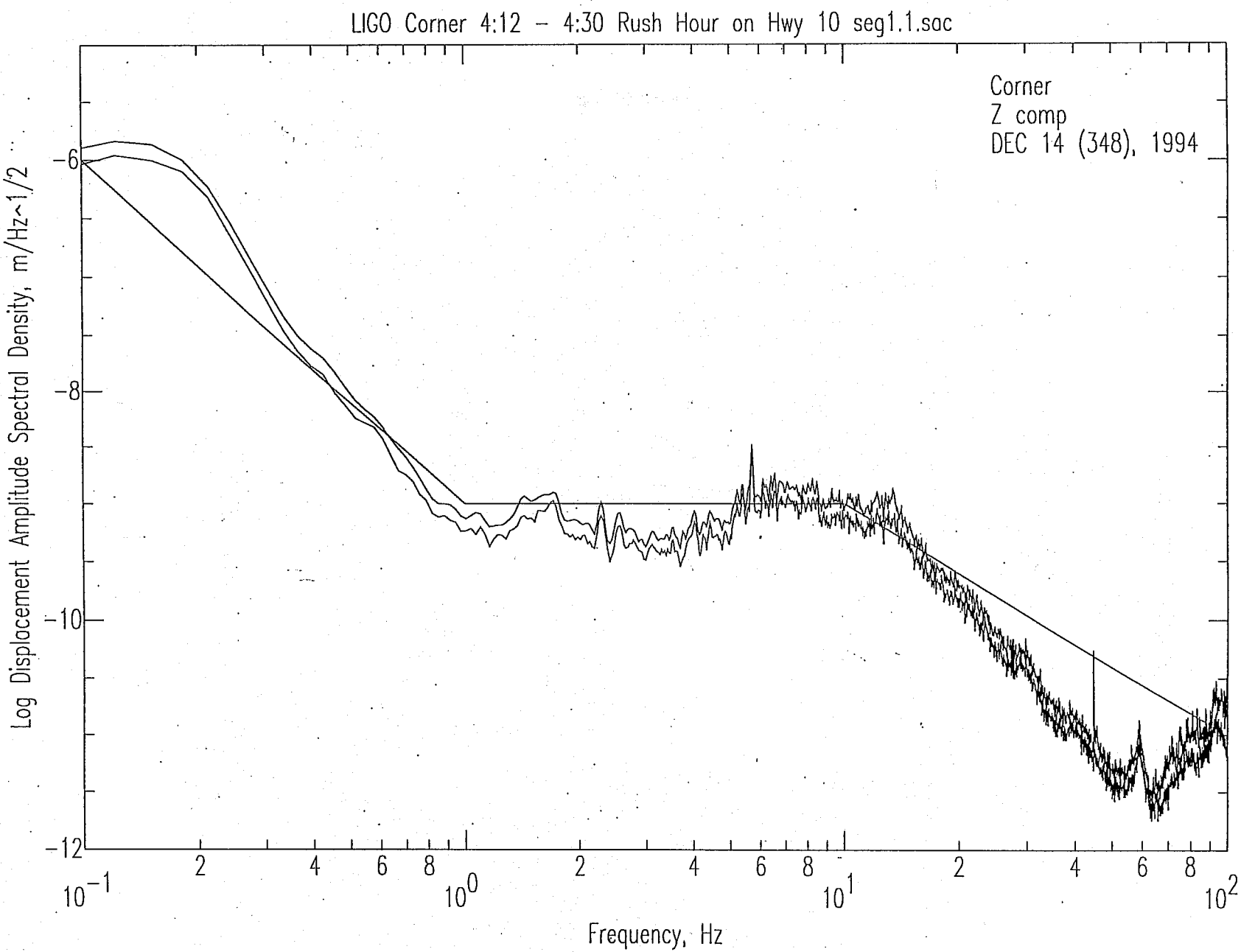

Figure 8.1-10: Vertical component amplitude spectra at the Corner on weekday afternoon during rush hour traffic. This time period corresponds to 720 - 1080 s of the 4 p.m. spectrogram in Figure 8.1-8.

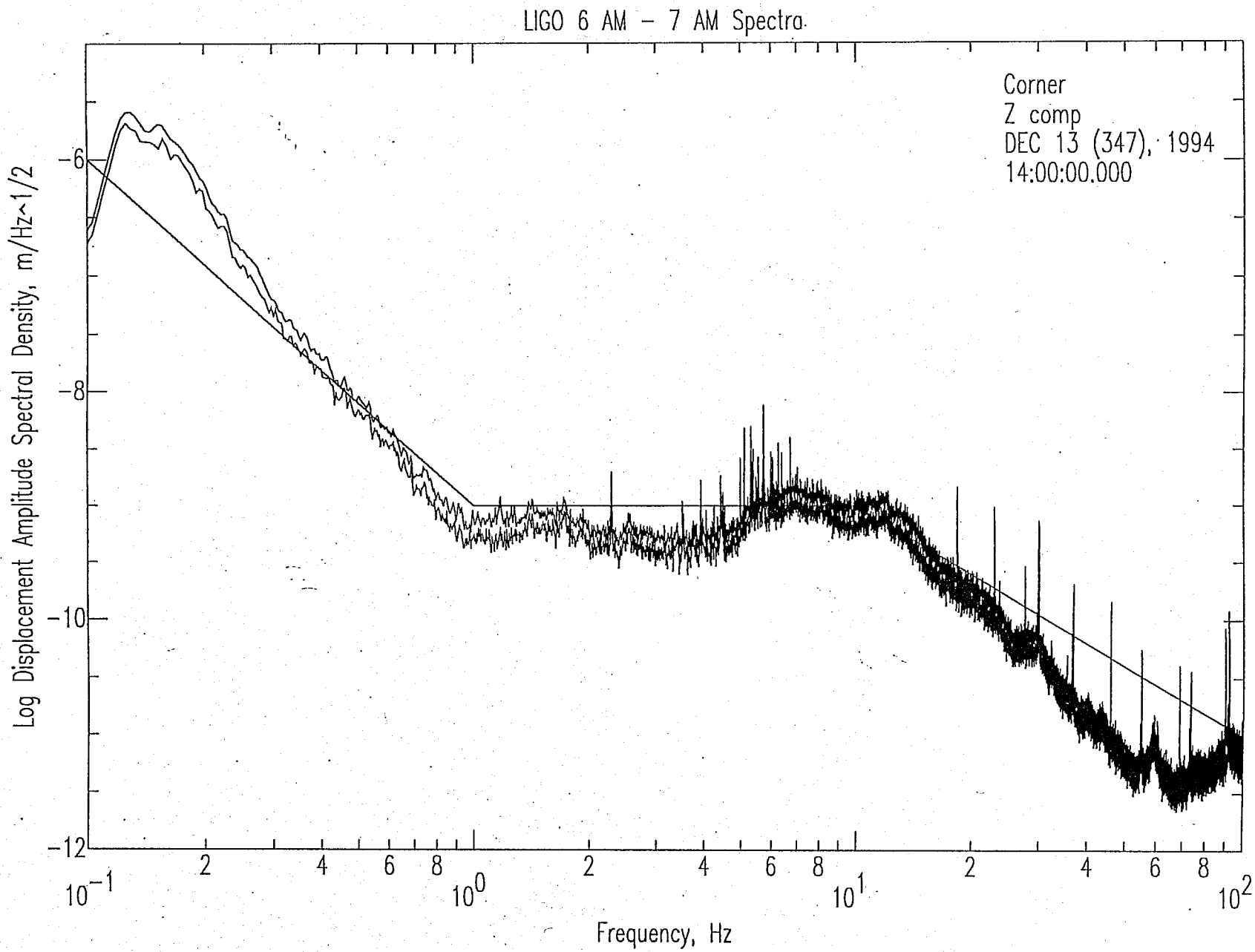

Figure 8.1-11: Vertical component amplitude spectra at the Corner during weekday morning rush hour.

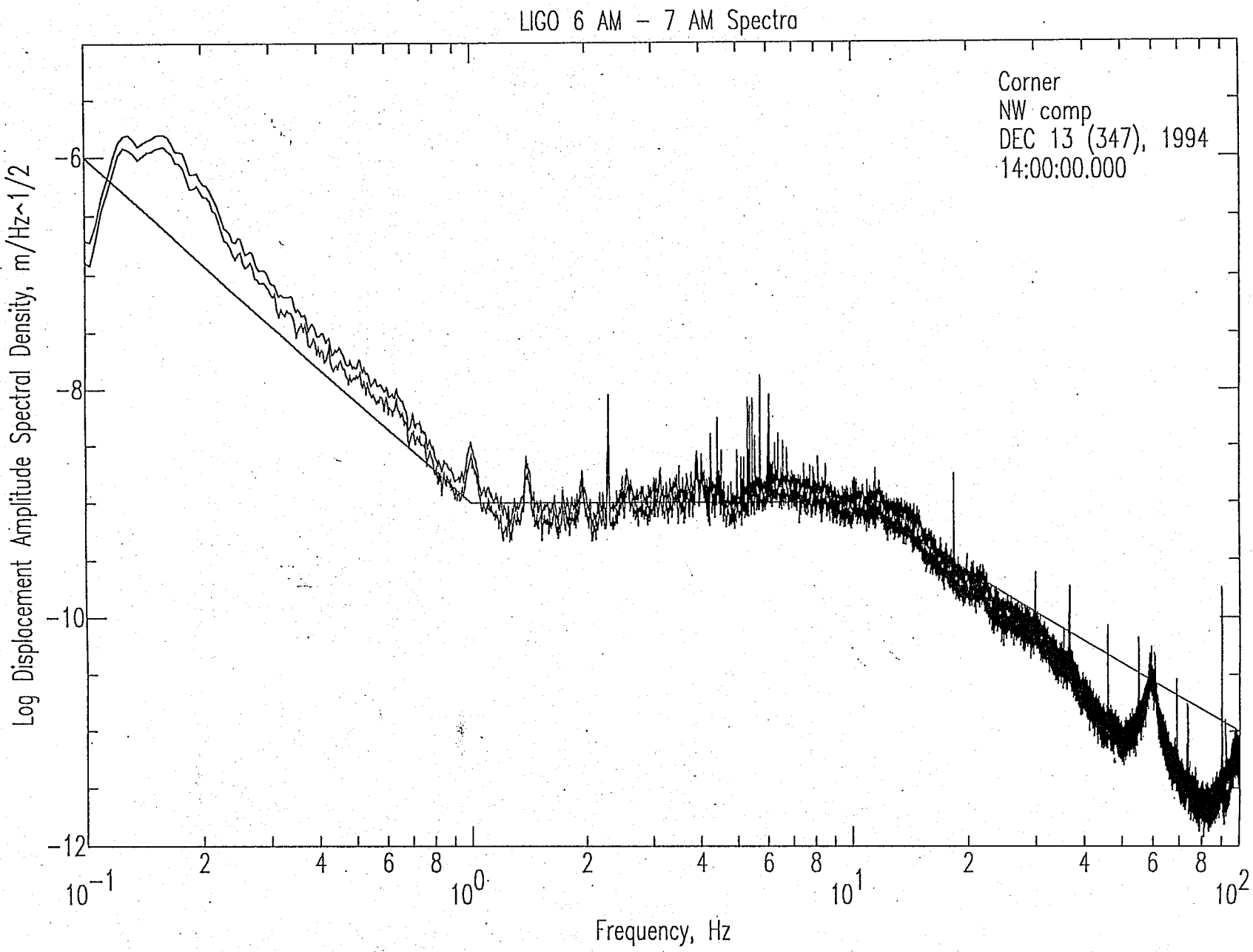

Figure 8.1-12: Northwest component amplitude spectra at the Corner during weekday morning rush hour.

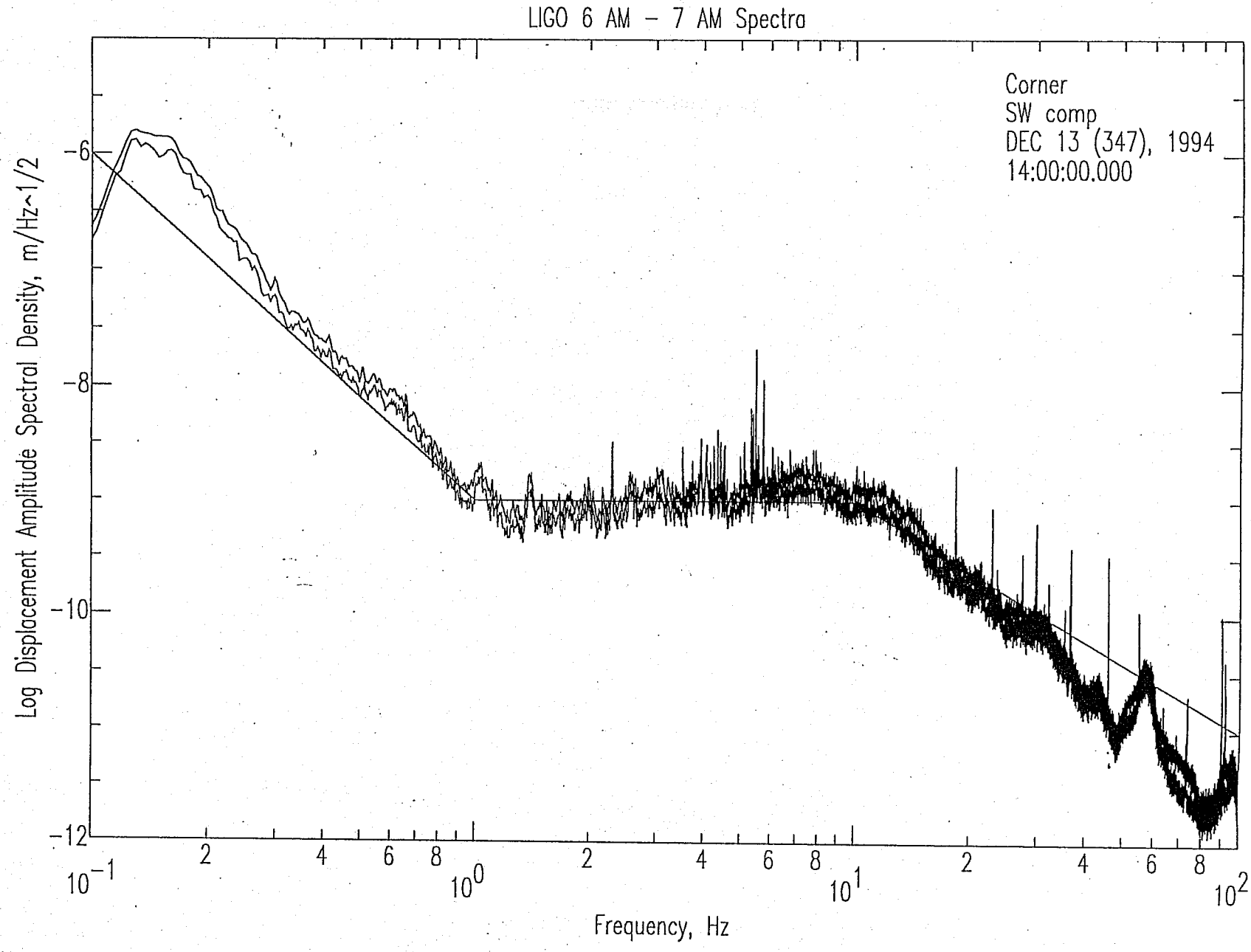

Figure 8.1-13: Southwest component amplitude spectra at the Corner during weekday morning rush hour.

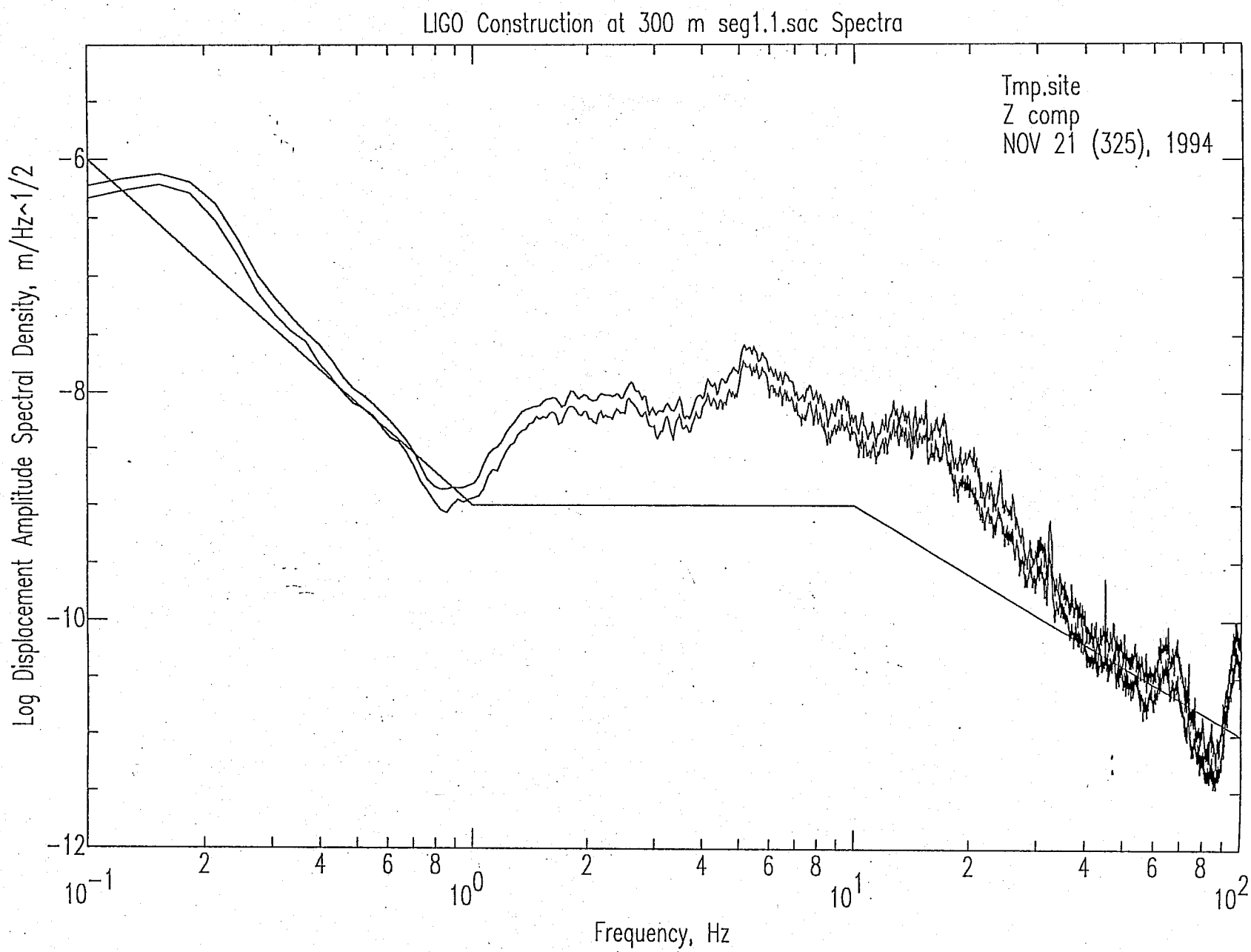

Figure 8.2-1: Vertical component amplitude spectra at a temporary site 300 m from construction activity.

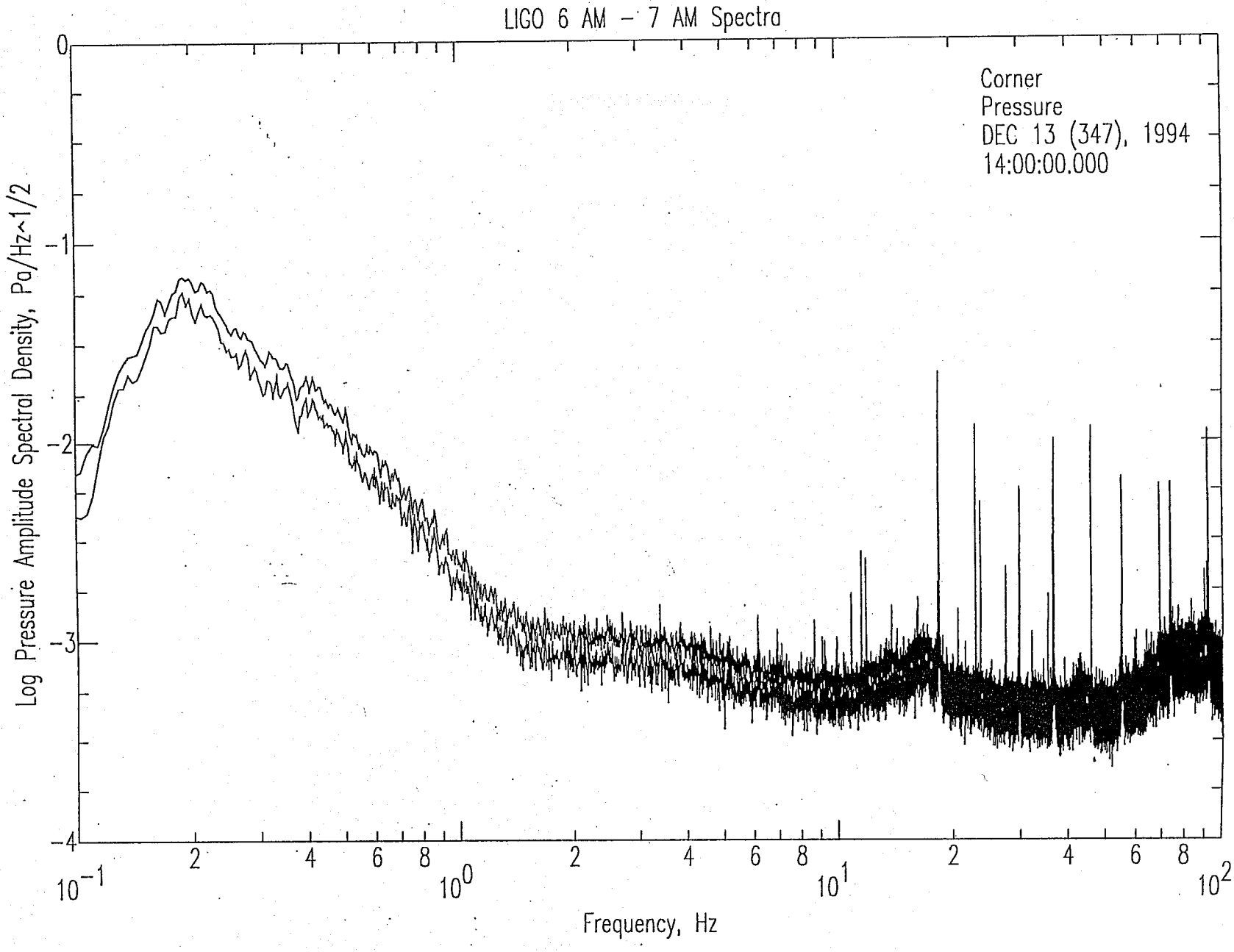

Figure 8.1-14: Sound pressure amplitude spectra at the Corner during weekday morning rush hour.

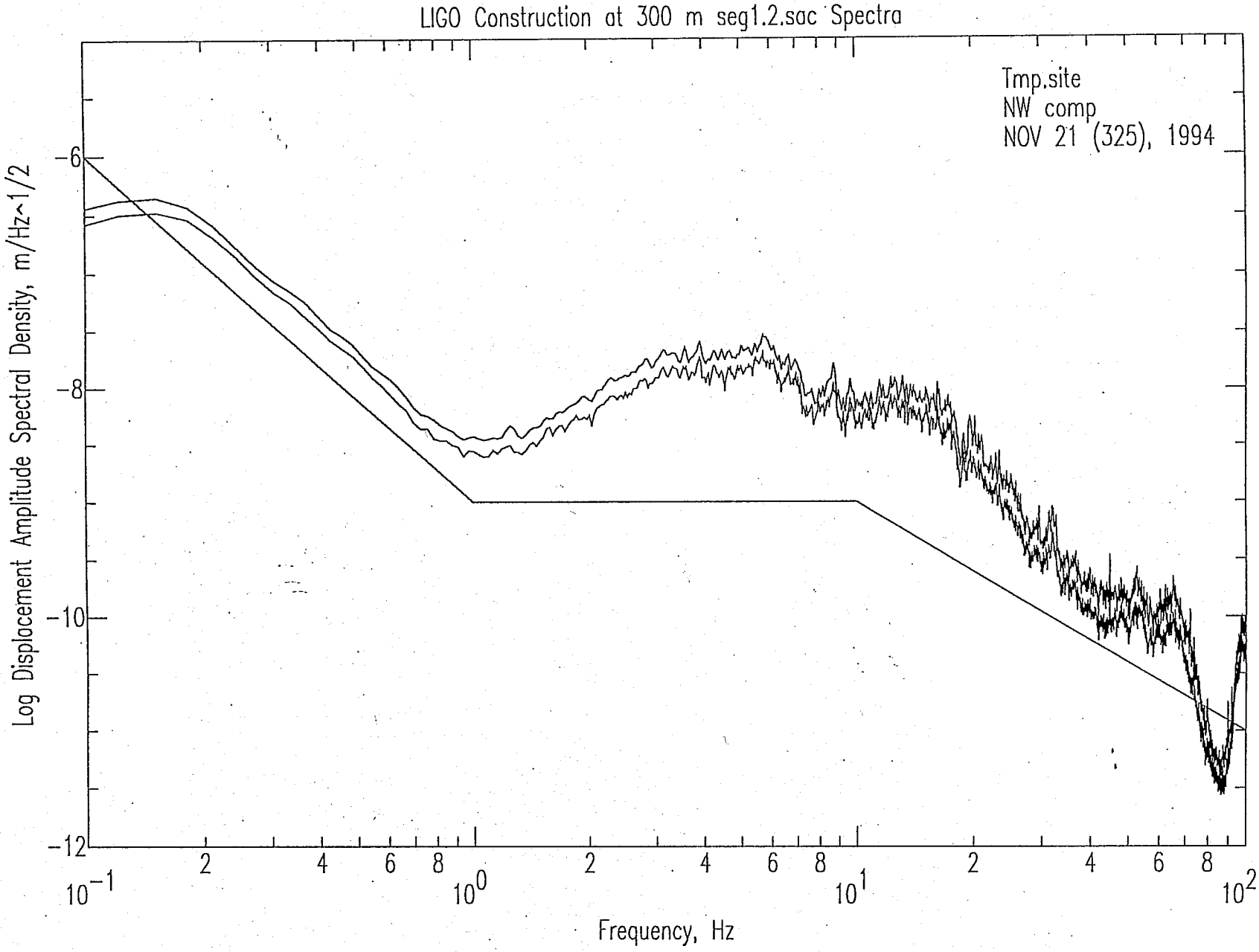

Figure 8.2-2: Northwest component amplitude spectra at a temporary site 300 m from construction activity.

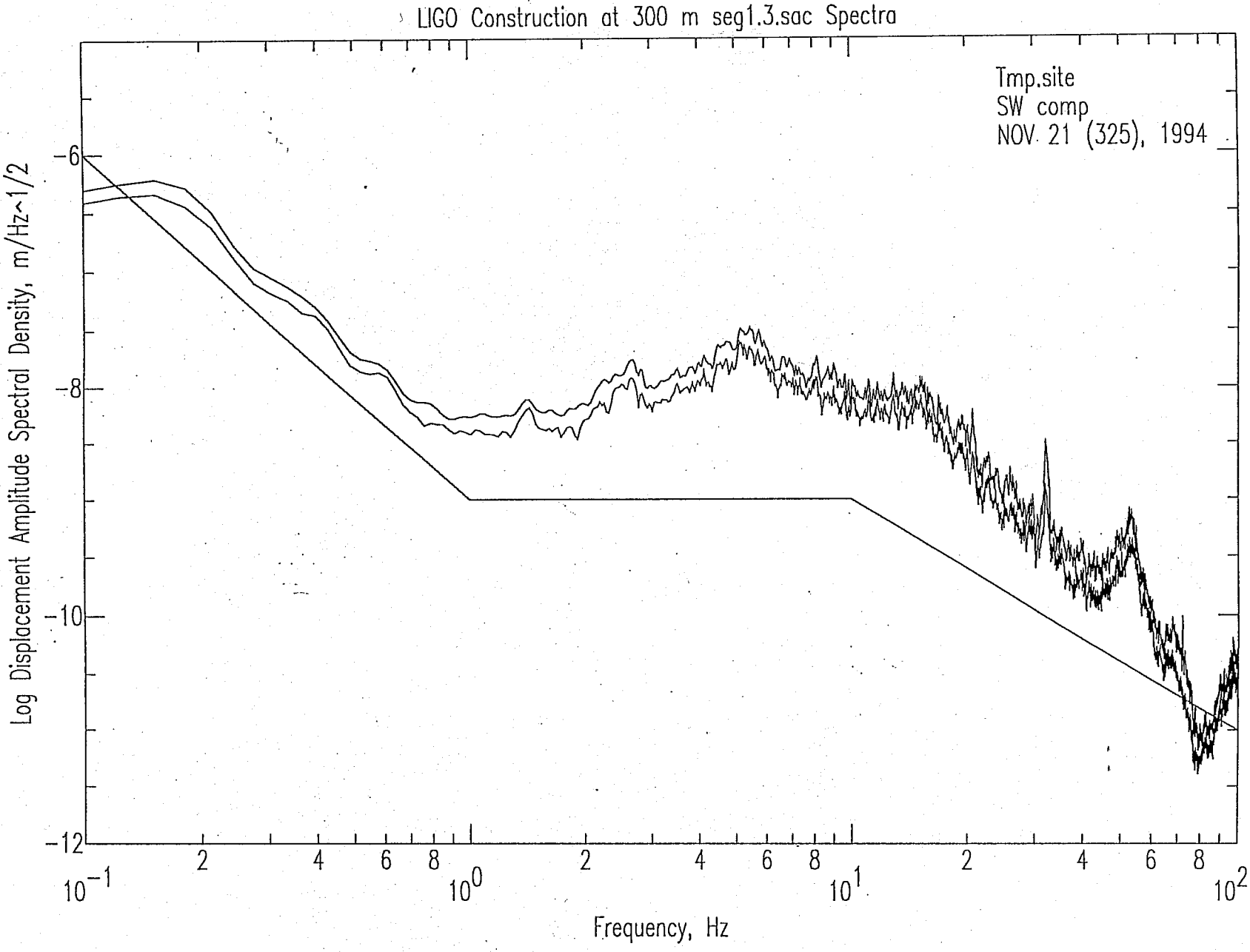

Figure 8.2-3: Southwest component amplitude spectra at a temporary site 300 m from construction activity.

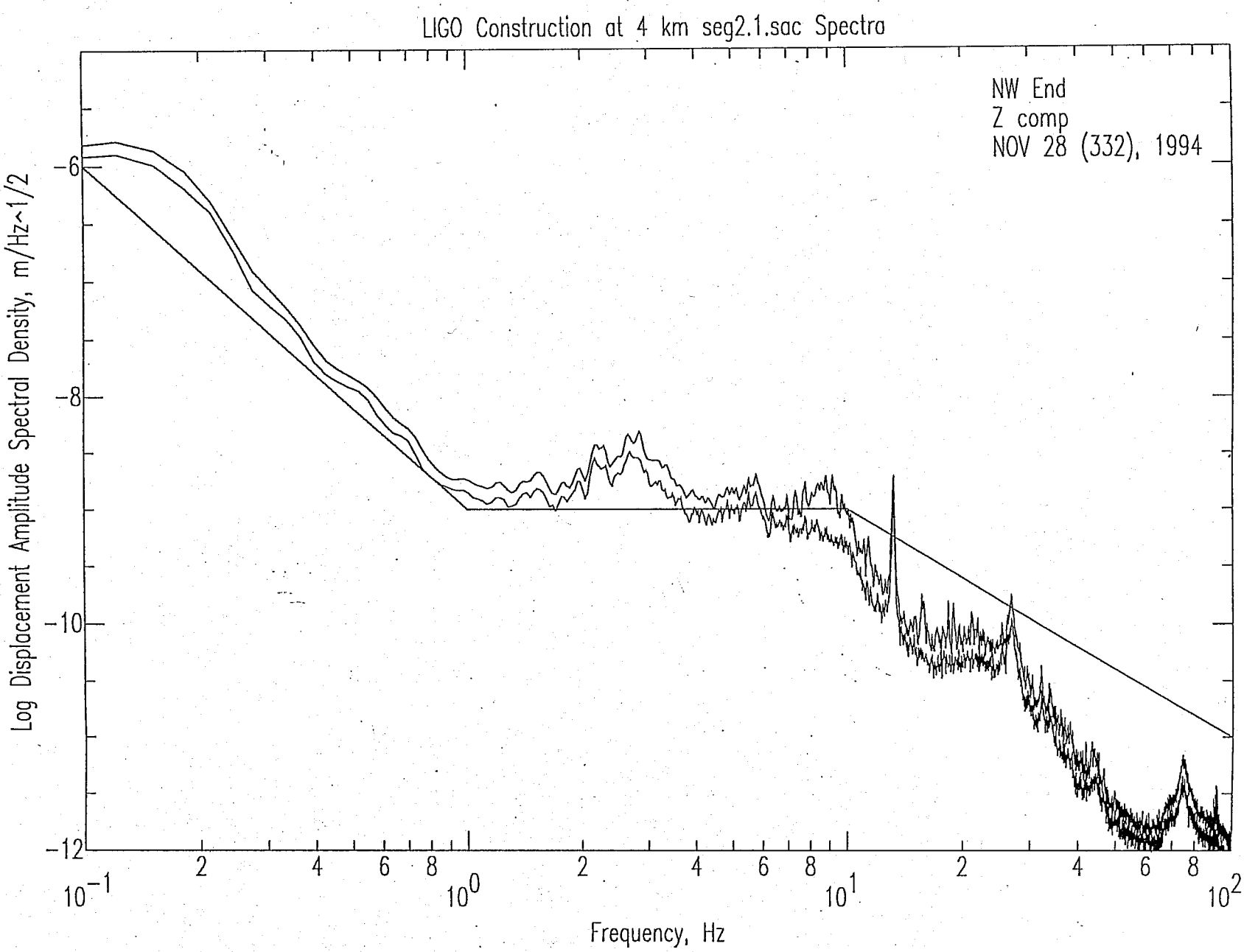

Figure 8.2-4: Vertical component amplitude spectra at the Northwest End site during construction activity at the Corner, 4 km distant.

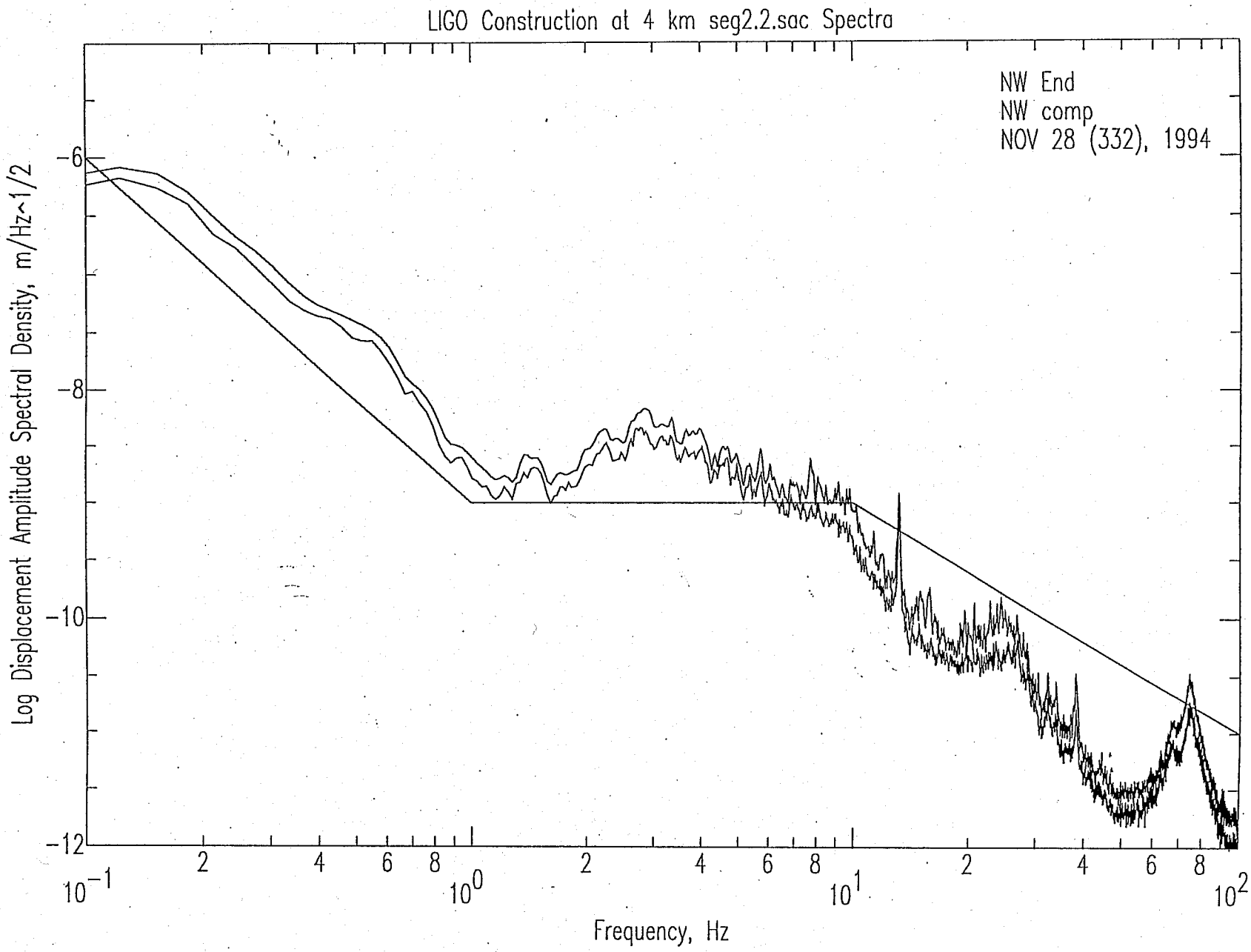

Figure 8.2-5: Northwest component amplitude spectra at the Northwest End site during construction activity at the Corner, 4 km distant.

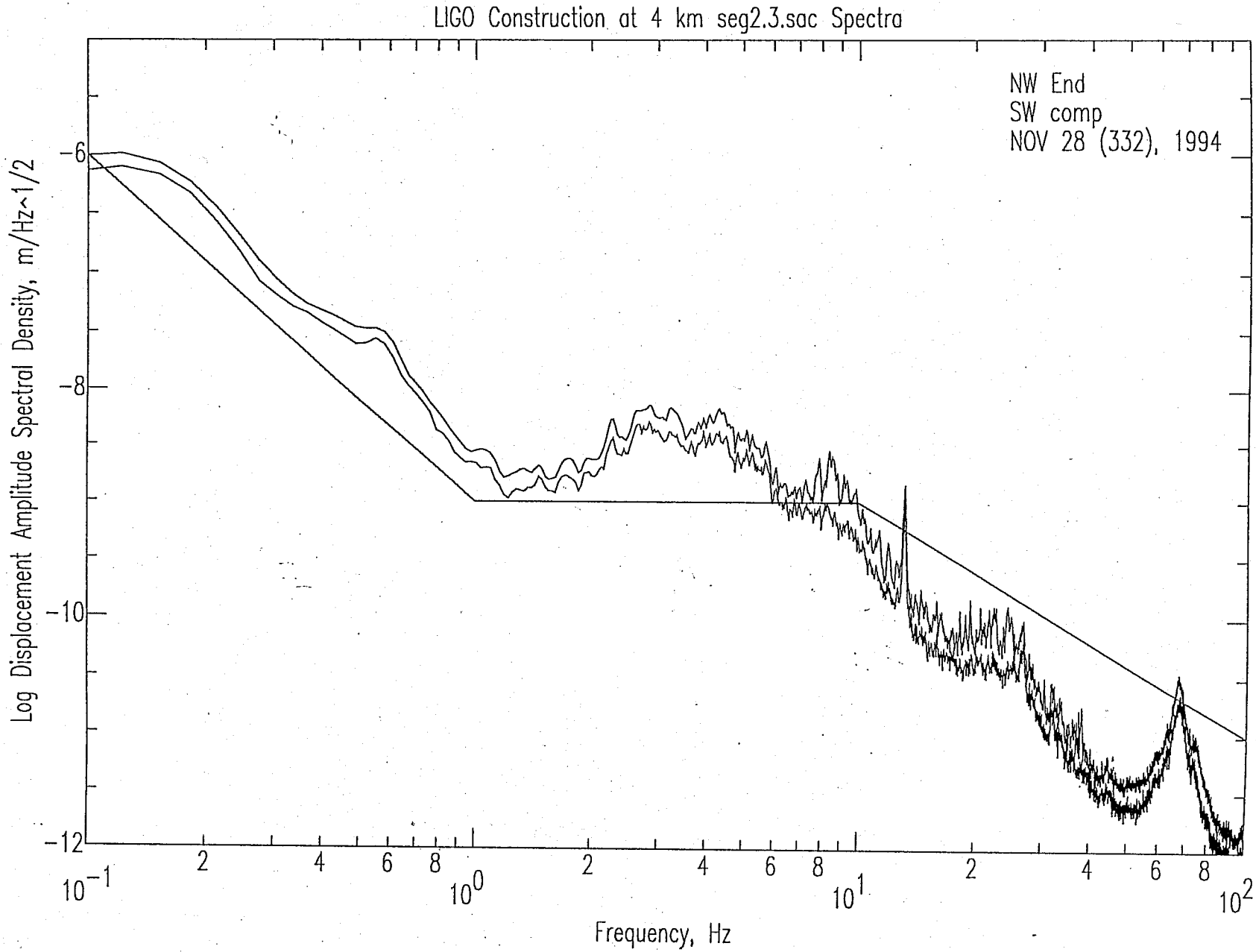

Figure 8.2-6: Southwest component amplitude spectra at the Northwest End site during construction activity at the Corner, 4 km distant.

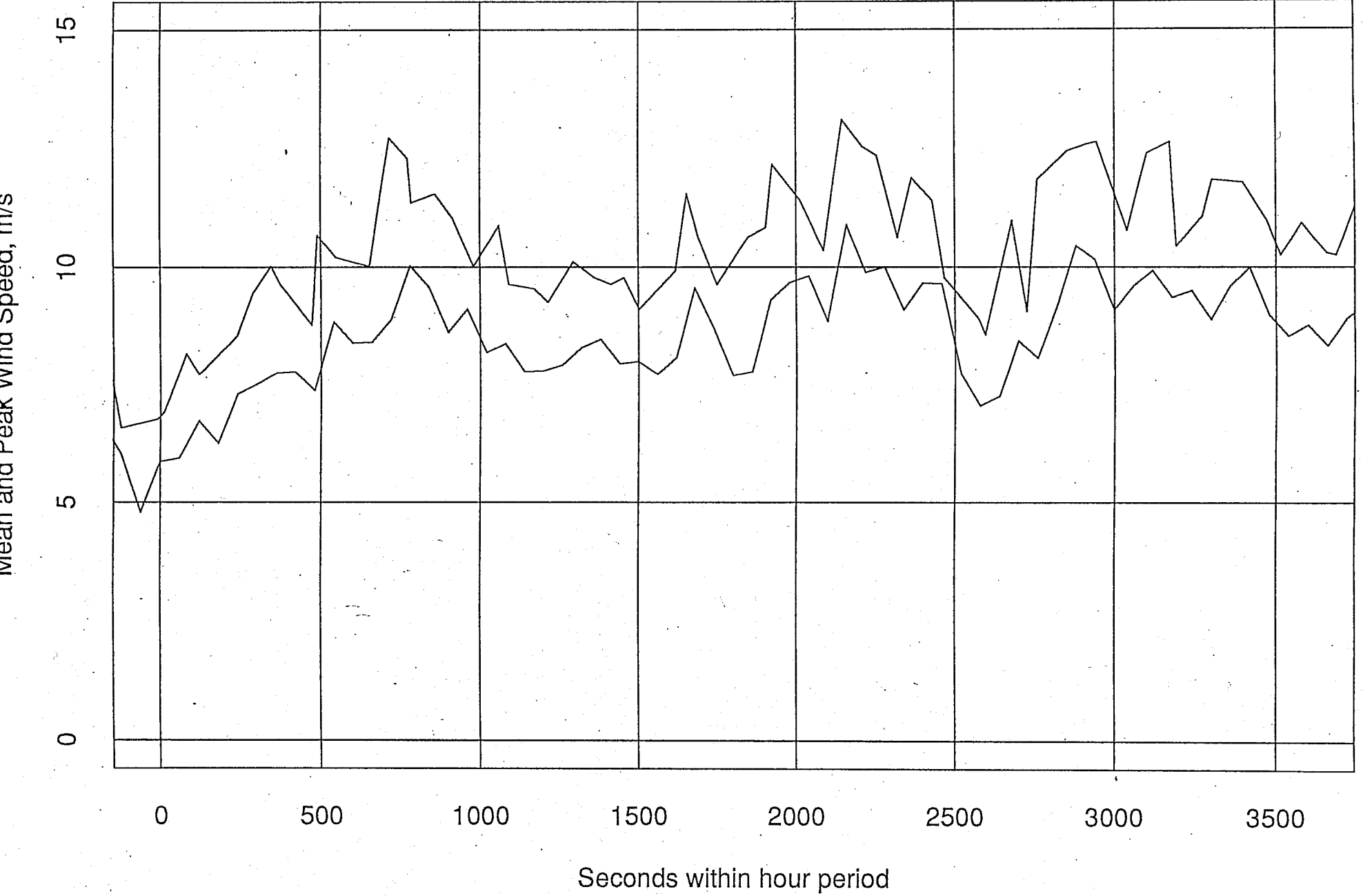

Figure 8.3-1: One-minute mean and peak wind speeds, Day 335, Hour 07 GMT at the Northwest End site.

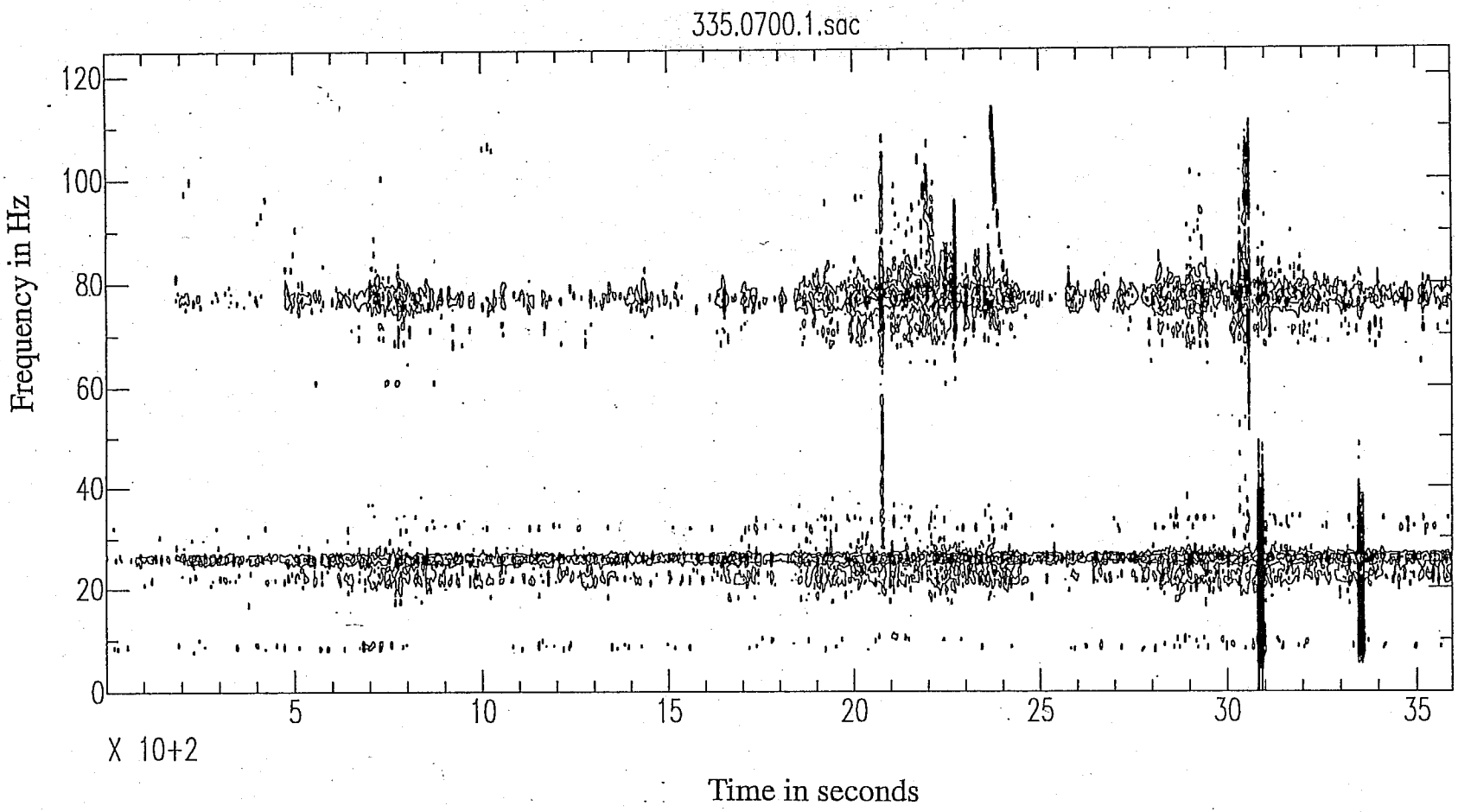

Figure 8.3-2: Spectrogram during Day 335, Hour 07 GMT at the Northwest End site. The wide-band noise bursts are caused by artillery practice.

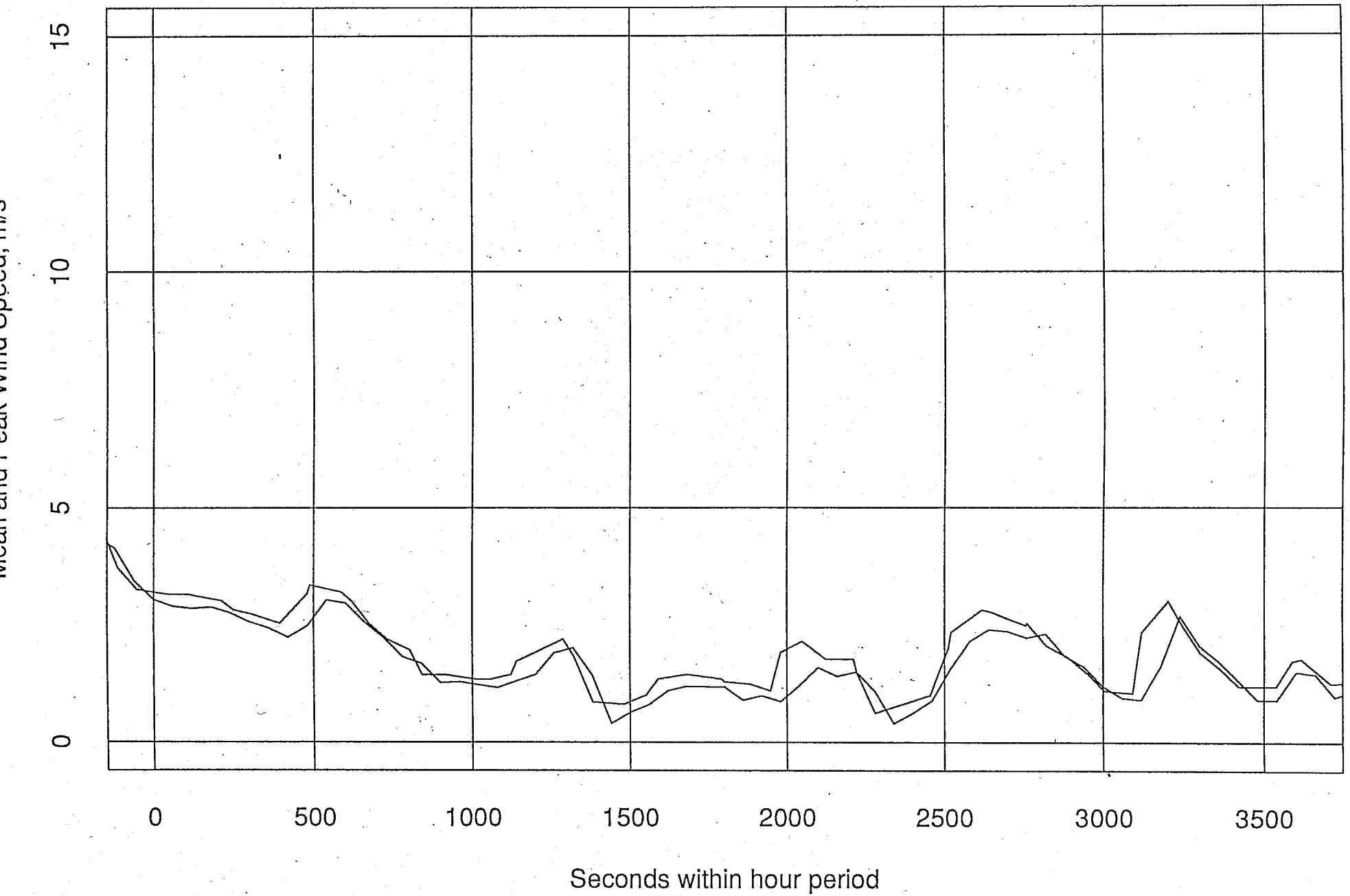

Figure 8.3-3: One-minute mean and peak wind speeds, Day 335, Hour 10 GMT at the Northwest End site.

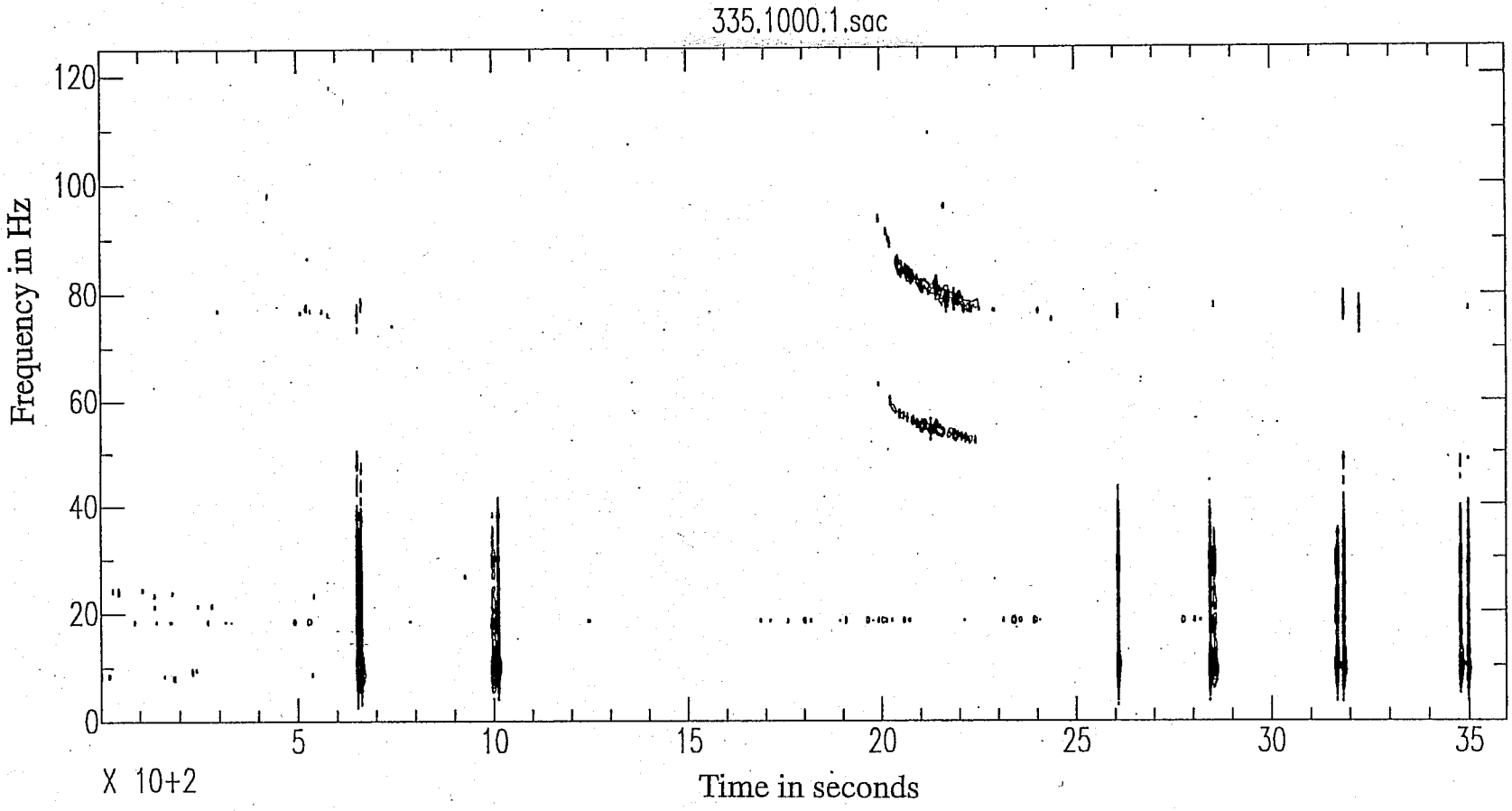

Figure 8.3-4: Spectrogram during Day 335, Hour 10 GMT at the Northwest End site. The wide-band noise bursts are caused by artillery practice.

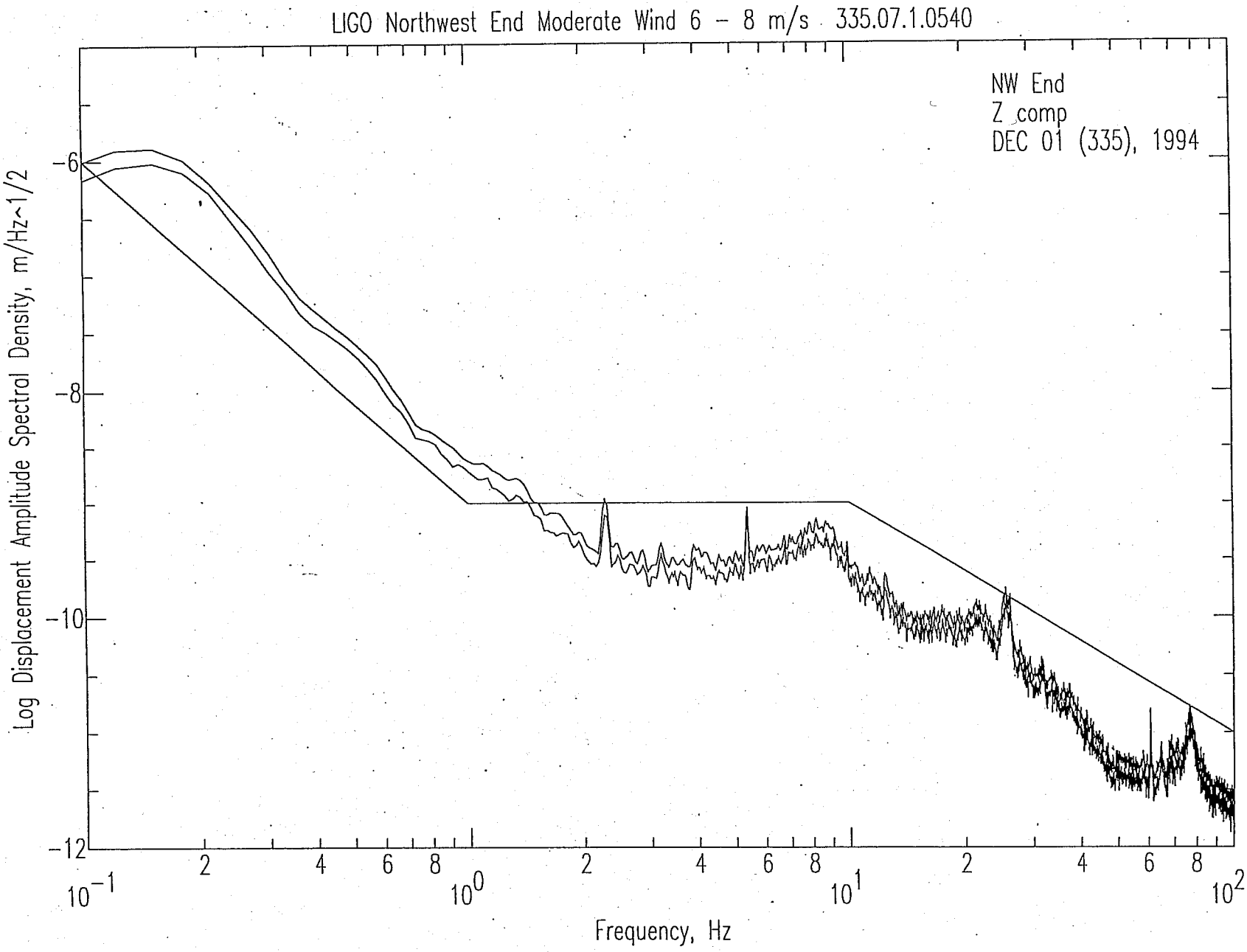

Figure 8.3-5: Spectra from a 6 minute sample taken from 540 to 900 s on Day 335, Hour 07 GMT at the Northwest End site.

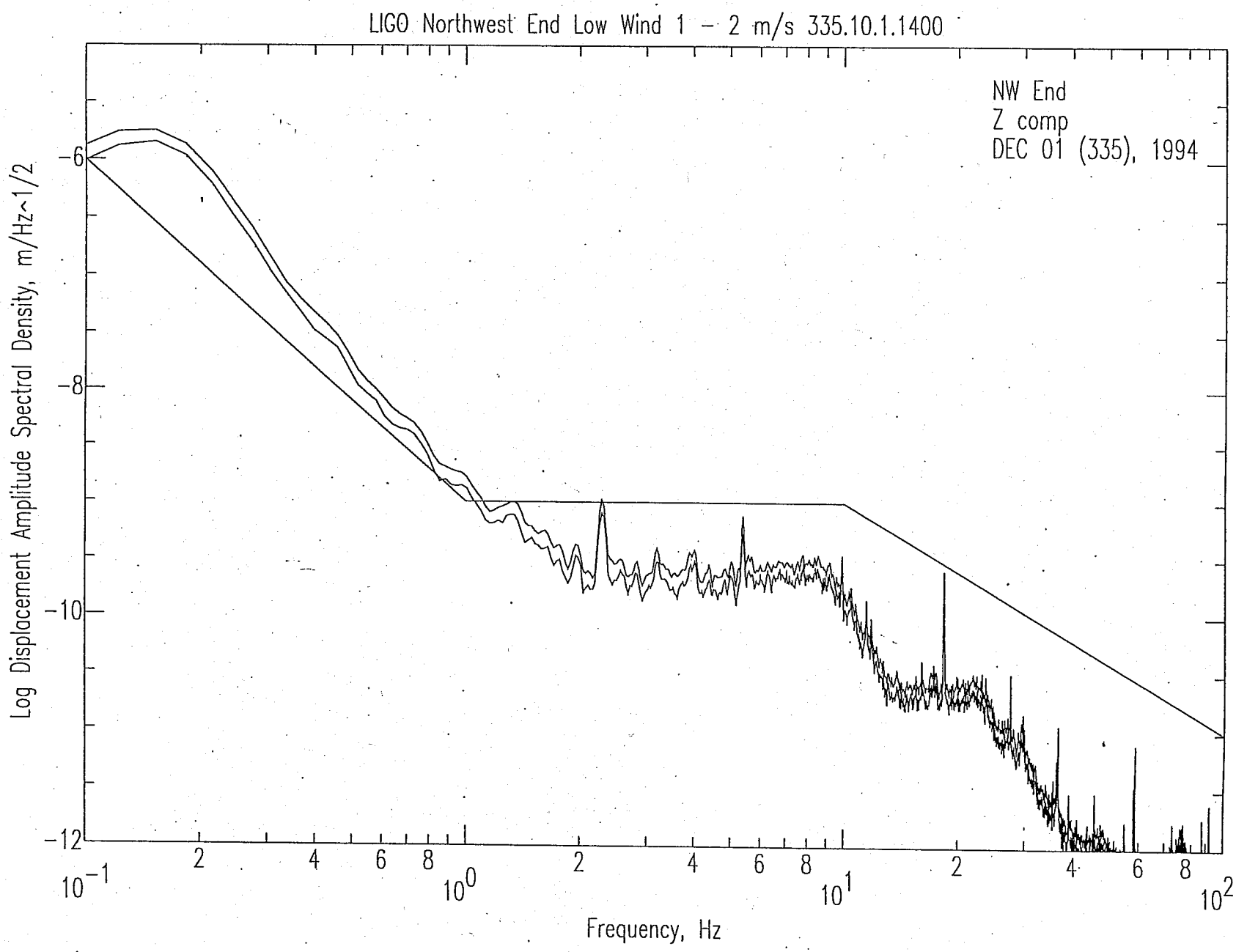

Figure 8.3-6: Spectra from a 6 minute sample taken from 1400 to 1760 s on Day 335, Hour 10 GMT at the Northwest End site.

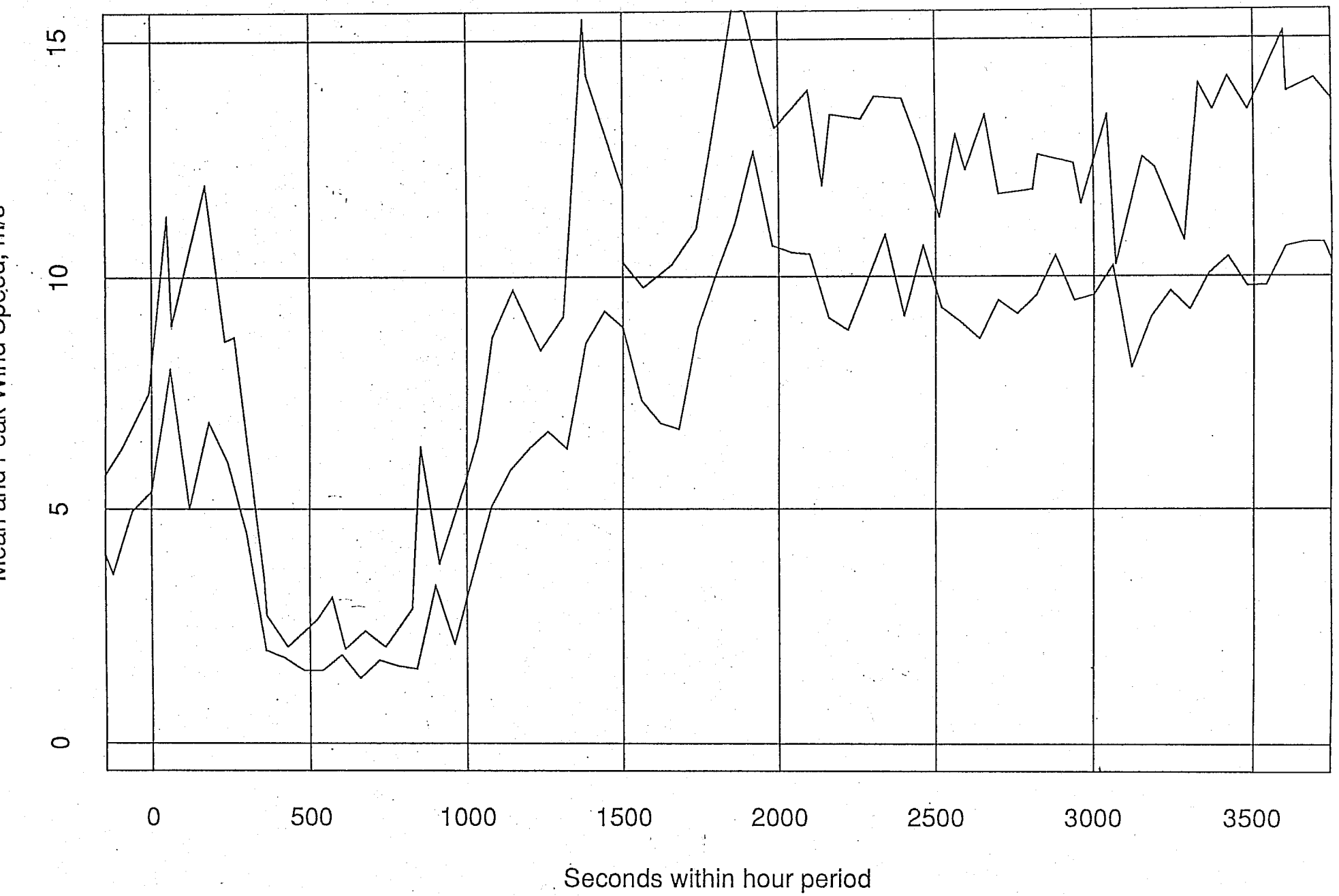

Figure 8.3-7: One-minute mean and peak wind speeds, Day 343, Hour 03 GMT at the Corner site.

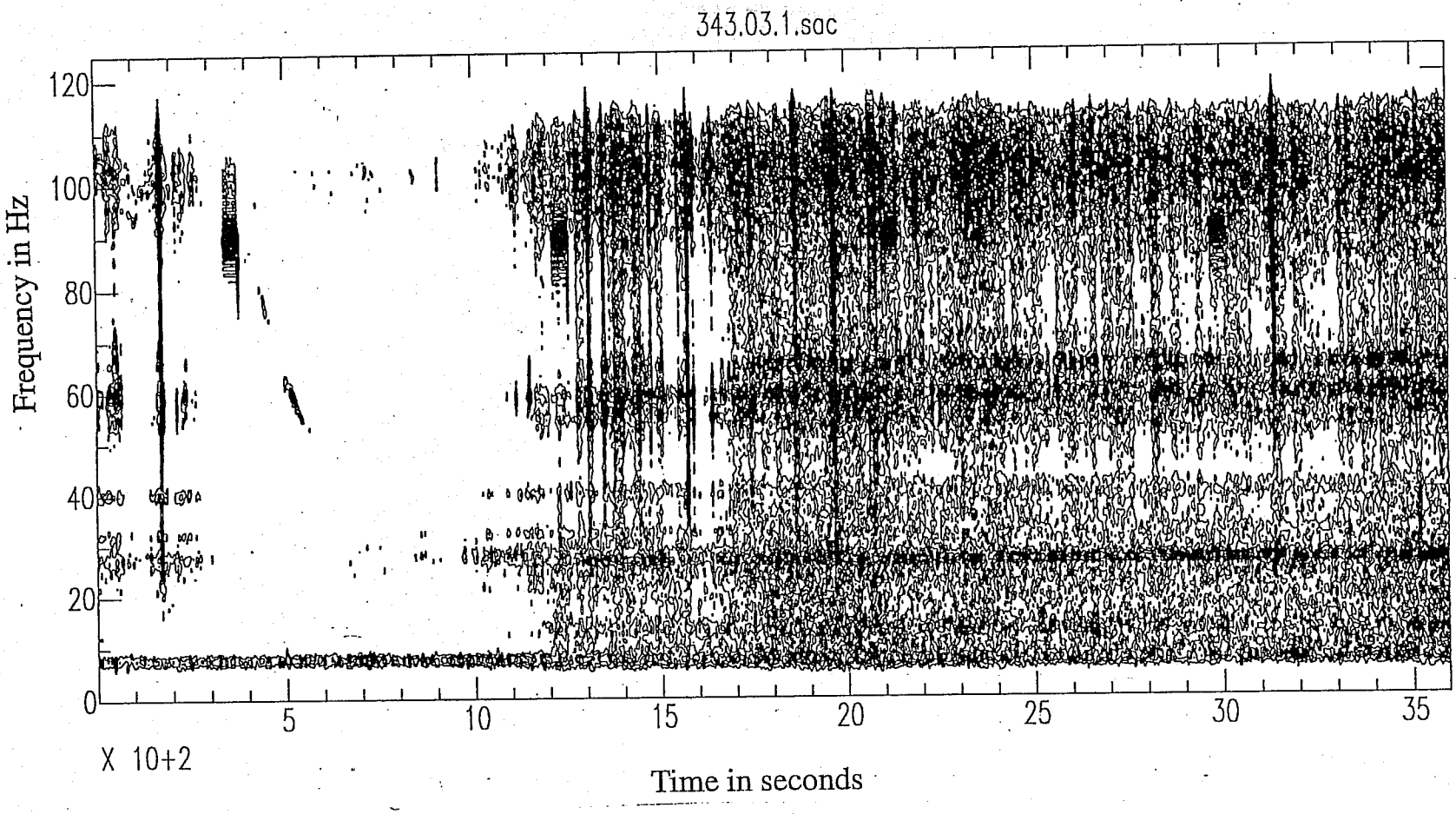

Figure 8.3-8: Spectrogram during Day 343, Hour 03 GMT at the Corner site.

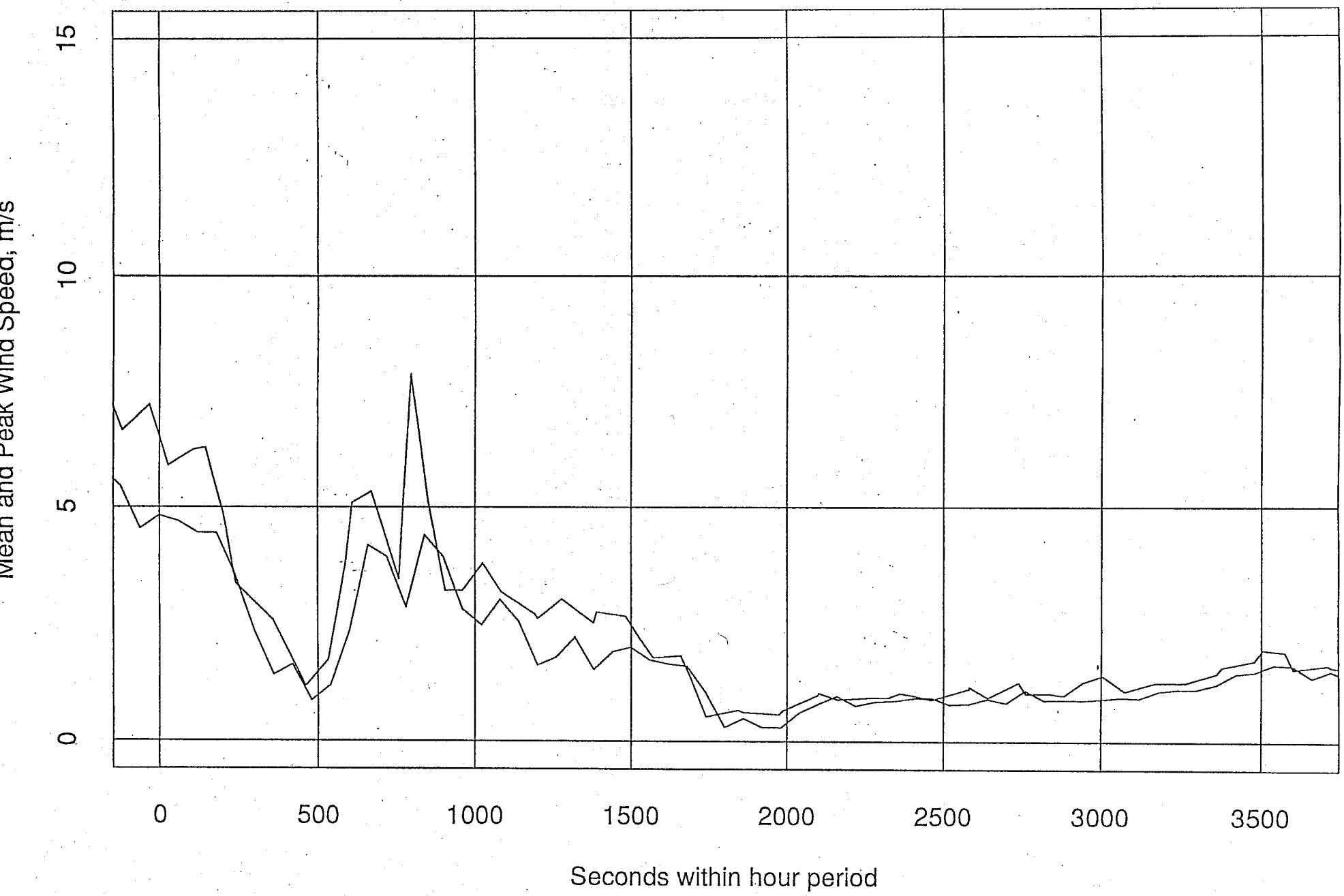

Figure 8.3-9: One-minute mean and peak wind speeds, Day 343, Hour 08 GMT at the Corner site.

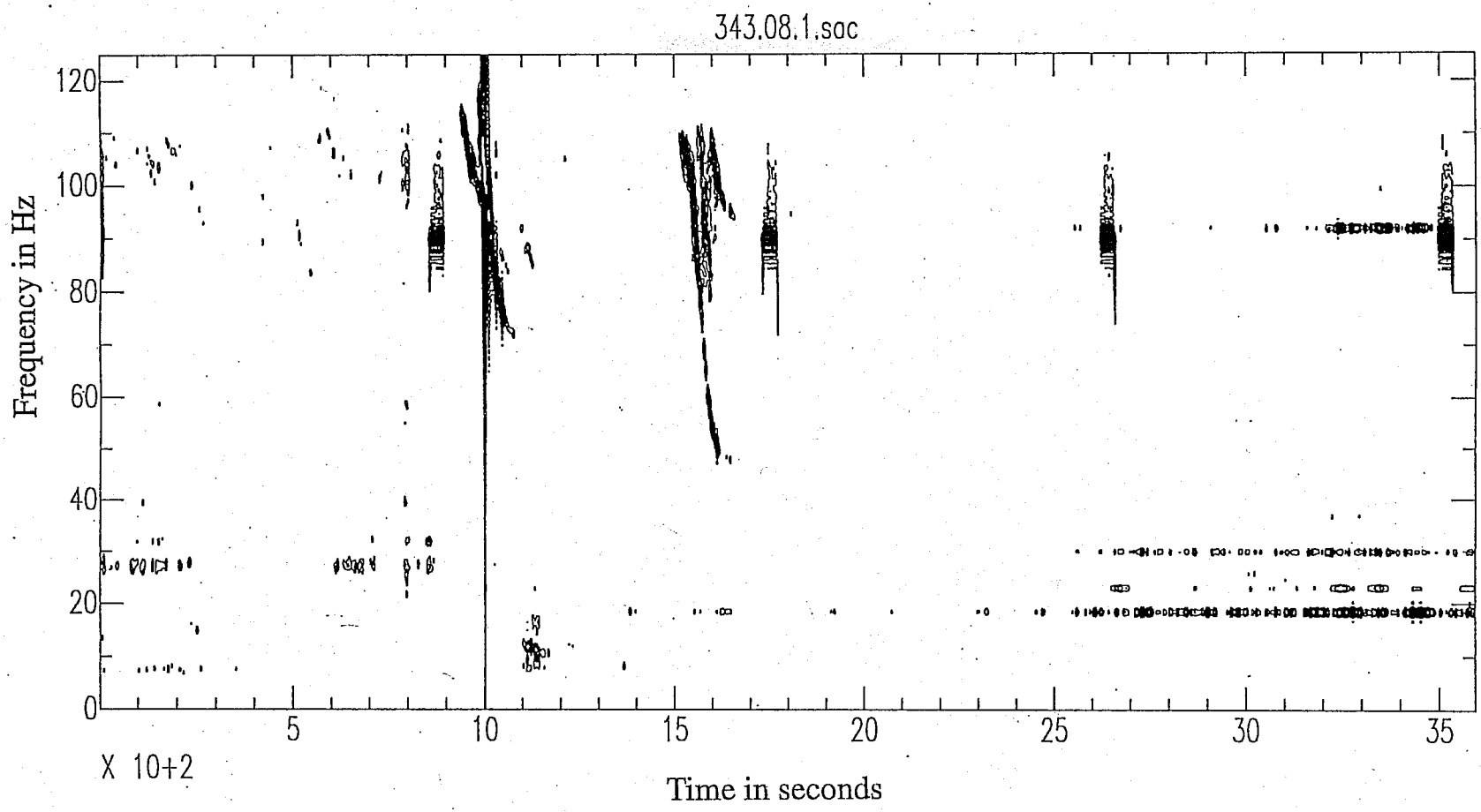

Figure 8.3-10: Spectrogram during Day 343, Hour 08 GMT at the Corner site.

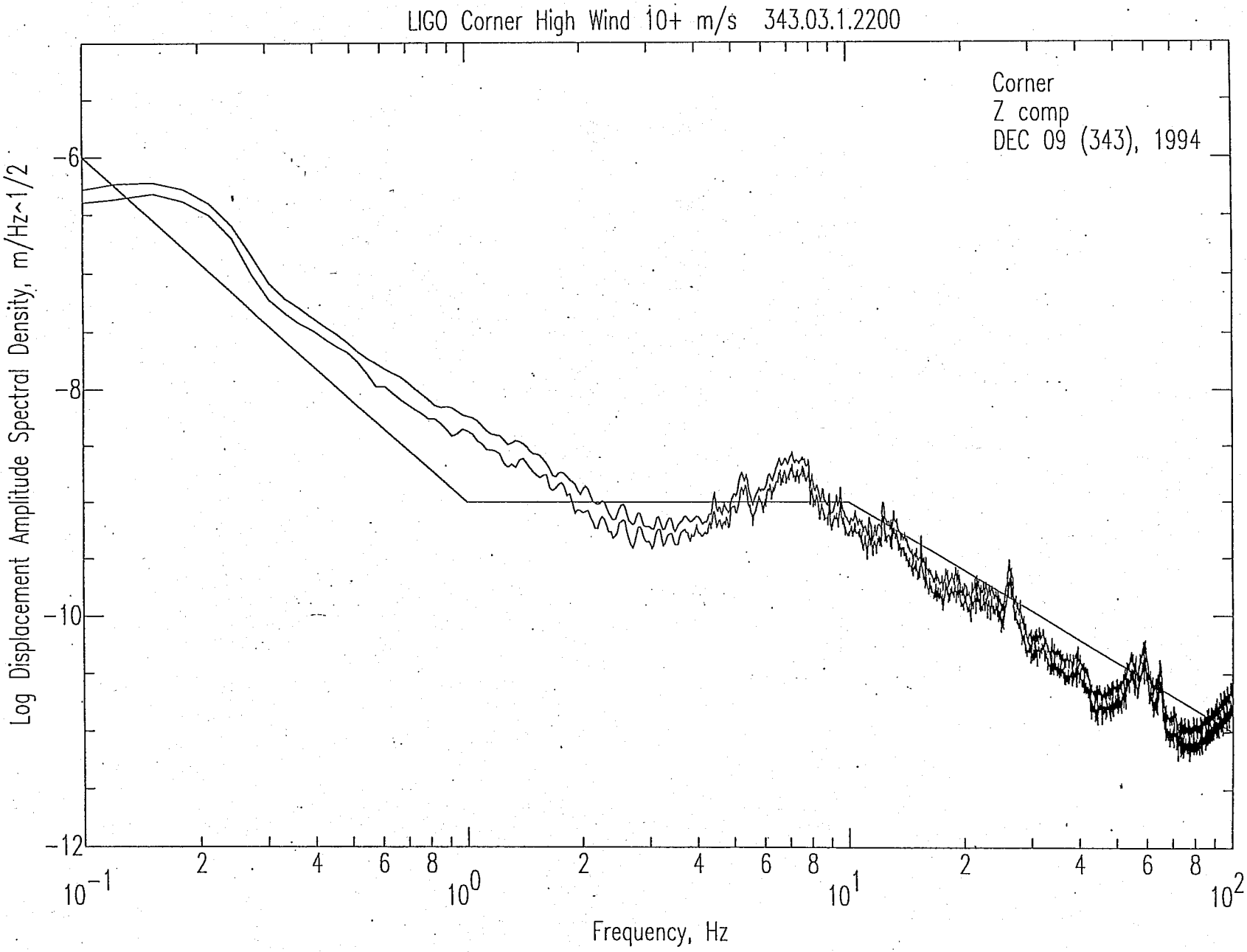

Figure 8.3-11: Spectra from a 6 minute sample taken from 2200 to 2560 s on Day 343, Hour 03 GMT at the Corner site.

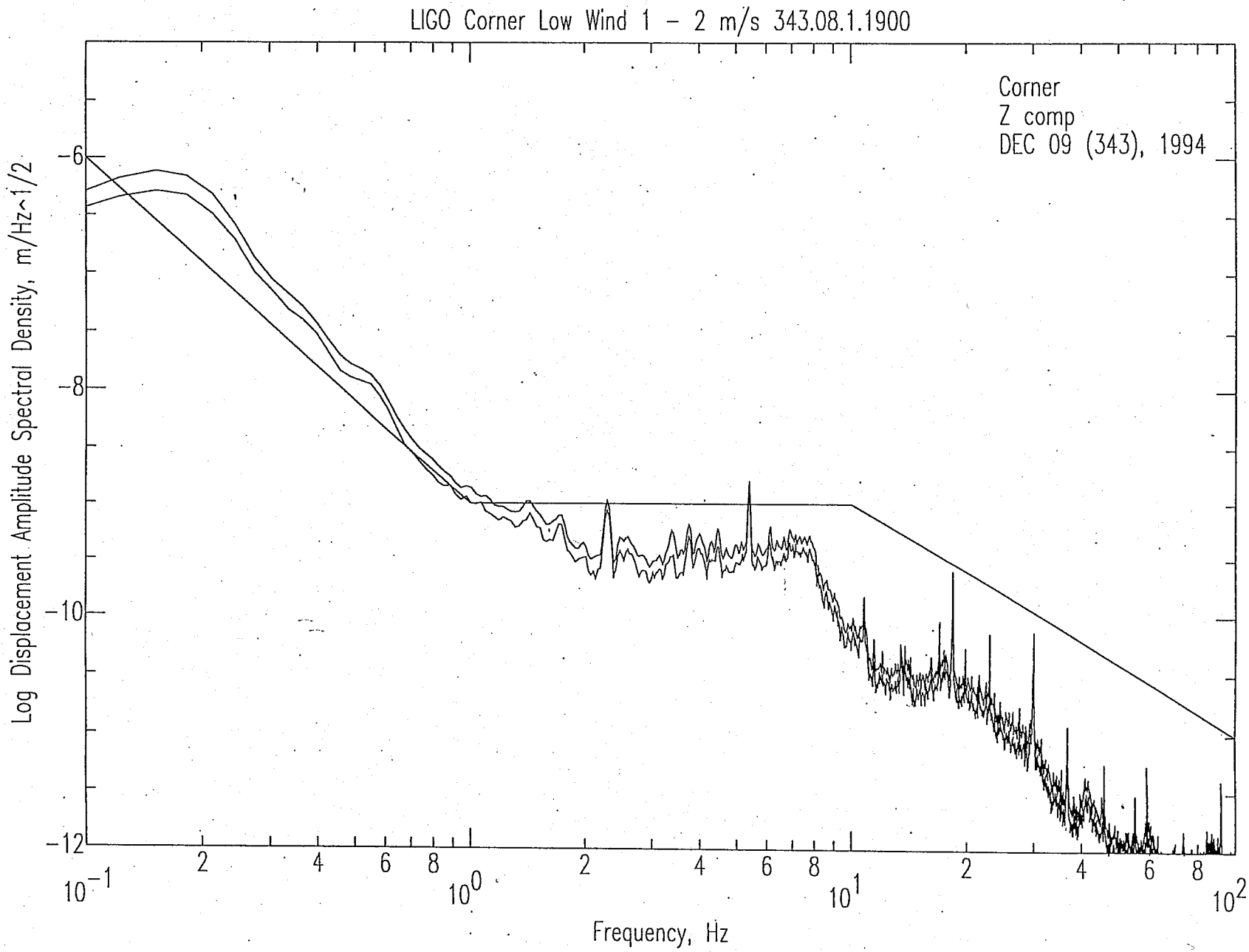

Figure 8.3-12: Spectra from a 6 minute sample taken from 1900 to 2260 s on Day 343, Hour 08 GMT at the Corner site.

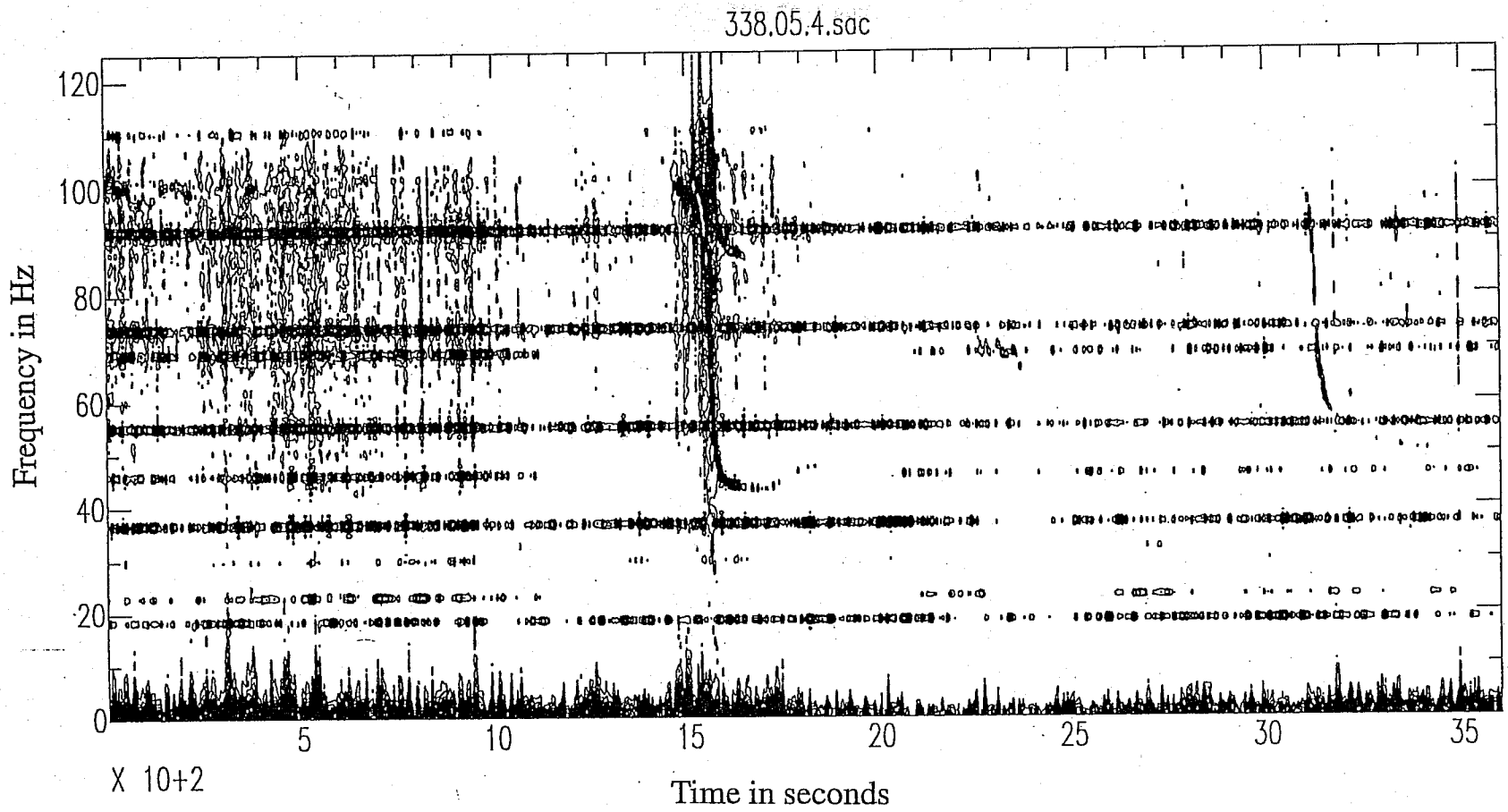

Figure 8.4-1: Acoustic spectrogram during Day 338, Hour 05 GMT at the Southwest End site. Line spectra are found in two distinct sets of multiples, one of which becomes intermittent after 1100 s.

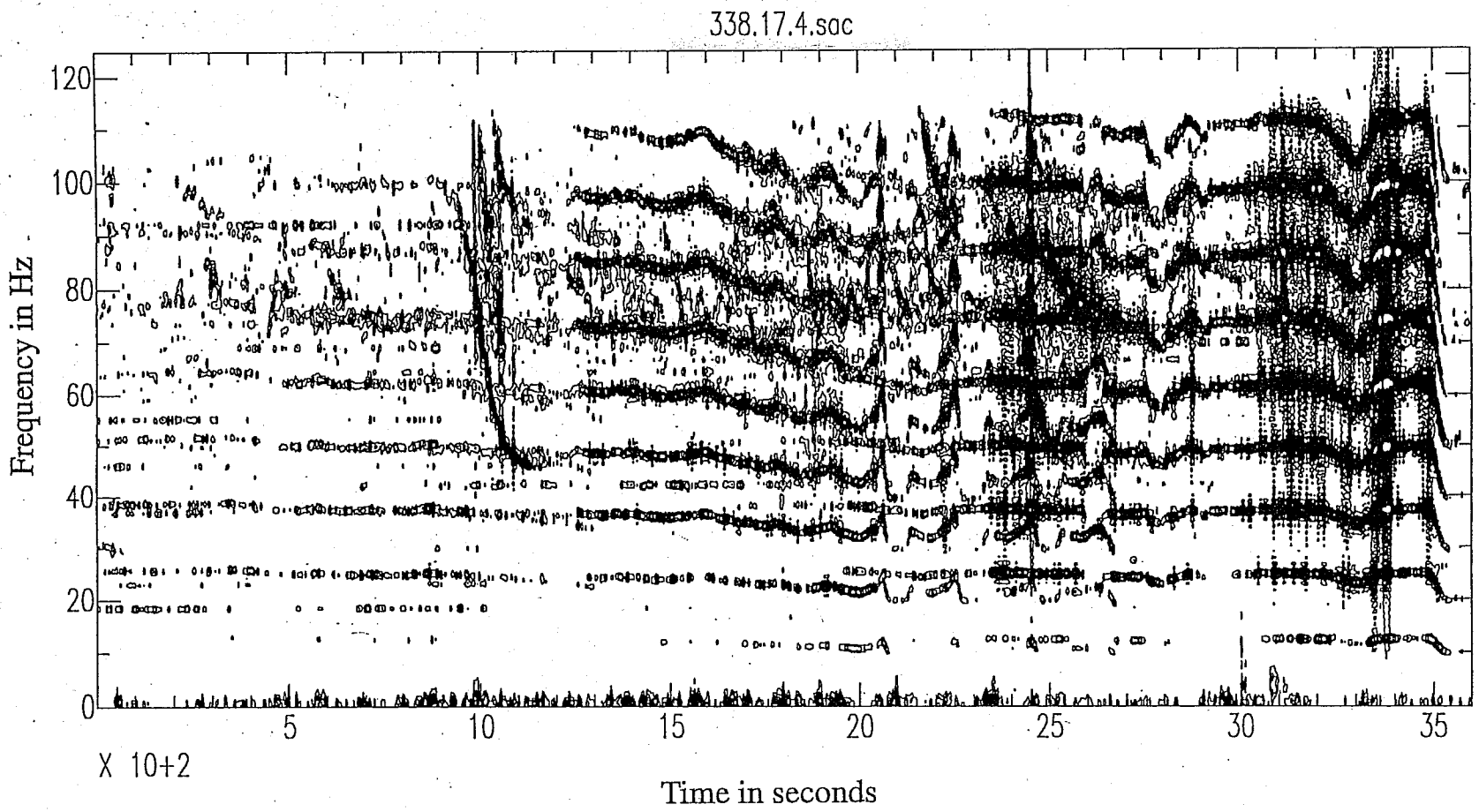

Figure 8.4-2: Acoustic spectrogram during Day 338, Hour 17 GMT at the Southwest End site. The line spectra in this example become louder, unsteady in frequency, and then abruptly terminate at the very end of the one hour period shown.

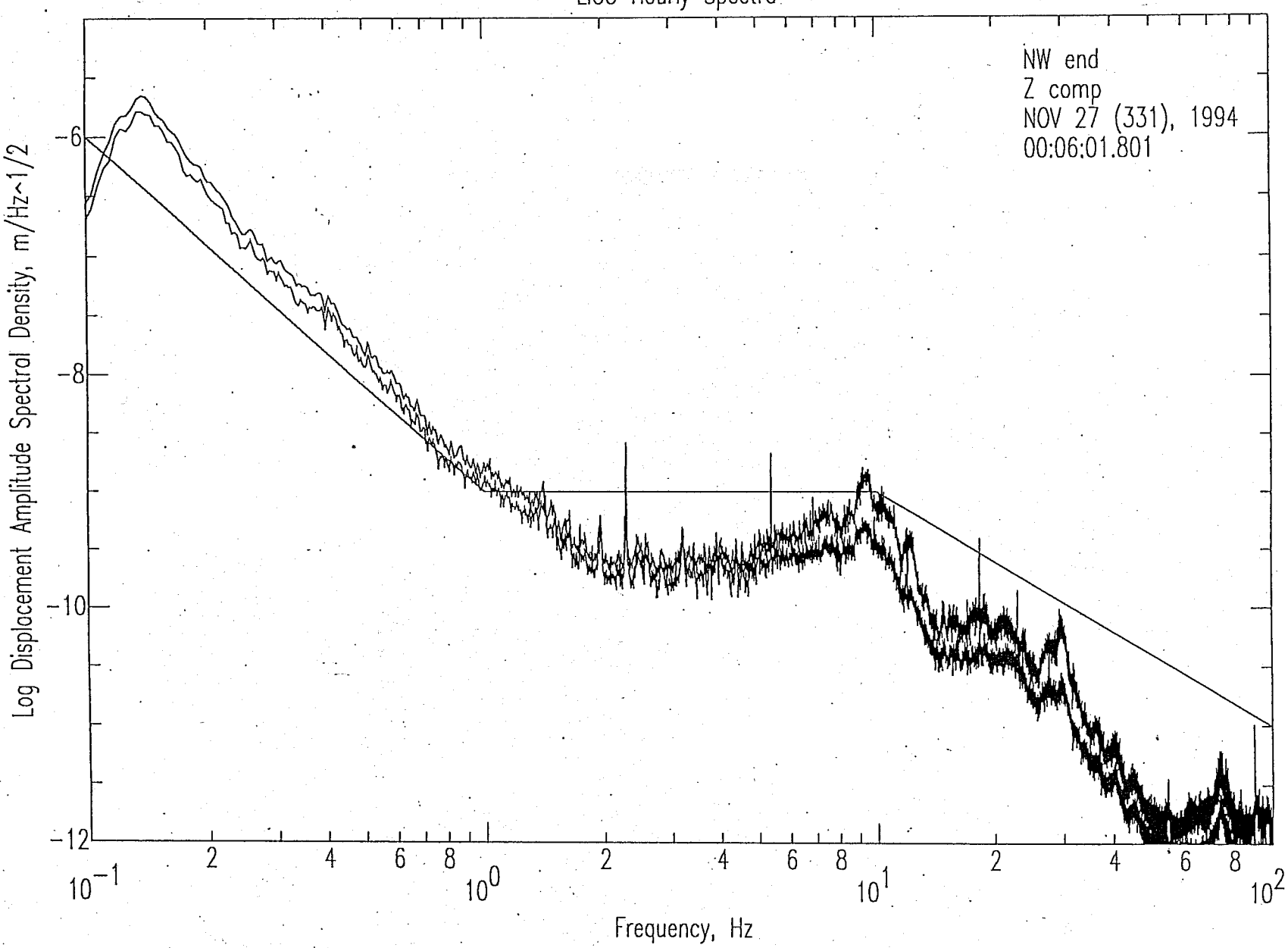

Figure 8.4-3: Median and r.m.s spectra of the vertical seismic signal for a one-hour period at the Northwest End during which artillery acoustic noise was observed. The r.m.s. spectrum is raised above the median spectra.

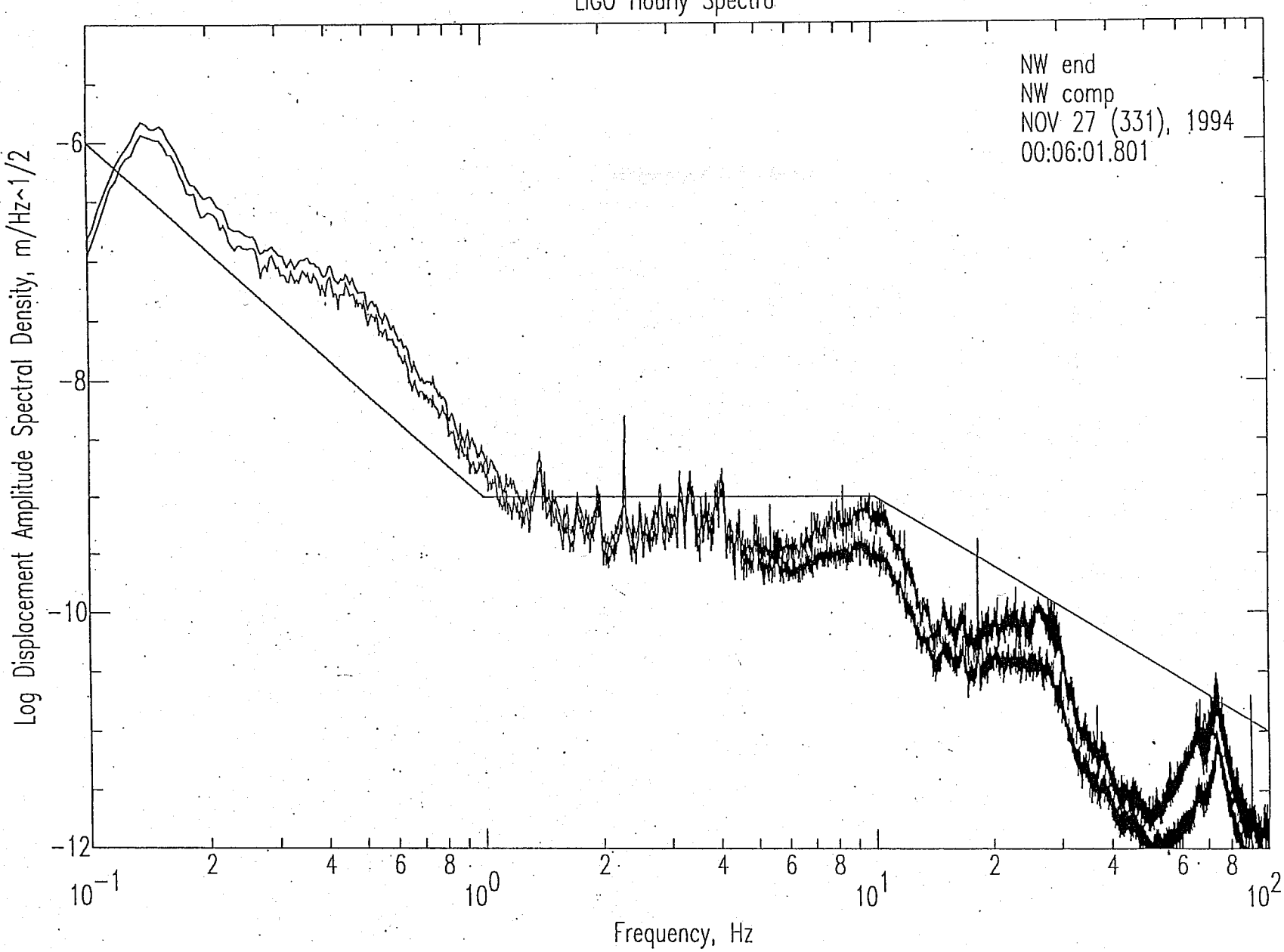

Figure 8.4-4: Median and r.m.s spectra of the northwest seismic signal for a one-hour period at the Northwest End during which artillery acoustic noise was observed. The r.m.s. spectrum is raised above the median spectra.

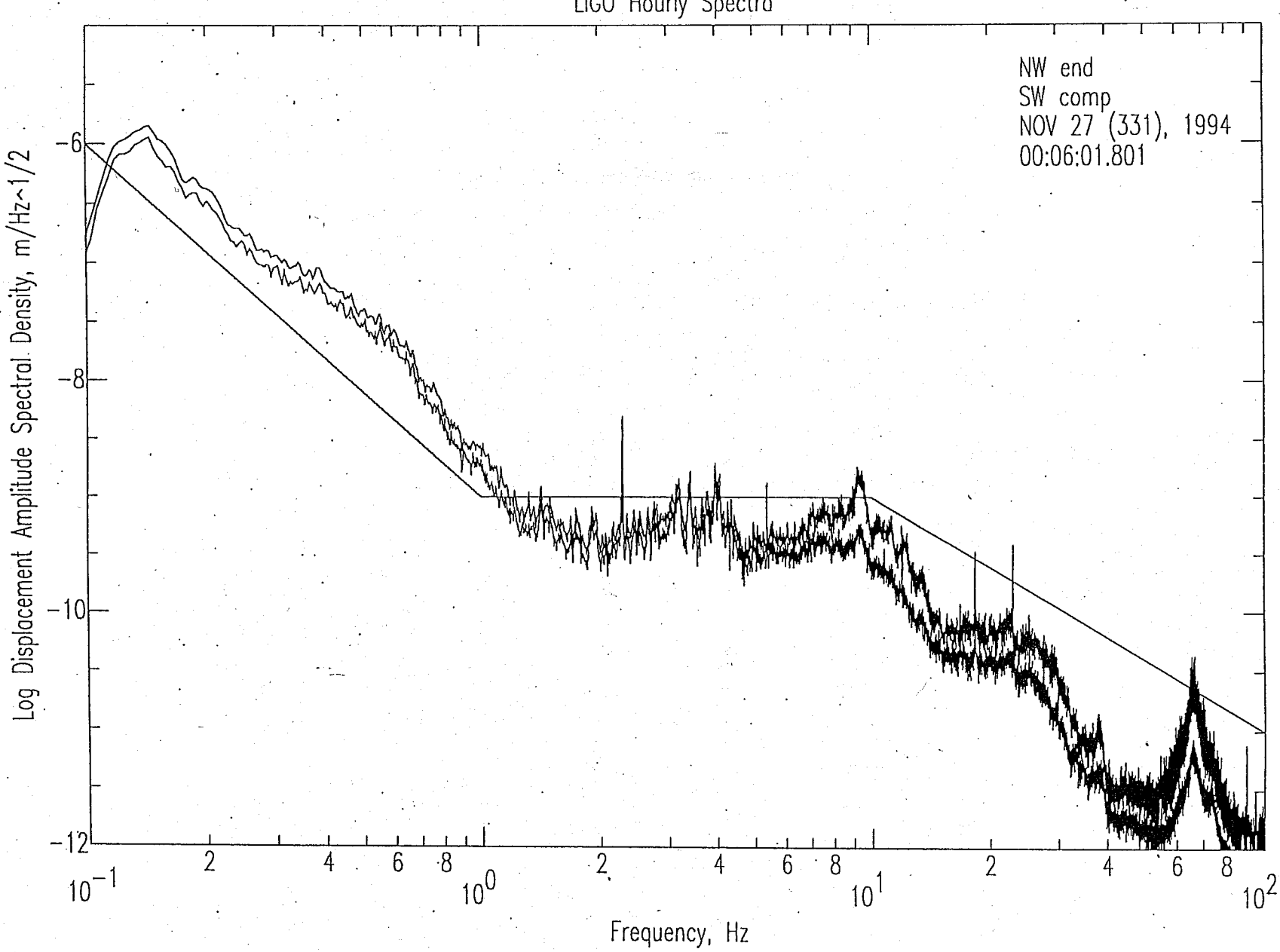

Figure 8.4-5: Median and r.m.s spectra of the southwest seismic signal for a one-hour period at the Northwest End during which artillery acoustic noise was observed. The r.m.s. spectrum is raised above the median spectra.

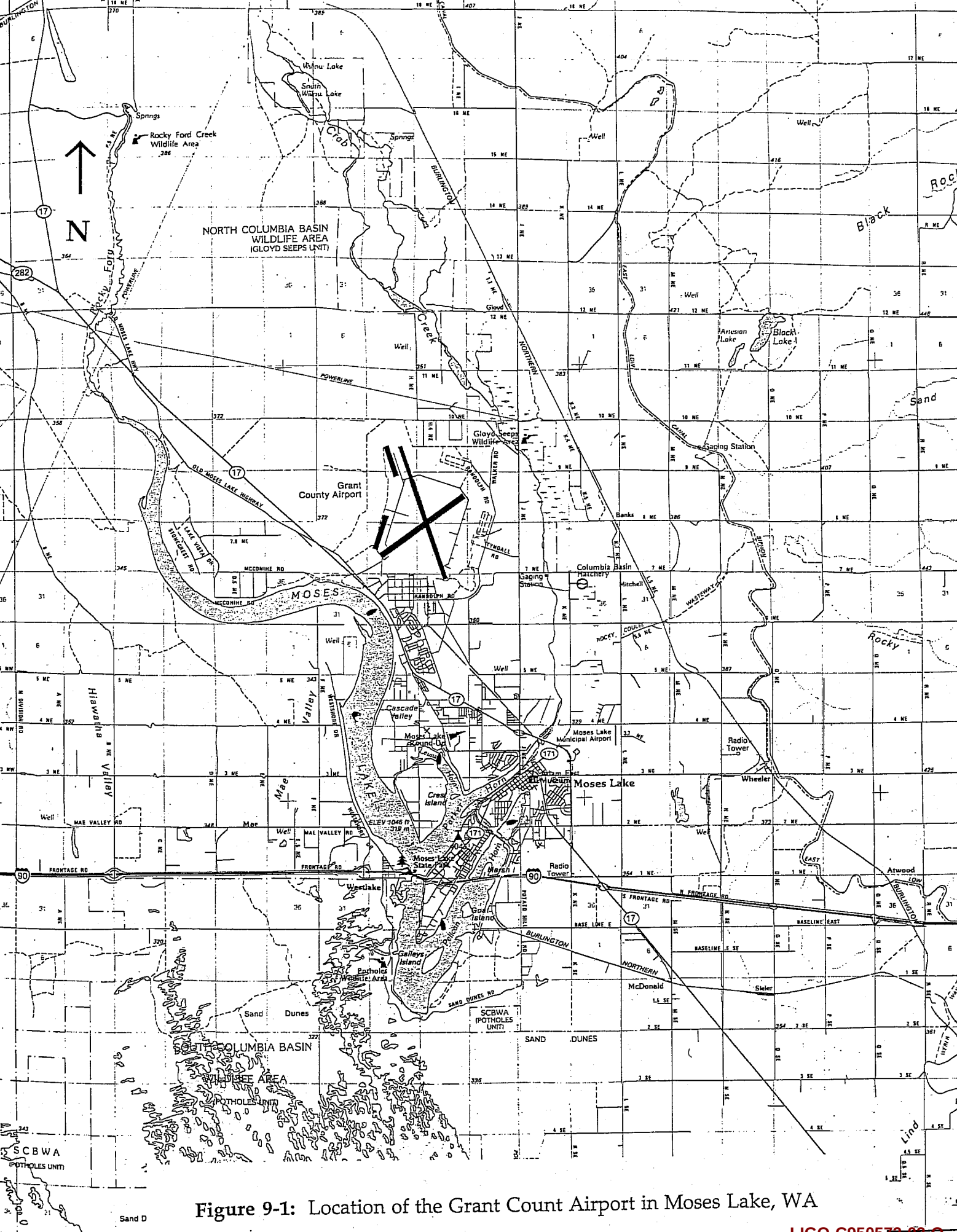

Figure 9-1: Location of the Grant Count Airport in Moses Lake, WA

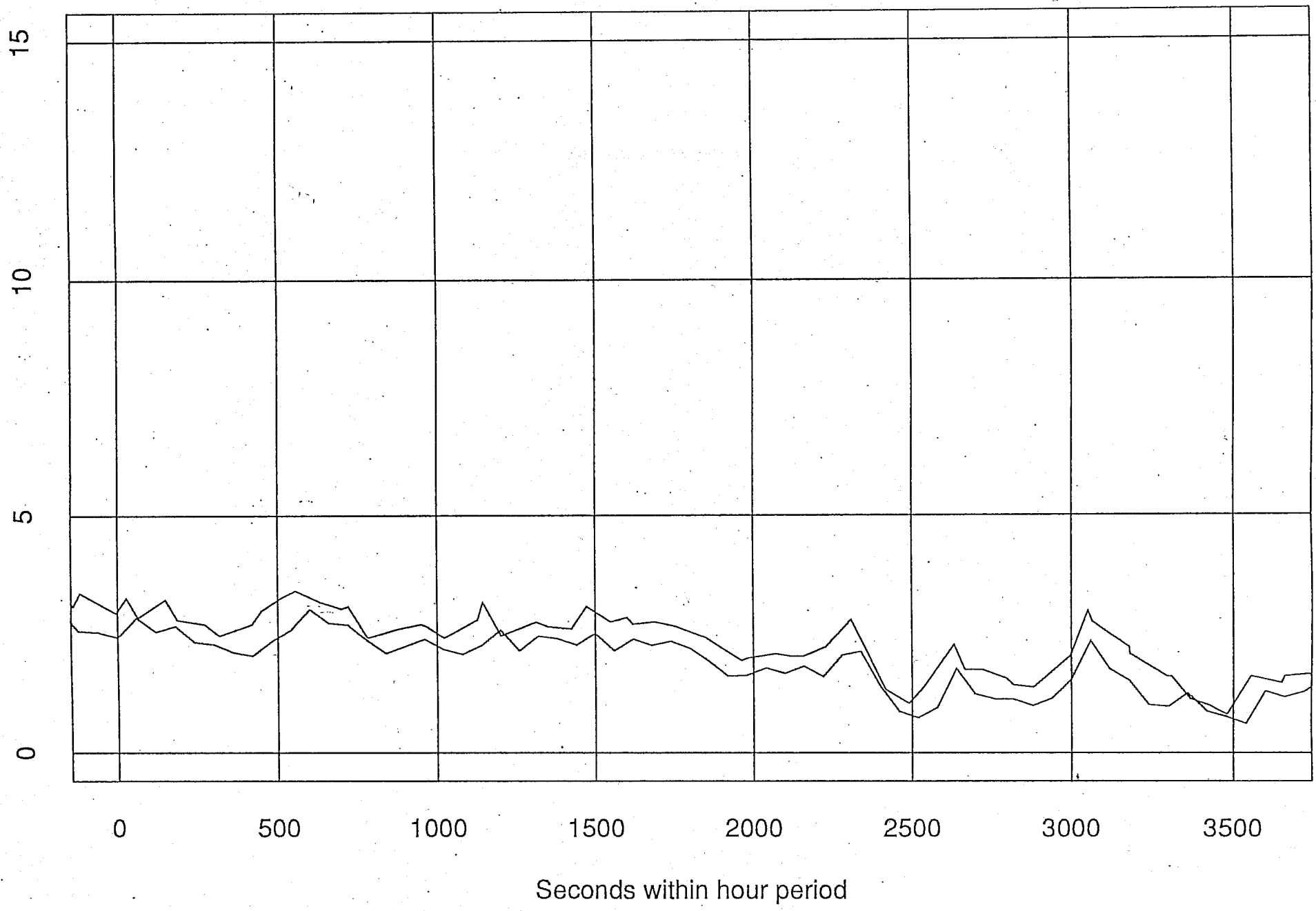

Figure 9-2: One-minute mean and peak wind speeds measured near the Moses Lake JAL aircraft hangar Day 238, Hour 04, during a low wind period.

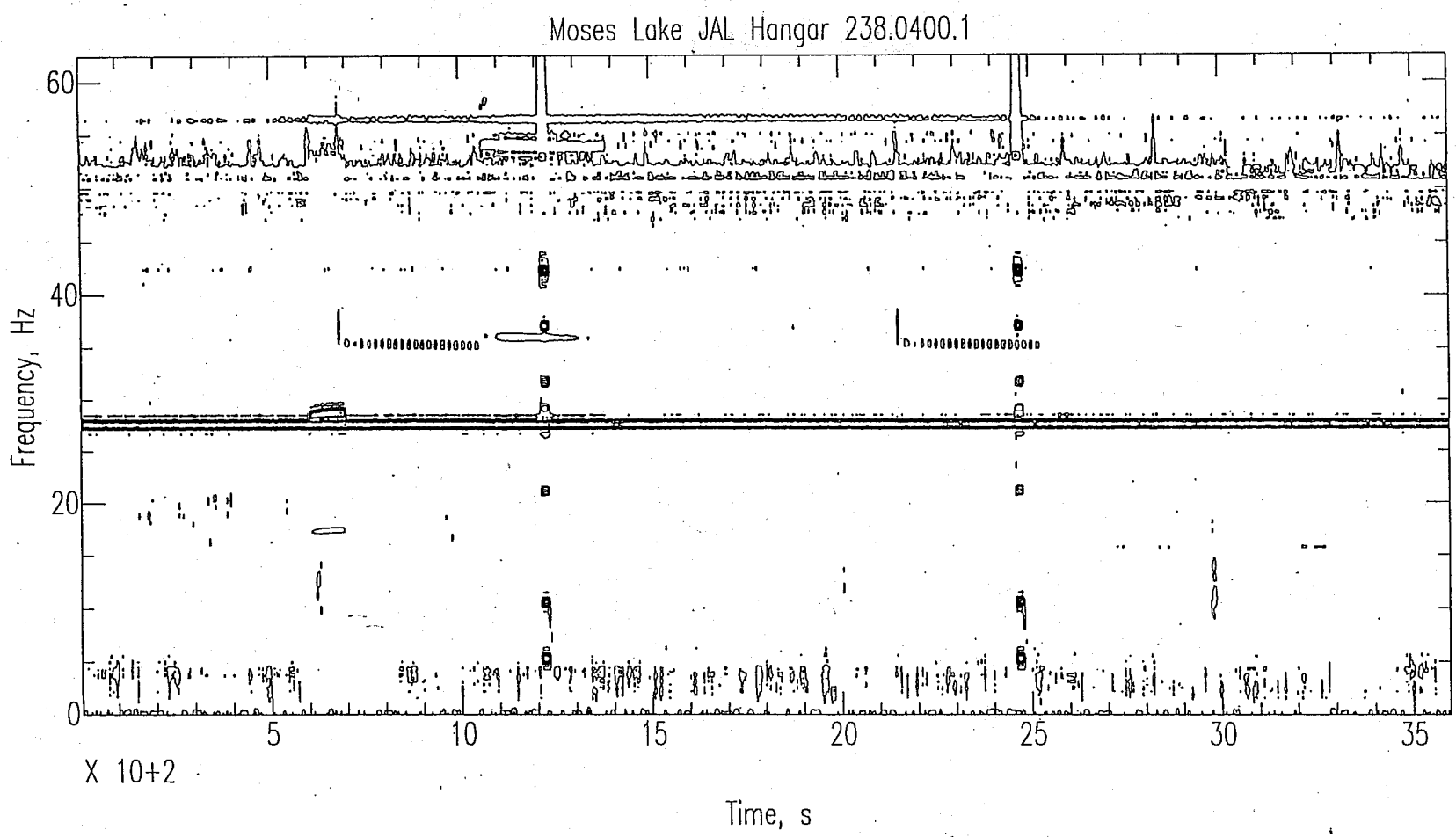

Figure 9-3: Spectrogram of the vertical seismic signal measured in the Moses Lake JAL aircraft hangar Day 238, Hour 04, during a low wind period.

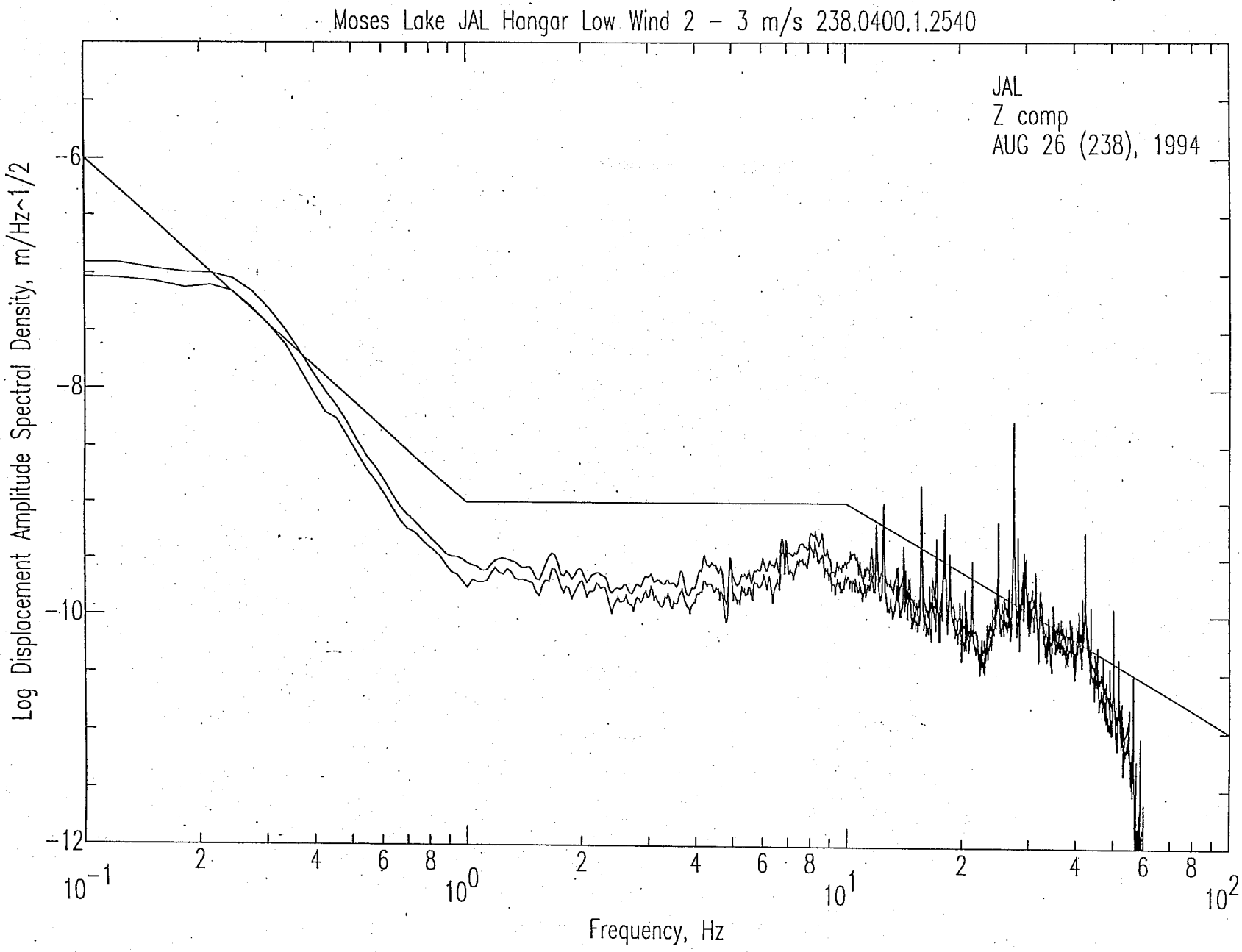

Figure 9-4: Median and r.m.s. spectra of the vertical seismic signal measured in the Moses Lake JAL aircraft hangar Day 238, Hour 04, during a low wind period. This spectrum is calculated from the time segment 2540 to 2900 s shown in Figures 9-2 and 9-3.

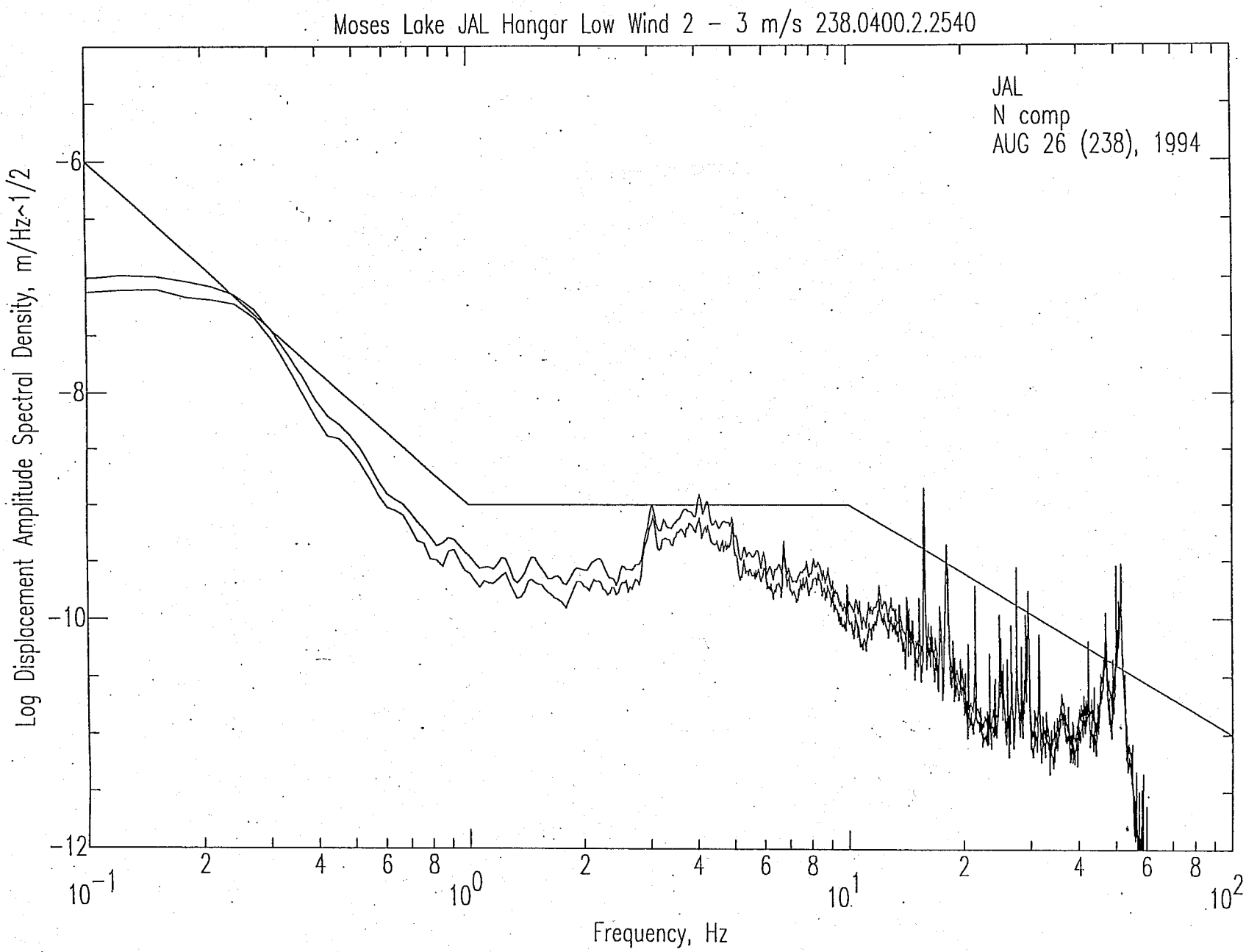

Figure 9-5: Median and r.m.s. spectra of the "north" seismic signal measured in the Moses Lake JAL aircraft hangar Day 238, Hour 04, during a low wind period. This spectrum is calculated from the time segment 2540 to 2900 s shown in Figures 9-2 and 9-3.

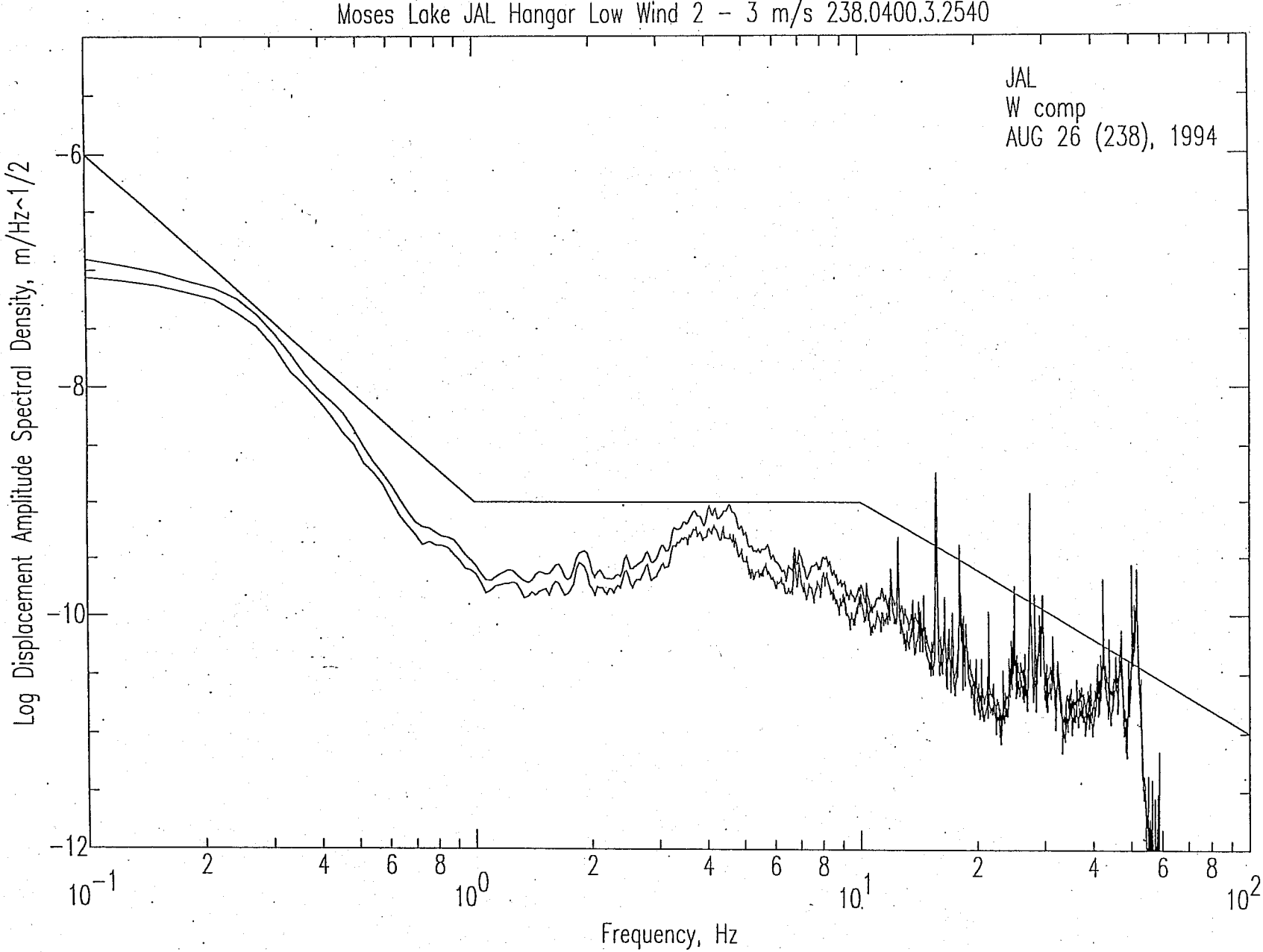

Figure 9-6: Median and r.m.s. spectra of the "east" seismic signal measured in the Moses Lake JAL aircraft hangar Day 238, Hour 04, during a low wind period. This spectrum is calculated from the time segment 2540 to 2900 s shown in Figures 9-2 and 9-3.

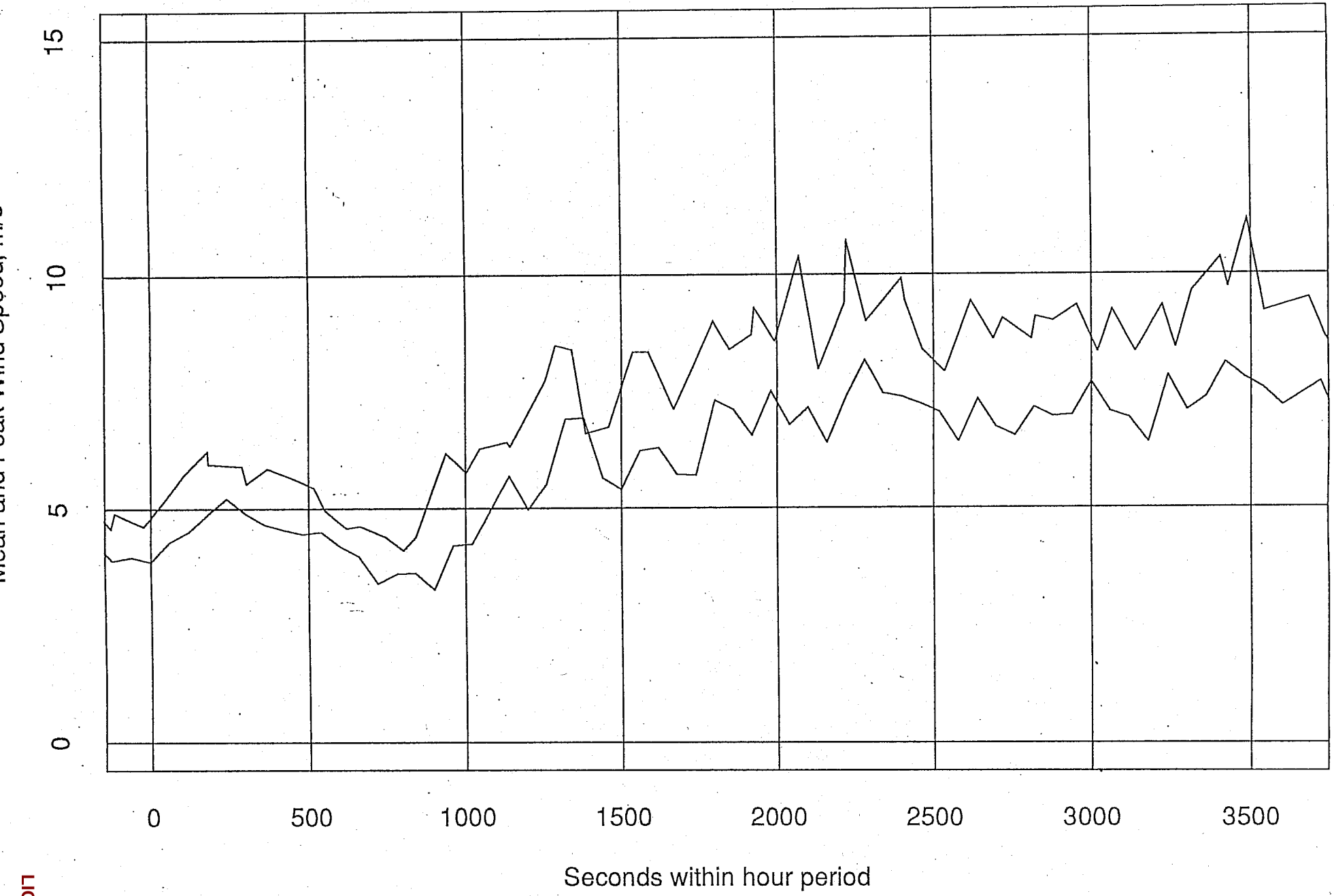

Figure 9-7: One-minute mean and peak wind speeds measured near the Moses Lake JAL aircraft hangar Day 238, Hour 01, during a moderate wind period.

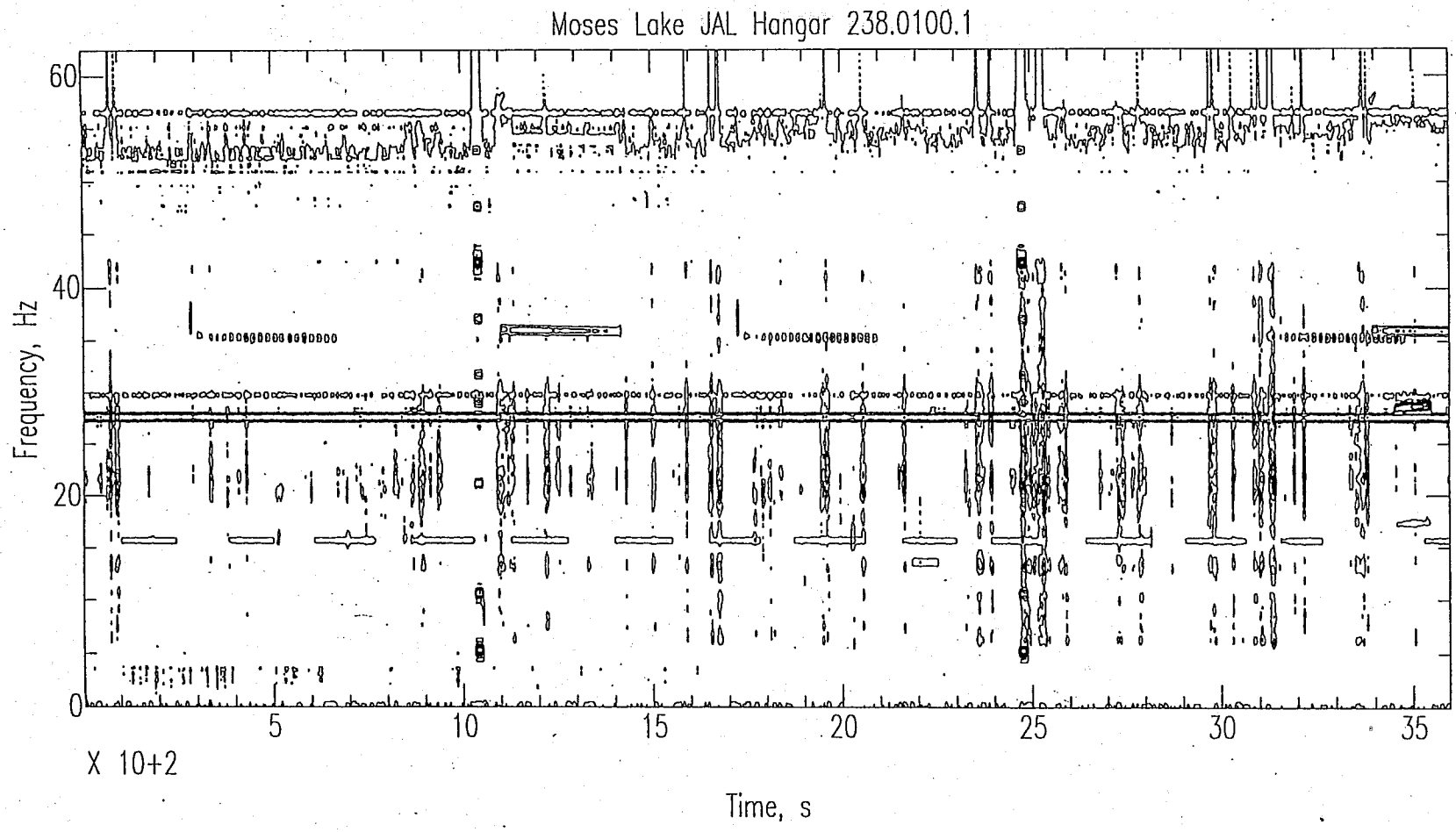

Figure 9-8: Spectrogram of the vertical seismic signal measured in the Moses Lake JAL aircraft hangar Day 238, Hour 01, during a moderate wind period.

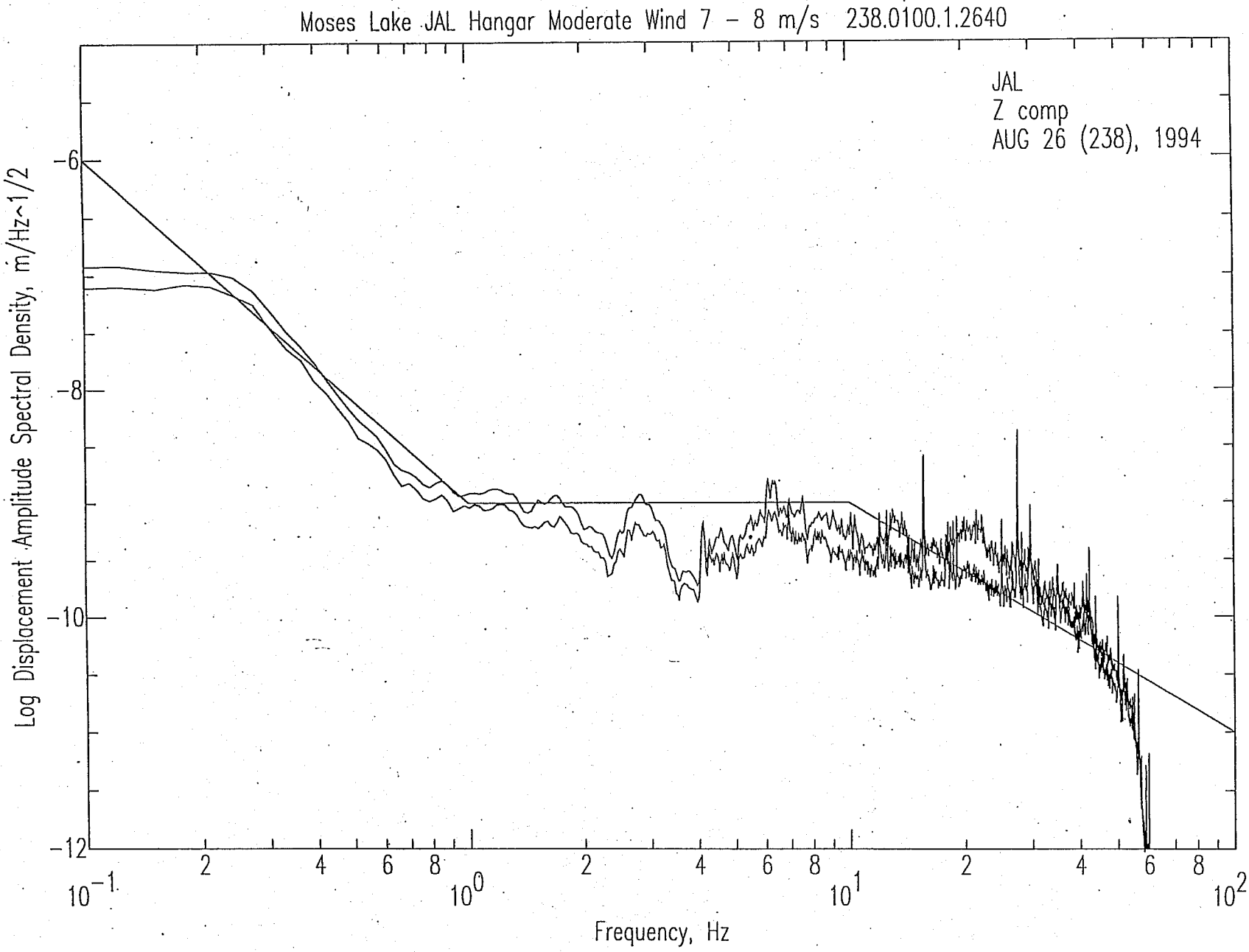

Figure 9-9: Median and r.m.s. spectra of the vertical seismic signal measured in the Moses Lake JAL aircraft hangar Day 238, Hour 01, during a moderate wind period. This spectrum is calculated from the time segment 2640 to 3000 s shown in Figures 9-7 and 9-8.

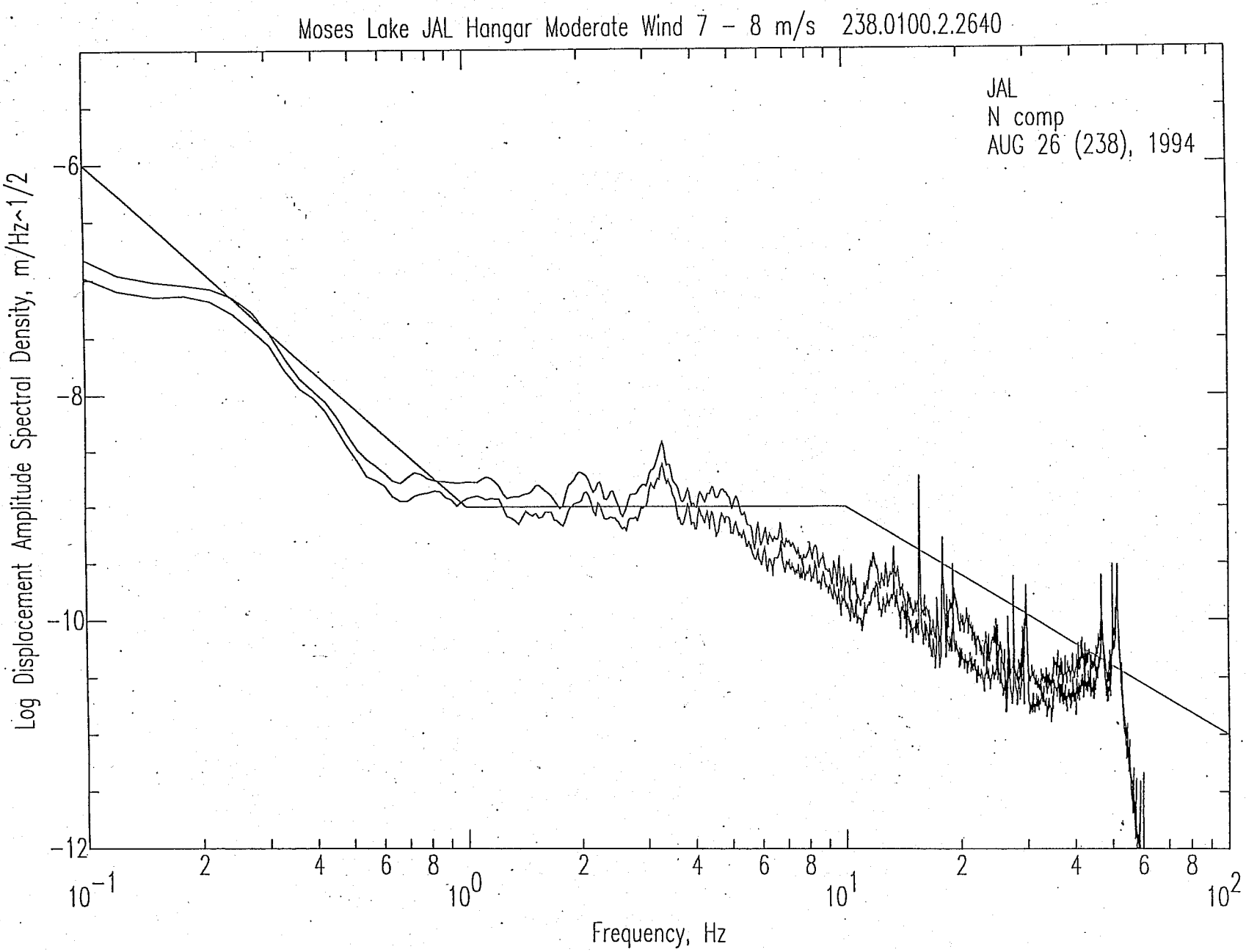

Figure 9-10: Median and r.m.s. spectra of the "north" seismic signal measured in the Moses Lake JAL aircraft hangar Day 238, Hour 01, during a moderate wind period. This spectrum is calculated from the time segment 2640 to 3000 s shown in Figures 9-7 and 9-8.

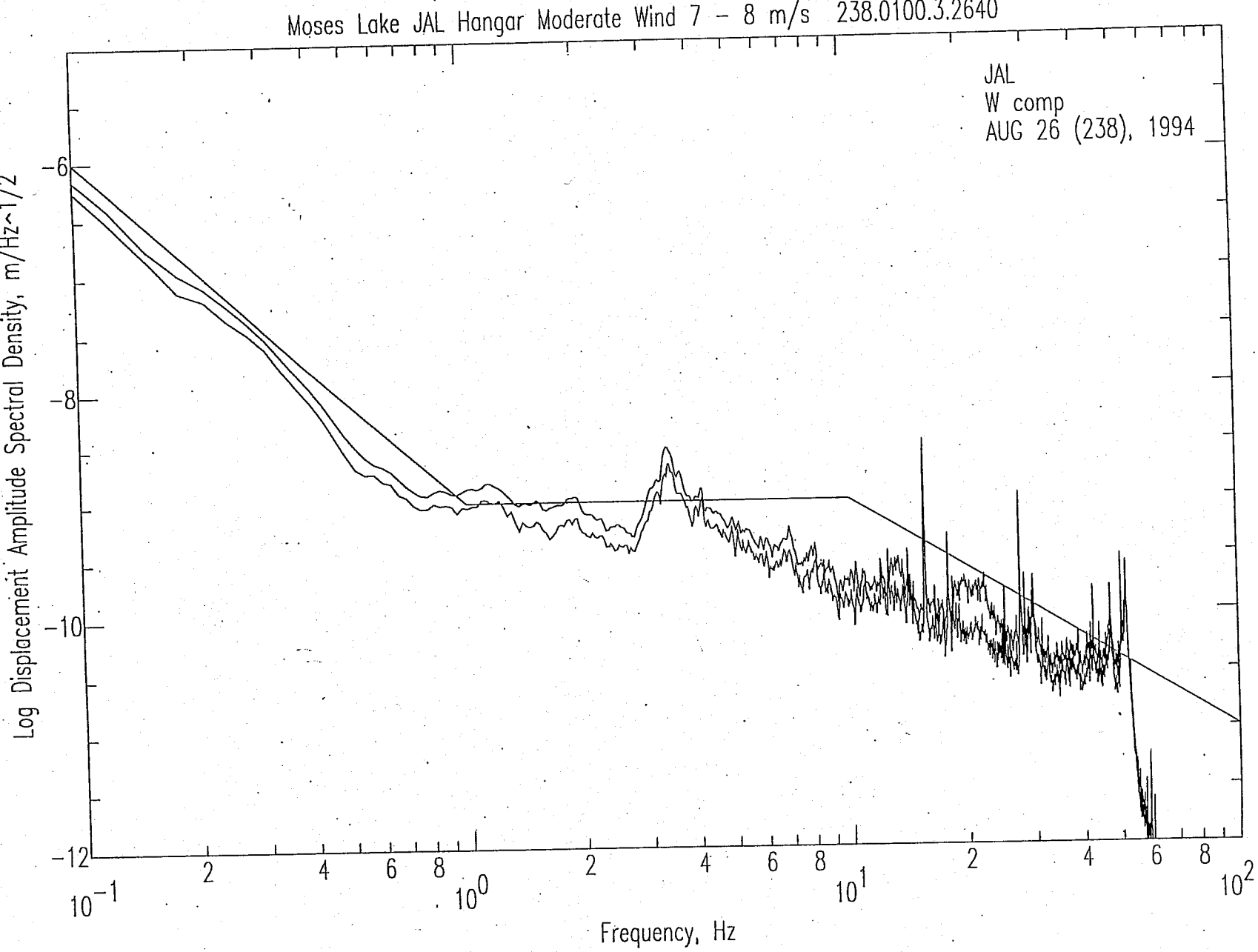

Figure 9-11: Median and r.m.s. spectra of the "east" seismic signal measured in the Moses Lake JAL aircraft hangar Day 238, Hour 01, during a moderate wind period. This spectrum is calculated from the time segment 2640 to 3000 s shown in Figures 9-7 and 9-8.